Nanostructure of Aggrecans in Natural and Engineered Intervertebral Discs

A thesis submitted to The University of Manchester for the degree of Master of Philosophy in the Faculty of Medical and Human Sciences

2013

Jude Michael Aldaco

Faculty of Medical and Human Sciences
School of Medicine

Table of Contents

List of Figures 9

List of Tables 11

Abstract 12

Declaration 13

Copyright 13

Acknowledgements 14

List of Abbreviations 15

Chapter 1 17

General Introduction 17

1.1 Introduction 18

1.2 The Spine 18

1.3 Structure of the Intervertebral Disc 19

1.3.1 Annulus Fibrosus 20

1.3.2 Nucleus Pulposus 21

1.3.3 Cartilaginous End Plate 21

1.4 Extracellular Matrix in the IVD 22

1.4.1 Collagens 22

1.4.2 Fibronectin Proteins and Elastin 22

1.4.3 Proteinases 23

1.4.4 Proteoglycans 23

1.4.4.1 Aggrecan 23

1.4.4.1.2 Aggrecan Structure 24

1.4.4.1.3 Aggrecan Globular Domains 24

1.4.4.1.4 GAG Chains 27

1.4.4.2 Other IVD Proteoglycans 28

1.5 Nutrition of IVD cells 29

1.6 Disc Degeneration of the IVD 31

1.6.1 Changes that Occur with Age 32
1.6.2 Genetics.....33
1.6.3 Mechanical Loading.....33
1.7. IVD Biochemical Consequences.....35
1.8 Current Treatments-for Low Back Pain and IVD Degeneration 35
1.9 IVD Tissue Engineering.....36
1.9.1 Co-cultures 36
1.9.2. Three Dimensional Scaffolds.....37
1.9.3 Growth Factors.....37
1.9.4 Mechanical Constraints.....38
1.10 Scaffolds for IVD Engineering 38
1.11 IVD Nucleus Pulposus Tissue Integrity.....39
1.12 Atomic Force Microscopy.....40
1.12.1 AFM modes.....41
1.12.1.1 Intermittent Contact AFM.....41
1.12.1.2 Peak Force Tapping Mode 42
1.13 Studying Aggrecan Structure at the Nanoscale.....43
1.14 Hypothesis.....46
1.15 Aims 47
Chapter 2 48
General Methods 48
2.0 General Methods 49
2.1 Isolation of Aggrecan from Bovine NP tissue (D1 and D1D1 Fractions) and Aggrecan Detection.....49
2.1.1 Aggrecan Extraction from Bovine NP Tissue.....49
2.1.2 Dissociative CsCl Density Gradient Centrifugation 50
2.1.2.1 CsCl Preparation and D1 Fraction Isolation 50
2.1.2.2 D1D1 Fraction Isolation.....51

2.1.3 Membrane and Sample Preparation for Dialysis and Freeze Drying.....51
2.1.4 Protein and Sulphated Glycosaminoglycan Quantification 52
2.1.5 Aggrecan Dot Blot 52
2.2 Surface Characterisation of APTES-mica.....53
2.2.1 Mica Preparation for Surface Roughness Analysis.....53
2.2.2 AFM Imaging (Intermittent Contact Mode) 53
2.2.3 Contact Angle Assessment for APTES-mica Surface 54
2.3 Imaging the Ultrastructure of Aggrecan 55
2.3.1 AFM Sample Preparation for Tissue Extracted Aggrecan.....55
2.3.2 AFM Imaging of Aggrecan Ultrastructure.....55
2.3.2.1 Intermittent Contact Mode 55
2.3.2.2 Peak Force Tapping Mode 55
2.4 Measuring Aggrecan Ultrastructure 55
2.4.1 Imaging Processing from AFM Height Images to RAW Files 58
2.4.2 Measurement of Aggrecan Core Protein Contour Length and GAG Brush Length 58
2.4.3 Measuring GAG Brush Width 58
2.5 Statistical Analysis 59
2.6 Gene expression 60
2.6.1 Gene Expression Analysis 60
2.6.1.1 RNA Extraction.....60
2.6.1.2 Reverse Transcription of RNA.....61
2.6.1.3 Quantitative Real Time Polymerase Chain Reaction.....61
Chapter 3 62
Optimisation of Methodology to Image and Analyse Aggrecan Ultrastructure by Atomic Force Microscopy.....62
3.1 Introduction 63
3.2 Aims 63

3.3 Experimental design....63
3.3.1 Aggrecan isolation....63
3.3.2 AFM imaging....63
3.3.3 Quantification of aggrecan dimensions....63
3.3.4 Statistical analysis....63
3.3 Results....64
3.4.1 D1D1 fractions isolated from bovine NP tissue....64
3.4.2 GAG and protein quantification....64
3.4.3 Immunodetection of aggrecan in the D1D1 Fraction obtained from Bovine NP Tissue....65
3.4.4 Assessment of Surface roughness of APTES-mica....65
3.4.5 Assessment of the APTES-mica Surface Chemistry....67
3.4.6 AFM Imaging of Isolated Aggrecan....68
3.4.7 Aggrecan Core Protein Length....70
3.4.8 Aggrecan GAG Brush Length....72
3.4.9 Quantification of Aggrecan GAG Chain Width....74
3.5 Discussion....76
3.5.1 Aggrecan Isolated From Nucleus Pulposus Tissue....76
3.5.2 The APTES-mica Surface is Suitable for AFM Imaging of Aggrecan Molecules....76
3.5.3 Comparison of CP Contour and GAG Brush Length to Other Studies. 77
3.5.3.1 Aggrecan Core Protein and GAG Brush Length Cleavage.....78
3.5.4 GAG Brush Width....80
3.5.4.1 GAG Brush Width Variations....81
3.5.4.2 GAG Brush Width Findings and other AFM Imaging Studies....82
3.6 Conclusion....82
Chapter 4....84
Modified Aggrecan Isolation Procedure from Alginate Constructs for AFM Imaging....84

4.1 Introduction 85
4.1.1 Alginate 85
4.1.2 Cellular Immobilisation with Alginate 87
4.2 Aims 88
4.3 Experimental design 88
4.3.1 Alginate Bead Preparation for Size Determination 88
4.3.2 Bovine NP Cell Expansion 89
4.3.3 Cell Encapsulation into Alginate Beads 89
4.3.4 Isolation of Aggrecan from Alginate Constructs 89
4.3.4.1 Dissociative CsCl Density Gradient Centrifugation (D1 fraction) 90
4.3.5 Aggrecan Dot Blot 90
4.3.6 Size Exclusion Chromatography for Separating Alginate from Aggrecan Molecules 91
4.3.7 AFM Sample Preparation and Imaging 91
4.3.8 Statistical Analysis 91
4.4 Results 91
4.4.1 Alginate beads size variability 91
4.4.2 NP Cells Synthesise Aggrecan in 3D Alginate Cultures 93
4.4.3 Aggrecan Obtained by Size Exclusion Chromatography 93
4.4.4 Aggrecan Synthesised by NP Cells in 3D Culture can be Imaged by AFM 94
4.5 Discussion 95
4.5.1 Manual Formation of Alginate Beads Lead to Low Size Variability 95
4.5.2 Isolated Aggrecan from Alginate Cell Culture 96
4.6 Conclusion 96
Chapter 5 97
Aggrecan Ultrastructure in Tissue Engineered NP Cell Seeded Constructs 97
5.1 Introduction 98
5.1.1 Growth factors 98

5.1.2 Gene expression 98
5.2 Hypothesis 98
5.3 Aims 99
5.4 Experimental design 99
5.4.1 Human NP Cell Expansion 99
5.4.2 Human NP Cell Encapsulation into Alginate beads 99
5.4.3 Isolation of Aggrecan from Alginate Beads for AFM Imaging and Gene Expression Analysis 100
5.4.4 Size Exclusion Chromatography 100
5.4.5 Identifying Fractionated Aggrecan with Immunoblotting 100
5.5 Results 100
5.5.1 Size Exclusion Chromatography and Immunobloting 100
5.5.1.2 D1 Isolated Aggrecan from Bovine NP Tissue 100
5.5.1.3 Aggrecan Isolated from Human NP Cells Seeded in Alginate 101
5.5.2 Gene Expression 102
5.5.3 AFM Imaging 103
5.5.3.1 Bovine NP Tissue 103
5.5.3.2 Human NP Cells 104
5.5.4 Aggrecan Dimensions 105
5.5.4.1 Bovine NP Tissue 105
5.5.4.2 Human NP Cells Cultured in Standard and Chondrogenic media 107
5.5.4.3 GAG Brush Width and Aggrecan Structural Changes 114
5.6 Discussion 115
5.6.1 Aggrecan Gene Expression 115
5.6.2 Aggrecan Ultrastructure and Media Conditions 116
5.6.3 Comparison to NP tissue 116
5.6.4 Aggrecan structural features and GAG brush width 117
5.6.5 Comparison to other studies 117

5.7 Conclusion 118
Chapter 6 119
6.1 General Conclusions 120
6.12 Characterising Aggrecan Ultrastructure from Bovine NP Tissue 120
6.13 Development of Aggrecan Isolation from Alginate for AFM Imaging 122
6.14 Media Conditions Influence Aggrecan Ultrastructure 123
6.15 Concluding Remarks 123
6.2 Future Work 124
6.21 Characterising Species and Tissue Differences in Aggrecan Structure 124
6.22 Cellular Distribution and ECM Accumulation in Alginate Constructs 125
6.23 Identification of Aggrecan Core Protein Heterogeneity 125
6.24 IVD Tissue Engineering: The Application of Human MSCs 126
6.24.1 The Seeding of Human Adult MSCs in Alginate Constructs 126
6.24.2 Stimulation of Chondrogenesis with Other Growth Factors 126
6.25 Investigating Changes in Aggrecan Structure and Micromechanics 126
Chapter 7 129
Appendices 129
7.1 Dimethylmethylene Blue (DMMB) Solution Preparation 130
7.3 IC tapping and PeakForce Tapping Mode Settings 131
7.4 Defining the Aggrecan Molecular Perimeter 131
7.5 Alginate Beads Size Determination 132
7.6 Standard and Chondrogenic Media Reagents 134
7.7 RT sample preparation procedure 134
7.8 Supplementary Data for CsCl Density Gradient fraction 135
8.0 References 138

List of Figures

Figure 1.1. Human Vertebral Column of the Spine. 19
Figure 1.2. Intervertebral Disc. 20
Figure 1.3. Annulus Fibrosus Lamellae Structure and Organisation. 21
Figure 1.4. Aggrecan Structure. 25
Figure 1.5. Aggrecan and MMPs Cleavage Site of Aggrecan CP. 26
Figure 1.6. CS and KS Linkage Regions. 27
Figure 1.7. Nutrient Gradient of IVD. 30
Figure 1.8. Normal and Degenerated IVD. 31
Figure 1.9. IVD Degeneration Factors. 32
Figure 1.10. Mechanical Load. 34
Figure 1.11. NP Tissue Engineering 39
Figure 1.12. Schematic Set-up of an Atomic Force Microscope. 41
Figure 1.13. IC-AFM (Tapping Mode) 42
Figure 1.14 Peak Force Tapping Mode 42
Figure 1.15. Electron Microscope Imaging of Proteoglycan Aggregates and Aggrecan Monomers 44
Figure 1.16. Montage of Aggrecan. 45
Figure 2.17 Experimental design for aggrecan isolation from bovine NP tissue 49
Figure 2.18 AFM Image Processing for Quantification of Aggrecan Morphological Parameters. 57
Figure 2.19. Calculating Aggrecan Morphological Parameters. 59
Figure 3.20. D1D1 sGAG and Protein Level in Top Gradient Fractions and D1D1 Fractions. 64
Figure 3.21. D1D1 Fraction Aggrecan Dot Blot. 65
Figure 3.22. AFM Height Images of Blank Mica and APTES-mica Surfaces. 66
Figure 3.23. Summary of RMS Surface Roughness of APTES-mica. 67
Figure 3.24. The Hydrophobicity/Hydrophilicity of the APTES-mica Surface. 68
Figure 3.25. Full-Length and Non-intact Aggrecan Molecules Found in Bovine NP Tissue. 69
Figure 3.26. Aggrecan Core Protein Contour Length Quantification for Aggrecan Extracted from Bovine NP Tissue. 71
Figure 3.27. Aggrecan GAG Brush Length Quantification for Bovine NP Tissue. 73
Figure 3.28. Aggrecan GAG Brush Width Quantification for Bovine NP Tissue. 75
Figure 3.29. MMPs and Aggrecanases Cleavage Sites. 79

Figure 3.30. GAG chain length influences CP contour length 80
Figure 4.31. Alginate Structure. Copied from Draget et al (1997) 86
Figure 4.32. Alginate Polymer Formation by Ionic Crosslink through Calcium Ions 87
Figure 4.33. Aggrecan Isolation from Alginate Beads 90
Figure 4.34. Alginate Bead Size. 92
Figure 4.35. Aggrecan Dot Blot 93
Figure 4.36. Isolation of Aggrecan from Alginate. 94
Figure 4.37. Aggrecan Isolated from Bovine NP Cells Embedded in Alginate Beads 95
Figure 5.38. SEC and Aggrecan Immunoblotting of D1 Isolated Bovine NP Tissue 101
Figure 5.39. SEC and Aggrecan Dot Blot Analysis from Human NP Cells. 102
Figure 5.40. Chondrocyte Markers in Human NP Cells under Standard and Chondrogenic Media Conditions. 103
Figure 5.41. D1-SEC Isolated Aggrecan from Bovine NP Tissue. 104
Figure 5.42. Aggrecan Isolated from Human NP Cells under Standard and Chondrogenic Media 105
Figure 5.43. D1 Isolated Aggrecan Dimension from Bovine NP Tissue. 107
Figure 5.44. Aggrecan Core Protein Length Quantification. 109
Figure 5.45. Aggrecan GAG Brush Length Quantification. 111
Figure 5.46. Aggrecan GAG Brush Width Quantification. 113
Figure 5.47. Correlation between Aggrecan GAG Brush Width and CP Length. 114
Figure 7.48. Determining Aggrecan Molecular Perimeter 132
Figure 7.49. Calculating mm^2/pixel with ImageJ 132
Figure 7.50 Determining Alginate Bead Size with ImageJ 133

List of Tables

Table 2.1 Primer and Probe Sequences used in the RT-PCR Analysis 61
Table 5.2. Sample details 99
Table 5.3. Summary of reported aggrecan dimensions from bovine NP tissue, human NP cells cultured from standard and chondrogenic media. 117
Table 7.4. APTES-mica RMS analysis Raw Data. 130
Table 7.5. Atomic force microscopy parameters for IC tapping and Peak force tapping mode 131
Table 7.6 Standard and Chondrogenic Media Formulation 134
Table 7.7. Reaction Mixture of RT 134
Table 7.8 D1D1 Fraction from Bovine NP tissue 135
Table 7.9. Bovine NP Cells D1 fractions 135
Table 7.10. Bovine NP Tissue D1 fractions 136
Table 7.11 Human NP Cells D1 Fraction for Standard Media 136
Table 7.12. Human NP Cells D1 Fraction for Chondrogenic Media 137

Word count: 24,765

Abstract

Degeneration of the intervertebral disc (IVD) is considered to be a major cause of low back pain. The IVD is composed of the nucleus pulposus (NP), surrounded by concentric layers of annulus fibrosus (AF). The NP is composed predominantly of fibrillar type II collagen and the hydrophilic proteoglycan aggrecan which resist tensile and compressive loads respectively. The degenerate IVD is characterised by the loss of aggrecan in the NP, which in turn is linked to a reduced load bearing capacity and hence low back pain. Given the important role that aggrecan plays in the IVD and that previous work has demonstrated that aggrecan ultrastructure varies species and tissue type, this project aimed to determine if aggrecan synthesized by cultured cells was comparable to aggrecan derived from tissue.

The first aim of this project was to adapt existing methodologies developed for cartilage to enable the visualization and characterisation of extracted aggrecan from IVD by atomic force microscopy (AFM). Following initial extraction, the presence of isolated aggrecan was confirmed with immunoblotting and the suitability of APTES-coated mica surfaces for aggrecan immobilisation and visualisation was determined by contact angle measurements (to confirm the hydrophilicity of the substrate) and AFM roughness analysis. Subsequent AFM imaging demonstrated that bovine tissue derived aggrecan was characterised by a core protein (CP) adorned with individual glycosaminoglycan (GAG) side chains. Although aggrecan CP length for IVD derived molecules was biomodally distributed (215 ± 2 nm and 371 ± 6 nm) and the CP of the shorter population was comparable to that reported for cartilage derived aggrecan (220 ± 142 nm), IVD extracted molecules were predominantly in the shorter form.

The above optimised methodologies were subsequently applied to aggrecan isolated from alginate constructs seeded with human NP cells and cultured in standard or chondrogenic media with TGF-β3 for 21 days. Newly synthesised aggrecan was isolated by GuHCl solubilisation and ultracentrifugation under dissociative conditions (D1) with size exclusion chromatography. Aggrecan molecules isolated from human NP cells cultured in standard and chondrogenic media (n= 300/culture condition) conditions were imaged by PeakForce AFM. AFM height imaging and data analysis revealed a significant difference (p<0.0001) between the CP lengths and GAG brush lengths of human NP cells under standard and chondrogenic media (CP: 314 ± 2 nm and 376 ± 2 nm; GAG brush length: 248 ± 3 nm and 290 ± 1 nm respectively). In addition, there was a significant and profound difference in GAG brush width (49 ± 2 nm and 57± 2 nm respectively) between aggrecan synthesised in the two media. Crucially however, neither culture condition induced human NP cells to synthesise aggrecan which was structurally comparable to that isolated from bovine IVD tissue.

In future investigations it will be necessary to not only characterise the structure of aggrecan derived from human IVD but also to i) optimise culture conditions that would lead to synthesis of aggrecan structures comparable to native healthy tissue, and ii) determine the effects of variable aggrecan structure on the mechanical function of the constructs with an overall objective to using ultrastructural approaches to optimise tissue engineering strategies.

Declaration

No portion of the work referred to in the thesis has been submitted in support of an application for another degree or qualification of this or any other university or other institute of learning.

Copyright

ii. Copies of this thesis, either in full or in extracts and whether in hard or electronic copy, may be made **only** in accordance with the Copyright, Designs and Patents Act 1988 (as amended) and regulations issued under it or, where appropriate, in accordance with licensing agreements which the University has from time to time. This page must form part of any such copies made.

iii. The ownership of certain Copyright, patents, designs, trademarks and other intellectual property (the "Intellectual Property") and any reproductions of copyright works in the thesis, for example graphs and tables ("Reproductions"), which may be described in this thesis, may not be owned by the author and may be owned by third parties. Such Intellectual Property and Reproductions cannot and must not be made available for use without the prior written permission of the owner(s) of the relevant Intellectual Property and/or Reproductions.

iv. Further information on the conditions under which disclosure, publication and commercialisation of this thesis, the Copyright and any Intellectual Property and/or Reproductions described in it may take place is available in the University IP Policy (see http://www.campus.manchester.ac.uk/medialibrary/policies/intellectual-property.pdf), in any relevant Thesis restriction declarations deposited in the University Library, The University Library's regulations (see http://www.manchester.ac.uk/library/aboutus/regulations) and in The University's policy on presentation of Theses

Acknowledgements

First I would like to express my gratitude to the NOWNano DTC for the opportunity and showing me a different side of science that I will never forget. I like to send my thanks to my fellow NOWNano DTC students (the first cohorts) especially to Donna, Thanasis, Roberto, and Adam for their friendship and memories during my postgraduate studies.

I would like to thank Prof. Nicola Tirelli and Prof. Tony Freemont for inviting me into the NOWNANO DTC to undertake this study, Dr. Dave Thornton and Dr. Karine Rousseau for advice and training in proteoglycan separation and dot blotting trouble shooting, Tony Bentley and Nick Odgen from PhotoGraphics, Dr. Nigel Hodson for the watchful eye in AFM training and troubleshooting, Dr. Anne White and Andy Fotheringham for tissue extraction training, Pauline Baird for everything laboratory related, Dr. Hamish Gilbert for immunoblotting training, Dr. Lei Wang and Dr. Ghislaine Robert-Nicoud for the use of the freeze dry facilities, Dr. Stephen Richardson for introducing me to alginate beads, and Sonal Patel for the RNA extraction and gene expression work. I would also like to thank my fellow postgraduate student, Chris, Kim, Francesca, Louise, Ricardo, and Shahnaz for the laughs in the postgraduate office, tearoom, and in the laboratory.

A huge expression of thanks to Prof. Judith Hoyland and Dr. Michael Sherratt for giving me a second chance and never giving up on me, for all the technical and practical support, constructive criticism, patience, guidance, and advice.

A very special thanks to my wife Lisa (my true love and best friend) and daughters Faith (little pukka pie) and Abbey (little spud) for making my life colourful and joyful during my studies and their patience, sacrifice, and support during these busy and trying times, and to Christ who has provided everything I need for the next epic endeavour.

List of Abbreviations

A1	Associative density gradient
AC	Articular cartilage
ACN	Aggrecan
ADAMTS	A disintegrin and metalloproteinase with thrombospondin motifs
AF	Annulus fibrosus
AFM	Atomic force microscopy
AGEs	Advanced glycation end-products
APTES	3-aminopropyltriethoxysilane
CEP	Cartilaginous end plates
CM	Chondrogenic media
COL1	Type I collagen
COL2	Type II collagen
CP	Core protein
CRP	Complement reactive protein
CS	Chondroitin sulphate
CsCl	Caesium chloride
D1	Dissociative density gradient
D1D1	Dissociative density gradient + Dissociative density gradient
ECM	Extracellular matrix
EGF	Epidermal growth factor
GAG	Glycosaminoglycan
Gal	Galatose
GalNAc	N-acetylgalactosamine
GlcNAc	N-acetyl-D glucosamine
Glu	Glutamic acid
Gly	Glycine
GuHCl	Guanidine hydrochloride
HA	Hylauronic acid or hyaluronan
IC	Intermittent contact mode (tapping mode)
IGD	Interglobular domain
IL-1	Interleukin-1
IVD	Intervertebral disc
KS	Keratan sulphate

LBP	Lower back pain
MMP	Matrix metalloproteinase
NP	Nucleus pulposus
PG	Proteoglycan
PLL	Poly-L-lysine
RMS	Root mean square
SA	Sialic acid
Ser	Serine
SLRP	Small leucine-rich proteoglycans
SM	Standard media
TIMPs	Tissue inhibitor of metalloproteinase
TNF-α	Tumour necrosis factor alpha
VCN	Versican
xyl	Xylose

Chapter 1

General Introduction

1.1 Introduction

At some point in their life two thirds of adults will experience low back pain (LBP) which is a major cause of disability in modern society (Deyo and Weinstein, 2001). LBP places a great socioeconomic burden on healthcare systems around the world as the world's population ages (Dagenais et al., 2008). For instance, in the UK alone LBP accounts for 15 % of all sick leave which costs over £12 billion in lost production, disability benefits, medical, and insurance costs (Maniadakis and Gray, 2000). Chronic LPB is considered to be multifactoral and the risk factors include demographic, health, occupational, psychological, and spinal anatomy (Adams, 2002, Rubin, 2007). Low back pain has been commonly associated with intervertebral disc (IVD) degeneration disease which leads to limited mobility and poor quality of life (Luoma et al., 2000, Benneker et al., 2005, Cheung et al., 2009). It has been demonstrated that up to 40% individuals with LBP display features of intervertebral disc degeneration (Cheung et al., 2009).

1.2 The Spine

The human vertebral column or spine consists of 24 non fused vertebrae that are separated into three regions which are cervical (C1-C7), thoracic (T1-T12), and lumbar (L1-L5) with two fused regions below the lumbar section called the sacrum (5 fused) and coccygeal (4 fused) bones (figure 1.1). The spine exists in a 'S' shape column that supports the head and trunk during posture and movement and encloses and protects the spinal cord, nerve roots, and vertebral arteries. The joints between each vertebrae, which are known as intervertebral discs (IVDs), are the main shock absorber of motion-induced mechanical stresses transmitted to the skull and brain (Izzo et al., 2013).

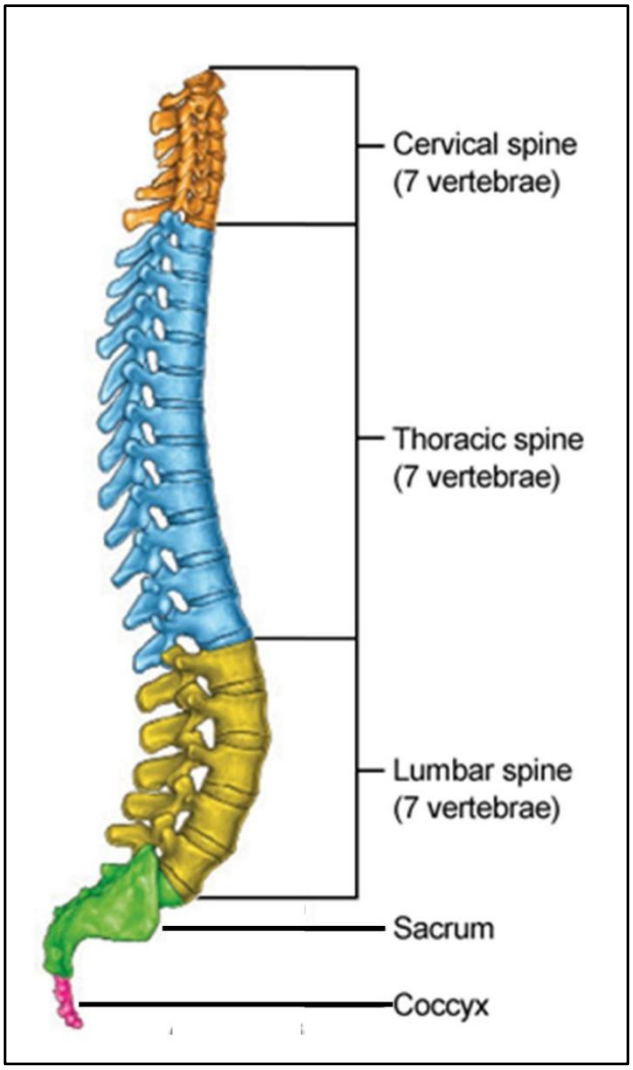

Figure 1.1. Human Vertebral Column of the Spine.

1.3 Structure of the Intervertebral Disc

The IVD consists of both fibrous and cartilaginous connective tissue. The twenty-three IVDs found along the human spine column provide six degrees of freedom to a spinal motion segment and serves as a central axial structure for cushioning mechanical loads (Hsieh and Twomey, 2010). IVD is not a uniform structure, but instead consist of three distinct layers called the annulus fibrosus (AF) layer, nucleus pulposus (NP) inner layer, and cartilaginous end plates (CEP) (figure 1.2).

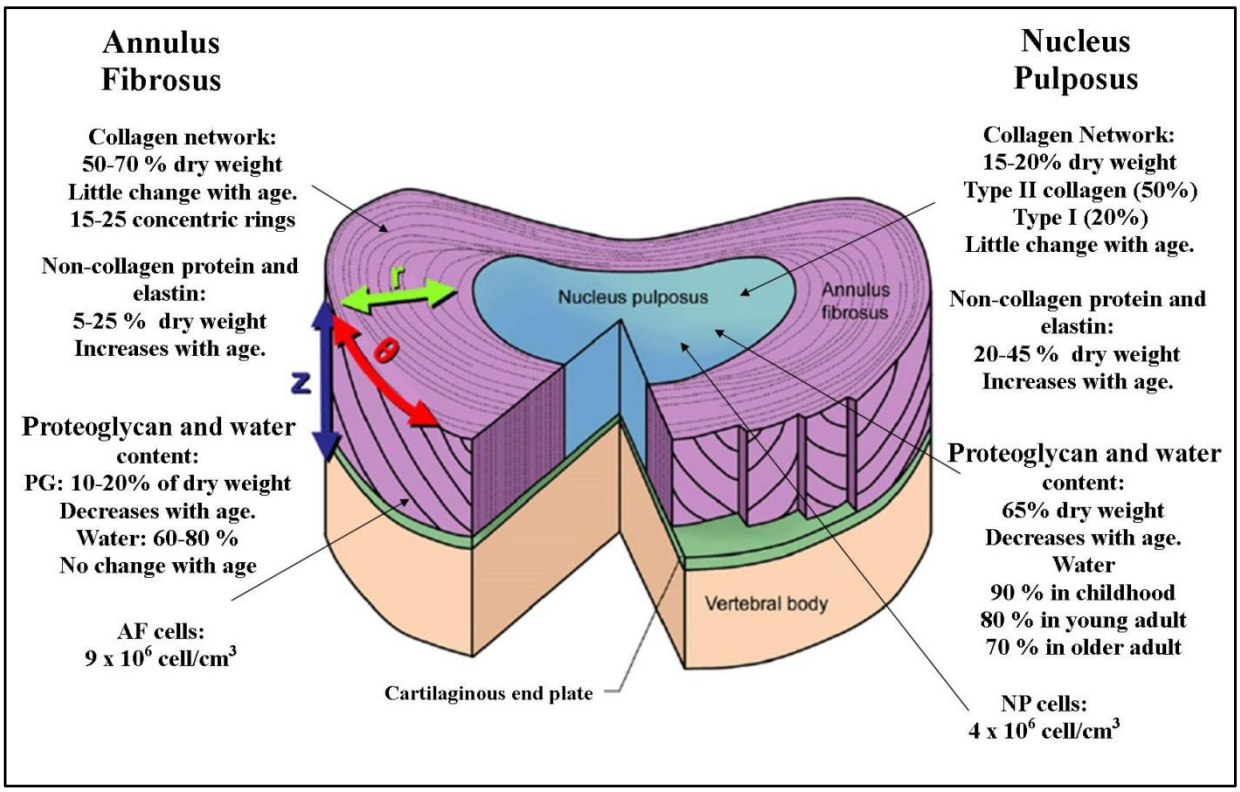

Figure 1.2. Intervertebral Disc.
Schematic illustration of the IVD structure and components for the AF and NP layers (Eyre and Muir, 1977, Lundon and Bolton, 2001, Pattappa et al., 2012). Radial direction (r) (from the NP outward), axial direction (z) (spinal long axis), and circumferential direction (θ) are the architecture of the IVD primary geometric axes. Image modified from Clouet et al. (2009) and Nerurkar et al. (2010).

1.3.1 Annulus Fibrosus

The AF consists of mainly collagen type I (50%), even though other collagen types are present such as types II and III. The AF structure is arranged in 15 to 25 concentric rings of highly organised collagen fibre bundles of multi-lamella. From a biomechanical view, each lamellae orientation alternates between +30º and -30º in a parallel direction (figure 1.3) to the vertical axis between each adjacent lamella (Hsieh and Twomey, 2010, Nerurkar et al., 2010). Earlier papers report the lamella band's geometry varies as a function of vertebral level and intradiscal region (Humzah and Soames, 1988). This was reported by the use of polarized light microscopy, X-ray crystallography, and electron microscopy showing collagen fibres angulation was regularly oriented in alternate sheets crossing at about 50-60° (Horton, 1958, Inoue, 1973). Both the inner and outer AF layers surround the NP layer where collagen type I content increases towards the outer layer and proteoglycan content decreases. AF cells in the outer layer are elongated and fibroblast-like, whereas cells in the inner layer are more spheroid and chondrocyte-like (Zhao et al., 2007).

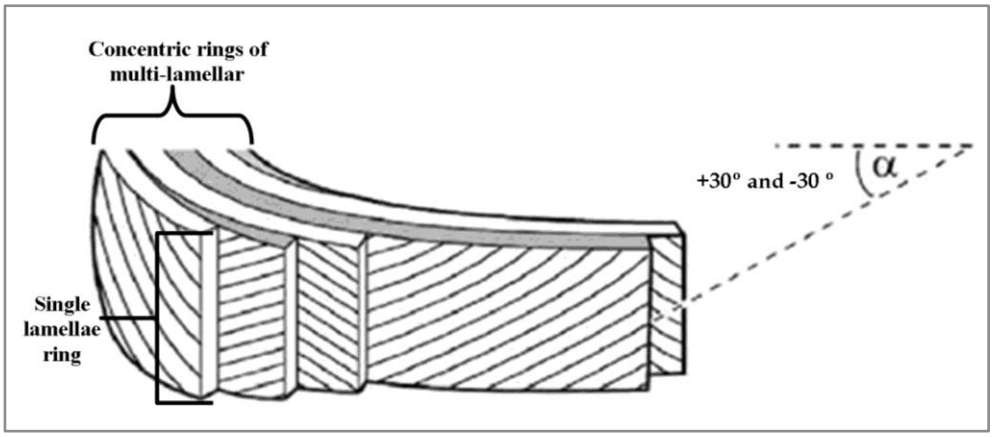

Figure 1.3. Annulus Fibrosus Lamellae Structure and Organisation.
The AF consist of number of concentric ring of lamellae with each ring containing collagen fibrils network arranged in an angle (α = +30º and -30º) that runs opposite in parallel to adjacent rings. Image modified from Adams and Roughley (2006).

1.3.2 Nucleus Pulposus

The nucleus pulposus (NP) which is the main tissue of focus of this study is surrounded by the AF and contains more of collagen type II (20%) and proteoglycans (PG) (60%). The large PG aggrecan is the main component that attracts and binds water molecules to provide a gelatinous consistency and compressibility integral to the shock absorbing properties of the disc. The accumulation of hydrophilic aggrecan creates a large osmotic swelling pressure. This is due to the negatively charged anionic groups on the chondroitin sulphate and keratan sulphate glycosaminoglycans (GAGs) chains on aggrecan that generate hydrostatic pressurisation to counter mechanical compression, while collagen type I in the AF resists biaxial tensile stresses and shear both within and between lamellae during mechanical stress (Hsieh and Twomey, 2010). In early development NP tissue is inhabited by a population of cells known as notochord cells, but these are subsequently replaced by NP cells (Trout et al., 1982, Urban et al., 2000). There is evidence however, that the nucleus pulposus of all vertebrates retains notochordal precursors throughout life (Risbud et al., 2010a).

1.3.3 Cartilaginous End Plate

The CEP is considered similar to articular cartilage (AC). The main component of the CEP is the water which is close to 80% after birth, but decreases below 70 % after 15 years of age. The ratio of proteoglycan to type II collagen (2:1) is similar to AC however lower than the NP which is 27:1. The CEP plays a key role for IVD structure, as a semi-permeable barrier for the diffusion of nutrients and bearing load. Structurally, the CEP covers the cortical bone surfaces of the superior and inferior vertebral bodies (Humzah and

Soames, 1988). During early development the foetal CEP is wide and vascularised along the AF layer, but by the age of 10, the AF layer becomes poorly vascularised. By adulthood (20 years of age) the CEP is calcified and decreases in size no longer covering the entire IVD (Hassler, 1969, Roughley, 2004).

1.4 Extracellular Matrix in the IVD

The ECM is mainly composed of water, PGs, and collagen fibrils, noncollagenous proteins, and elastin that vary between tissue (Hardingham and Fosang, 1992, Hascall et al., 1994, Roughley, 2004). NP and AF areas possess specific amounts of collagen types and proteoglycans which influence their unique biological and physiological attributes. The mechanical function of the matrix depends on not only the composition but also the architecture of the matrix components and both composition and architecture differ between the main IVD tissues lamella (Hsieh and Twomey, 2010, Nerurkar et al., 2010). This is due to the different specialised disc cell types in each layer that produce not only collagen fibrils types and proteoglycans, but also key proteins such as proteolytic enzymes that synthesise and breakdown the surrounding ECM, and other proteins that inhibit their activity (Sztrolovics et al., 1997, Nagase and Kashiwagi, 2003, Le Maitre et al., 2004, Le Maitre et al., 2007b).

1.4.1 Collagens

The IVD contains multiple collagen types. Types I and II being the main framework components of each layer. Collagen type I is found mainly in the inner and outer AF with collagen type II found in abundance in the NP region. Collagen type I and II account for 80% of the total collagen found in the IVD. Other collagens include III, V, VI, IX, XI, and XIV. All collagens are found to be in three functionalities- fibrillar, fibril-associated, and pericellular. The fibrillar collagens are types I, II, III, V, and XI and make up the majority of the collagen framework while fibril-associated collagens reside on the surface of the fibrillar collagens (e.g. type IX resides on the surface of type II collagen). Pericellular collagens such as type VI and X surround disc cell in both the AF and NP tissue.

1.4.2 Fibronectin Proteins and Elastin

Proteins are found in abundance in the IVD extracellular matrix and hold a variety of active functions. Two key proteins are fibronectin and elastin. Fibronectin plays an important role in linking disc cells to the surrounding ECM, and the accumulation of fragmented fibronectin promotes an increasing catabolic event linked to disc degeneration (Oegema et al., 2000). Elastin plays a vital role along with collagen in both AP and NP

layers and has the ability to recoil after being stretched. In the AF, elastin, runs parallel to the collagen type I fibrils whereas in the NP elastin are arranged radially and axially in order to restore deformation during mechanical bending (Yu, 2002, Smith and Fazzalari, 2009).

1.4.3 Proteinases

Proteinases are another group of proteins found within the IVD extracellular matrix, and play vital role in ECM remodelling and degradation (Vo et al., 2013). The two proteinases involved in this process are matrix metalloproteinase (MMPs) and aggrecanases. It is important to comment that disc properties depend on the balance between ECM synthesis and breakdown, and if this balance is maintained then, damaged tissue can normally be restored (Colombini et al., 2008). MMPs include collagenases (MMP1, 8, and 13), stromelysins (MMP3), gelatinases (MMP2 and 9) and membrane metalloproteinases are involved in the normal turnover degradation of collagen, aggrecan, versican, and link protein (Roberts et al., 2000). In the normal IVD working environment, MMPs are regulated and secreted in a latent form (proenzyme form) and activated by proteolytic cleavage, but inhibited by tissue inhibitor of metalloproteases (TIMPs) (Le Maitre et al., 2004). TIMP-1 and 2 are two main inhibitors that target active MMPS in the IVD matrix and bind irreversibly into a complex in a 1:1 stoichiometeric fashion (Le Maitre et al., 2007b). Aggrecanases include a disintegrin and metallloprotease with thrombospodin motifs (ADAMTS 1, 4, 5, 8, 9, and 15) are expressed by the NP disc cells and breakdown aggrecan by targeting cleavage sites of unique amino acid sequence along the aggrecan core protein (Nagase and Kashiwagi, 2003, Struglics et al., 2006, Le Maitre et al., 2007b). Like MMPs, ADAMTS also have TIMP-3 which target and inhibit their enzyme activity.

1.4.4 Proteoglycans

1.4.4.1 Aggrecan

Aggrecan is the most prevalent proteoglycan mainly residing in the NP. The attraction to water molecules by the highly negative charge GAGs increases the swelling pressure to the ECM which allows the IVD to withstand high compressive loads (Wilke et al., 1999). The functions of PGs are not only structural but they also act as key regulating factors in tissue development. Hyaluronan a non-sulphated GAG is abundant throughout the AF and NP sections associate with aggrecan via a link protein to form a supramolecular structure called aggregate.

1.4.4.1.2 Aggrecan Structure

Aggrecan is a multi-modular proteoglycan that has a core protein (CP) (250-350 kDa) with three functional domains known as G1, G2, and G3 (Doege et al., 1991, Hardingham and Fosang, 1992, Kiani et al., 2002, Dudhia, 2005, Chandran and Horkay, 2012). The globular domains G1 and G2 are separated by a short region called the interglobular domain (IGD), and G2 and G3 are separated by a GAG attachment region consisting of CS and KS known as CS1 and CS2 (figure 1.4a).

1.4.4.1.3 Aggrecan Globular Domains

The G1 domain is the N-terminal of the CP containing three structural motifs called N-terminal immunoglobulin-fold (Ig-fold or A) and two proteoglycan tandem repeat sequences (B1 and B2) that form a double loop structure by disulphide bonding (Sandy et al., 1990). The functional aspect of G1 is the attachment to hyaluronic acid via the link protein's (LP) own Ig-folds (A) that interacts noncovalently with G1-Ig-folds (A) while both B1 and B2 motifs from G1 and LP interact with HA to form a high molecular weight aggregate (>200 MDa) illustrated in figure 1.4b-c (Heinegard and Hascall, 1974, Hardingham and Fosang, 1992, Neame and Barry, 1993, Watanabe et al., 1997).

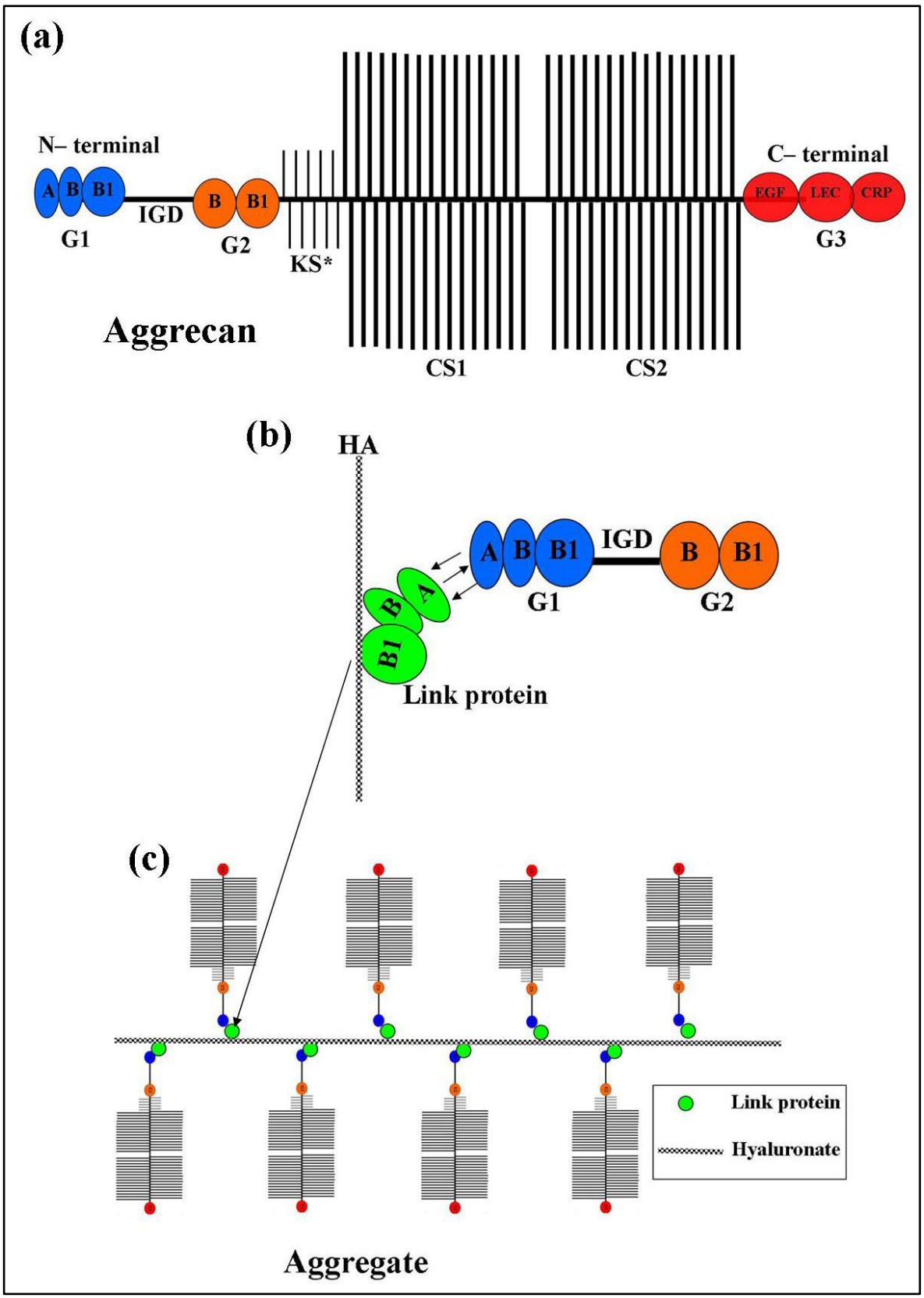

Figure 1.4. Aggrecan Structure.

(a) Aggrecan consist of three regions G1, G2, and G3. Between G2 and G3 reside the two types GAG chains made of disaccharide sugar D-glucuronic acid and N-acetyl-D-galactosamine for CS; D-galactose and N- acetyl-D-galactosamine for KS. (b) Link protein (LP) and G1 binding to immunoglobin fold (A) and a proteoglycan tandem repeat (loops B and B1).G1 and link protein bind to hyaluronan (HA) . Aggrecan binds to hyaluronan to form aggregates via link. (c) A series of aggrecan monomers bind to HA to a supramolecular structure known as aggregate. [Images adapted from Hardingham and Fosang(1992).] * = keratan sulphate II.

The G2 domain possess the same two proteoglycan tandem repeat sequence (B1 and B2) motifs with no Ig-fold, having no interaction with LP or HA. The IGD contain a number of proteolytic cleavage site that are susceptible to MMPs and aggrecanases (ADAMTS) (Lohmander et al., 1993, Sztrolovics et al., 1997, Le Maitre et al., 2004, Pockert et al., 2009). ADAMTS-4 and 5 targets Glu^{373}–Ala^{374} bound in the IGD whereas MMP cleave between Asn^{341} and Phe^{342} (Nagase and Kashiwagi, 2003, Le Maitre et al., 2007b). Figure 1.5 summaries the current knowledge of CP cleavage sites for aggrecan in humans.

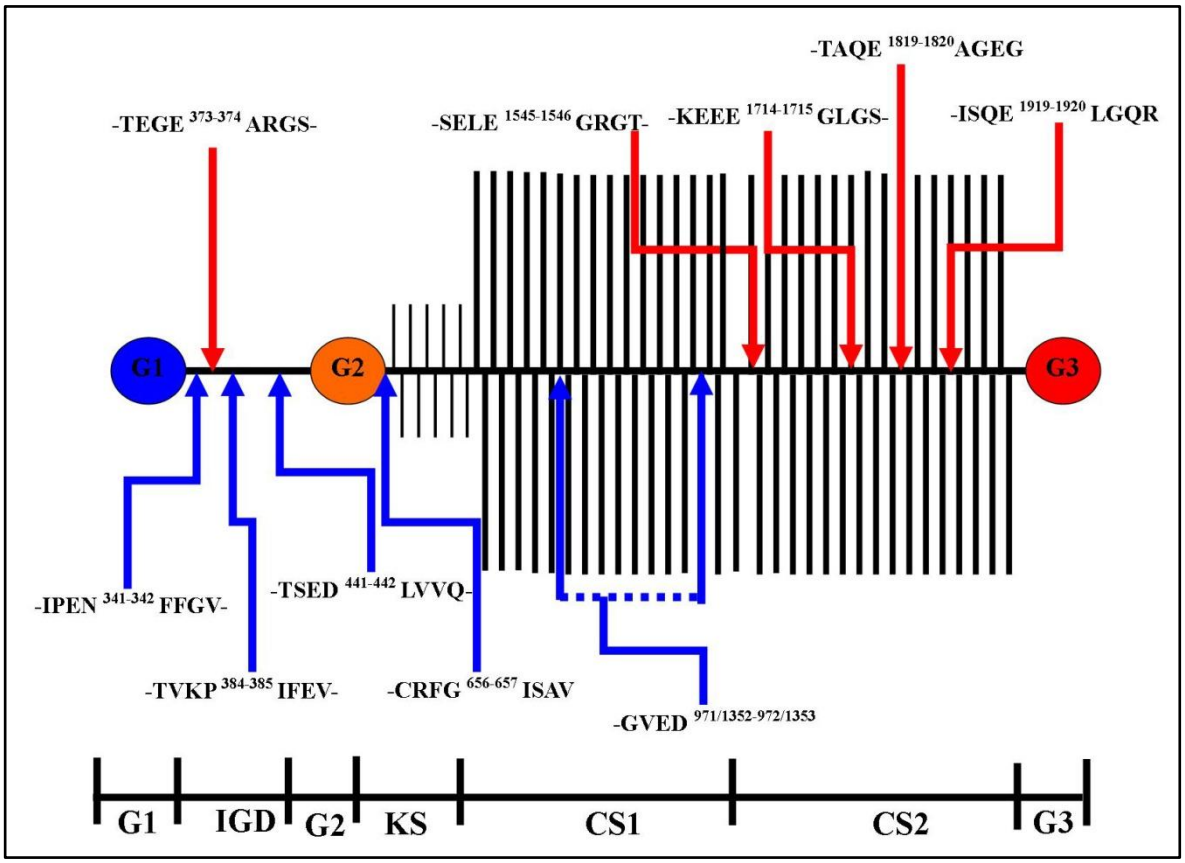

Figure 1.5. Aggrecan and MMPs Cleavage Site of Aggrecan CP.
Schematic representation of human aggrecan with cleavage sites of aggrecanase (red) and MMPs (blue). G1= globular domain 1, IGD= interglobular domain, G2= globular domain 2, KS= keratan sulphate II, CS1= chondroitin sulphate domain 1, CS2= chondroitin sulphate domain 2, and G3= globular domain 3. [Adapted from Struglics et al., (2006)]

The G3 domain is the C-terminal end of the core protein and possess three motif structures known as epidermal growth factor (EGF), C-type lectin, and sushi or complement reactive protein (CRP) (Perkins et al., 1991, Brissett and Perkins, 1998). Both CRP and C-type lectin are always present whereas EGF motif is variable (Luo et al., 2000). The functional aspect of G3 is post-translational processing of the core protein and aggrecan secretion (Zheng et al., 1998)

1.4.4.1.4 GAG Chains

Chondroitin sulphate is the main component of the glycosaminoglycan (GAG) chains attached to the aggrecan core protein which comprises of one uronic acid (glucuronic acid (GlcA)) and one aminosugar (N-acetylgalactosamine (GalNAc)) that form the repeating disaccharide unit whereas keratan sulphate II(KS) consist of N-acetyl-D glucosamine (GlcNAc) and galatose (Gal). The attachment site to the core protein for CS is known as a tetrasaccharide linkage region (figure 1.6a). This region consist of four monosaccharides starting with xylose (Xyl) which is covalently bonded by serine residues (flanked glycine residues) from the core protein via an O-linked glycosidic bond (Silbert and Sugumaran, 2002). This is followed by two successive Gal and one GlcA residues. KS linkage (figure 1.6b) differs which is branched with a GalNAc which is covalently bonded by serine residues from the core protein via an O-linked glycosidic bond. However two branch chain extension is form with two pair of Gal-GalNAc and Gal-SA (sialin acid) where only the Gal- GalNAc residue undergoes GAG chain polymerisation (Funderburgh, 2000).

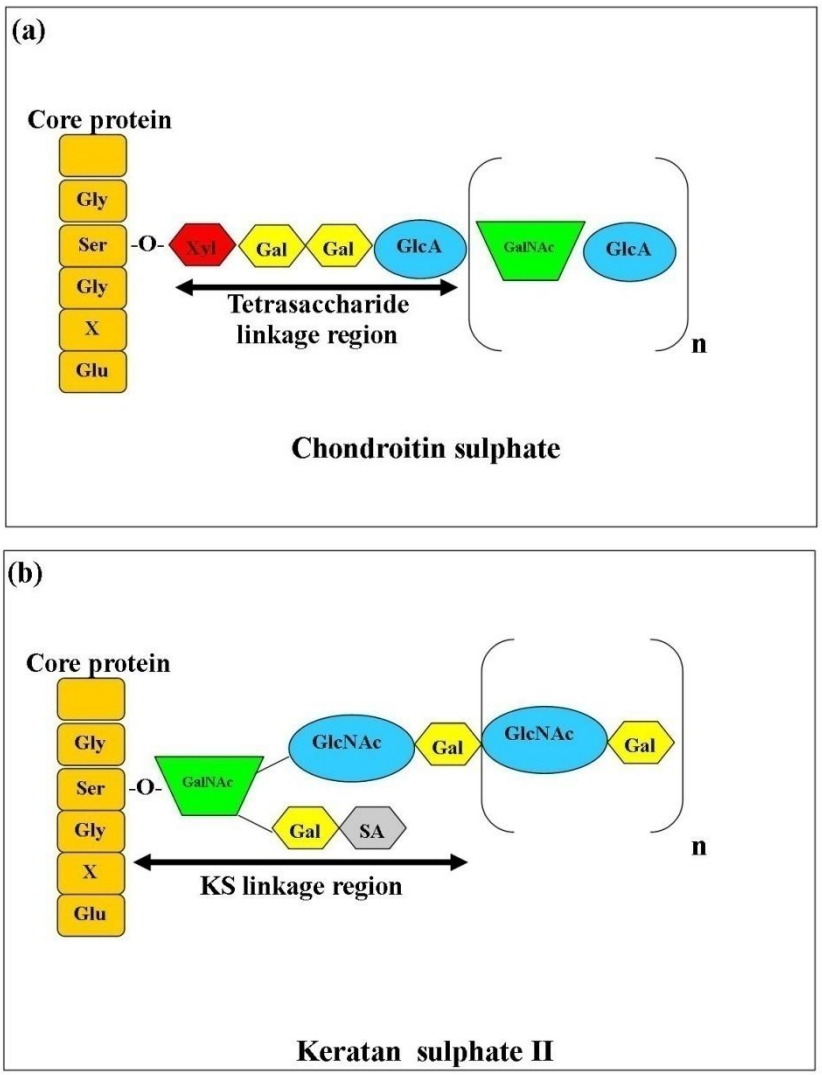

Figure 1.6. CS and KS Linkage Regions.

(a) GAG-core protein tetrasaccharide linkage region for CS. (b) GAG-core protein linkage region for keratan sulphate II. Gly= glycine; Ser= serine; Glu= glutamic acid; Gal= galatose; GalNAc=N-acetyl-galatosamine; GlcNAc= N-acetyl-D glucosamine; SA= sialic acid

The GAG attachment region of the core protein consist of three regions known as KS domain, CS1, and CS2 are located between G2 and G3 domain are covalently bounded to a dense population of negative charge CS chains (100 chains at ~20 kDa) and a less dense KS population (30-60 chains at 5-15 kDa)) (Rosenberg and Schubert, 1967, Kiani et al., 2002, Heinegard, 2009). KS domain is composed of a amino acid repeat motif that varies between species whereas the CS1 region contain a variable number of 19 amino acid tandem repeat that exhibits length polymorphism that influence the number of CS chain attached (Barry et al., 1994, Doege et al., 1997). CS2 domain contains four aggrecanases cleavage site, but no MMP cleavage sites. Importantly, the negatively charged CS1 and CS2 domain account for the major function of aggrecan as a structural proteoglycan creating a large osmotic swelling pressure and drawing water into the tissue. The net negative charge of the IVD extracellular matrix derives from these chains, and on average CS consists of two charges per disaccharide whereas KS consists of one charge (Urban and Maroudas, 1979). The concentration of fixed negative charge and fixed charge density depend on aggrecan concentration and CS/KS ratios which changes with age and spine/disc position.

Human IVD aggrecan is a metabolically stable, long lived protein (e.g. white matter of the brain, eye lens, cartilage and, skin,) that exists as two distinct populations: aggrecan which aggregates with link protein and hyaluronan (aggregating), and a non-aggregating aggrecan population (Jahnke and McDevitt, 1988, Sivan et al., 2006). IVD aggrecan is more highly sulphated with KS than AC and found to be 30% less aggregated and more heterogeneous with many non-aggregating proteoglycans derived from aggrecan (Donohue et al., 1988, Roughley et al., 2006). Another distinct feature of IVD aggrecan is the proteoglycan content being 27 times more than AC (Mwale et al., 2004). Aggrecan has a crucial importance in the stability of NP tissue for clinical approaches in IVD regeneration (i.e. NP tissue engineering). Specific separation (density gradient centrifugation) and analytical (AFM) techniques are required in order to study IVD aggrecan in more detail.

1.4.4.2 Other IVD Proteoglycans

Although aggrecan is the most abundant PG in both the NP and AF tissues other PGs are also present. They include versican, perlecan, lubricin, and small leucine-rich

proteoglycans (SLRP) which include a range of species (decorin, biglycan, fibromodulin, keratocan, lumican, proline arginine-rich protein (Prolargin, PRELP), chondroadherinand, asporin) which have been reported in the IVD (Melrose and Roughley, 2014). Structure and functional roles are being revealed in recent years. For an example, versican which is abundant in the AF is thought to control periodicity of disc cell differentiation (Zhang et al., 1999). SLRPs have numerous biological roles that are coming into light such as a function in collagen organisation, sequestering growth factors, and stimulating inflammation (Kalamajski and Oldberg, 2010, Iozzo and Schaefer, 2010).

1.5 Nutrition of IVD cells

The IVD is an avascular and aneural tissue regarded as a highly hypoxic, acidic, and nutrient deprived environment with a physiologically harsh ECM (Brodin, 1955b, Diamant et al., 1968, Mobasheri, 1998, Urban, 2002). The maturing IVD become less vascularised due to the calcified CEP that will restrict the diffusion of nutrient. This is important since NP and AF cells rely on diffusion of nutrients such as glucose and oxygen from capillaries from adjacent vertebra where the nearest blood vessels can be 8mm away (Brodin, 1955a, Brodin, 1955b, Urban et al., 2004). The IVD microenvironment has about 1-5% oxygen which has an effect on glucose transport and metabolism, and disc cells must obtain a critical concentration greater than 0.5 mmol/L of glucose to maintain vitality (Urban et al., 2004). Disc cells have overcome these conditions by utilising anaerobic glycolysis in order to metabolise glucose for adenosine triphosphate (ATP) production. Anaerobic glycolysis and low oxygen concentrations result in the production of lactic acid as a metabolite by-product giving a disc pH range of 6.9 to 7.2 (Bartels et al., 1998). Nutrient diffusion and the disc cells at various location will operate at different metabolic rates and hence build up a nutrient gradient of oxygen, glucose, and lactic acid along the disc (Urban et al., 2004, Grunhagen et al., 2006, Fassett et al., 2009) (figure 1.7).

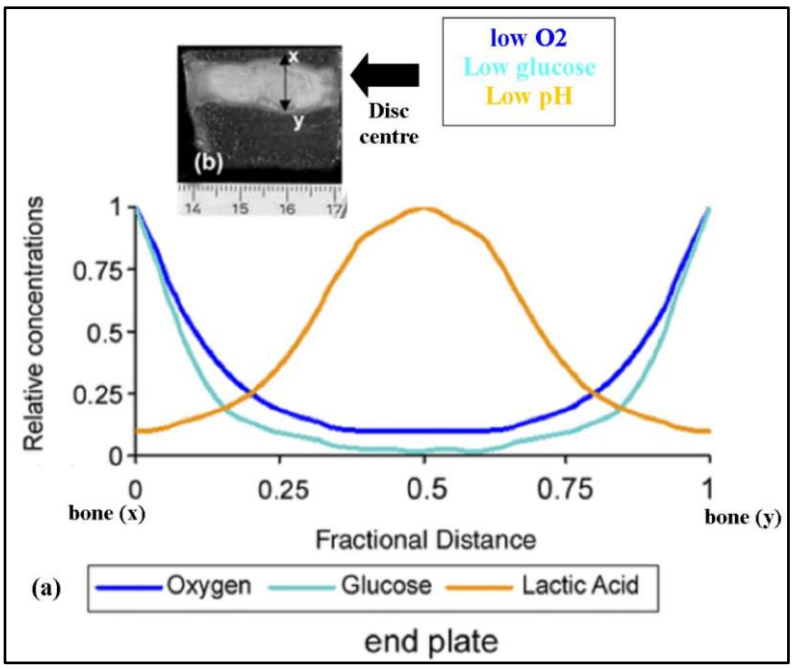

Figure 1.7. Nutrient Gradient of IVD.

(a) Distinct fall in glucose and glucose levels and a rise in the metabolic by-product lactic acid towards the centre of IVD. (b) A human sagittal section of the IVD showing the dimensions of the disc and the direction of the gradient shown in a. Images modified from Urban et al., (2004) and Grunhagen et al., (2006).

The decrease in pH plays a vital role in the IVD microenvironment resulting in glycosaminoglycan production, tissue inhibitor of metalloproteinase (TIMP) production, and cell viability (Masuda and Lotz, 2010). These hypoxic, acidic, and nutrient deprived conditions results in a low disc cell population in the NP and AF having approximately 4 x 10^6 cells/cm^3 and 9 x 10^6 cells/cm^3 respectively (Maroudas et al., 1975, Roughley, 2004, Richardson et al., 2007).

1.6 Disc Degeneration of the IVD

IVD degeneration pathology (figure 1.8) can be described as the loss of fibrous and cartilaginous connective tissue, narrowing of space between vertebral bodies (i.e. loss of disc height), and local mechanical dysfunction resulting from an aberrant cell-mediated response to progressive structural failure (Adams and Roughley, 2006, Colombini et al., 2008).

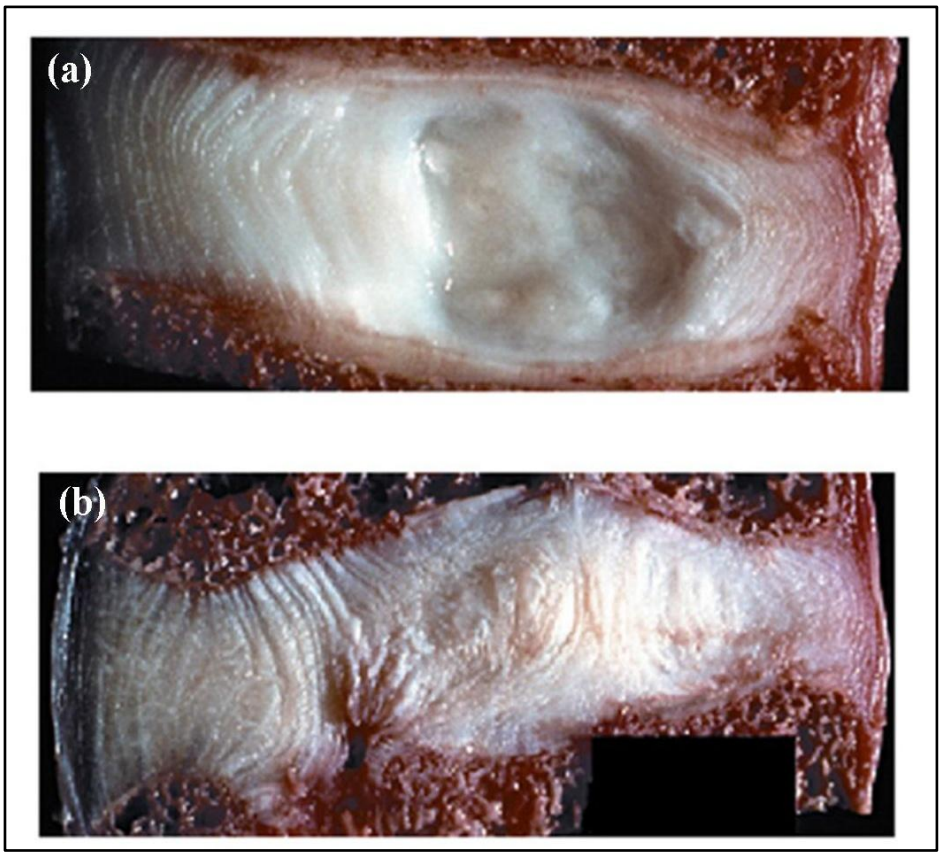

Figure 1.8. Normal and Degenerated IVD.
Mid-sagittal sections of IVDs (a) Young normal IVD (grade 1). (b) Degenerated disc (grade 3). Image modified from Adams et al., (2009)

The IVD disc cells play a pivotal role in IVD degeneration as their cellular metabolism is altered affecting the tissue composition of the ECM and its functional properties initiating disc degeneration (figure 1.9). Degeneration is influenced by a number of factors such as age (Buckwalter, 1995, Zhao et al., 2007), genetic polymorphisms (mutations) (Chan et al., 2006, Battie et al., 2008), and mechanical loading (Lotz et al., 2004, Setton and Chen, 2006, Adams, 2004) resulting in adverse biochemical consequences (Urban et al., 2004, Zhao et al., 2007).

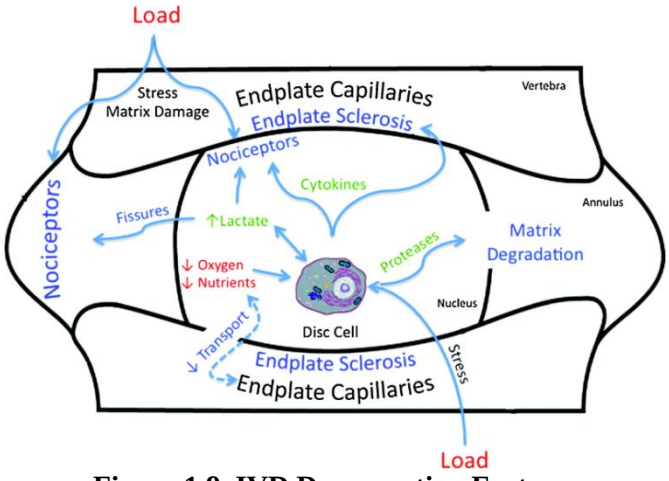

Figure 1.9. IVD Degeneration Factors.

A schematic summary of the major key factors (age, mechanical, and genetic (not shown)) that contribute to progressive disc degeneration implicating IVD disc cells as the key effectors in disc degeneration. Figure reproduced from Masuda et al (2010)

1.6.1 Changes that Occur with Age

The disc cells rely on metabolite transport by diffusion, but age related calcification of the CEP diminishes the blood supply contributing to low cell density and proliferation in both the NP and AF tissue (Buckwalter, 1995, Zhao et al., 2007). Low cell nutrition and age promotes the changes in composition of IVD ECM, especially proteoglycans in the NP layer where they degrade. GAG chain content changes with age resulting in keratan sulphate increase and chondroitin sulphate decrease which impairs aggrecan's affinity to attract water molecules (Lyons and Sweet, 1986, Johnstone and Bayliss, 1995). The synthesis of collagen type I replaces the diminishing formation of aggrecan and collagen type II. As abnormal collagen formation increases in NP layer this leads to an onset of aberrant cross-links by non-enzymatic glycosilation end products known as advanced glycation end-products (AGEs) (DeGroot et al., 2004, Verzijl et al., 2000). AGEs are the spontaneous reaction of reducing sugars such as pentosidine from degraded proteoglycans with collagen. Collagen cross-links (between lysine and arginine residues) formed in the NP layer interact with AGEs which in turn attack the physical and chemical properties of collagen leading to tissue stiffness and inhibition of matrix turnover (Adams and Roughley, 2006). Therefore the loss of hydration and presence of AGEs in the NP layer reduces the IVD's hydrodynamic pressure resulting in loss of shock absorbing capacity and the disc elastic deformability.

Diminishing nutrient supply and age affects disc cell biology through cell senescence and programmed cell death (apoptosis). Recent studies link cell senescence with aging and disc degeneration with signs of cell senescence indictors such as senescence associated β-galactosidase, decreasing telomere length, and increase expression of $P16^{INK4A}$ (Le Maitre

et al., 2007a, Gruber et al., 2007, Kim et al., 2009b). What is interesting is that both types of cell senescence appear to contribute to natural disc aging and pathological degeneration. The first type of cell senescence is replicative senescence, resulting from shortening of the telomeres from repeated cell division. The second type is stress induce premature senescence which results from various stress factors such as reactive oxygen species, mechanical load, and inflammatory mediators (e.g. IL-1) (Zhao et al., 2007). The combination of the two types contribute to age related degeneration meaning replicative senescence occurs naturally during disc aging whereas stress induce premature senescence can increase the onset of disc degeneration by its three factors .

Apoptosis or programmed cell death (PCD) is another cellular activity implicated in disc degeneration. PCD has been recently a new focus of research linking PCD and disc degeneration. Zhao (2006) discuss in their review that disc cells undergo PCD via different signal transduction pathways in response to different 'stimuli'. These stimuli are age related mechanical load and biochemical changes that were observed through various methodologies from animal models and human disc cells.

1.6.2 Genetics

Identical twin studies have shown 50-70% of IVD degeneration is contributed from genetic factors (Sambrook et al., 1999, Adams and Roughley, 2006, Battie et al., 2008). Current research has identified a number of mutations that affect genes encoding ECM components and proteases involved in their turnover (Chan et al., 2006, Tegeder, 2009, Mayer et al., 2013). For an example, aggrecan's retention of water is affected by the aggrecan gene AGC1 from variable number of tandem repeats (VNTR) polymorphisms. These variable numbers of amino acid sequences found in VNTRs affect the number chondroitin sulphate (CS) chain attachment to the aggrecan core protein (Doege et al., 1997, Rodriguez et al., 2006). Aggrecan molecules with a different number of CS chains affect the hydration of the NP layer and its tissue properties, therefore individuals that carry shorter alleles have an increased risk of early age-related disc degeneration associated with VNTRs (Solovieva et al., 2007). Other genes associated with disc degeneration are collagens (COL9A3, COL11A1, COL11A2, and COL1A1), vitamin D receptor, cartilage intermediate layer protein, metalloproteinsase-3 (MMP3), and thrombospondin-2.

1.6.3 Mechanical Loading

Biomechanical loading and trauma contribute mechanical stress to the IVD (Setton and Chen, 2006). The responses to these physical stimuli play a vital role to IVD degeneration.

As previously mentioned applied stress affects cellular activity and the disc remodels to build a matrix that minimises the stress (Hutton et al., 1999a, Wenger et al., 2005). The constant abnormal chronic loading or trauma can initiate a cascade of events that form a cycle of effects leading to IVD degeneration (Gilbert et al., 2010). Mechanical loading affects the response in both AF and NP cells. The cellular response is the key feature in this situation through metabolic changes that modify the surrounding ECM environment (Maclean et al., 2004). These progressive changes have a significant change in hydrostatic pressure, tensile strain, and fluid loss due to changes to proteoglycan and collagen rate of synthesis (Handa et al., 1997). Cellular response also includes the production of proteases that contribute to ECM degradation resulting in loss of matrix integrity and failure to response to continual biomechanical loading. Figure 1.10 summarises the effects of abnormal chronic loads on the IVD that lead to progressive degeneration (Colombini et al., 2008).

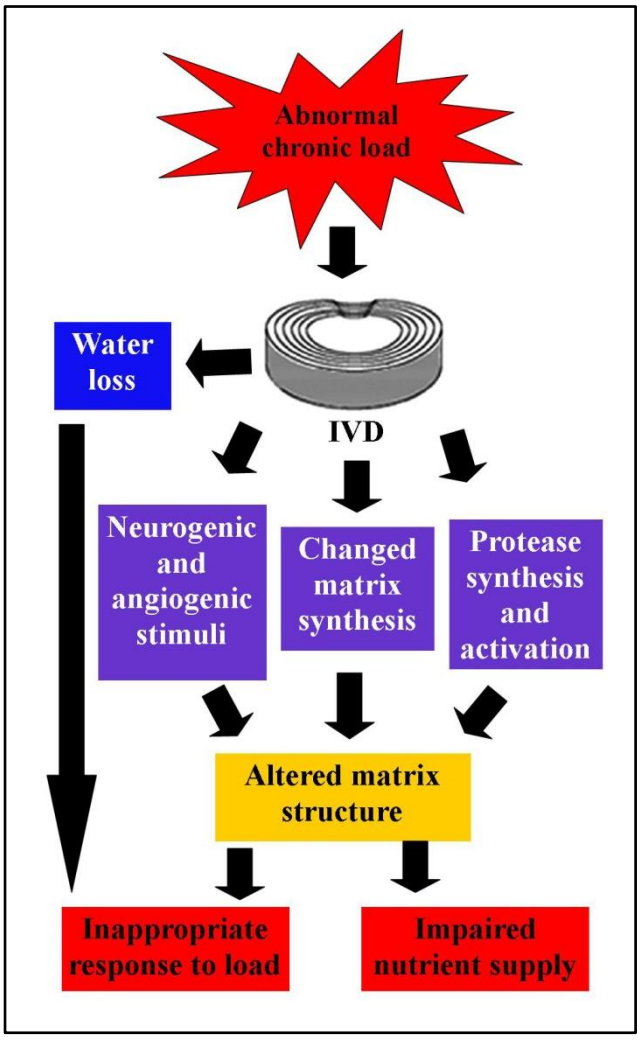

Figure 1.10. Mechanical Load.
One of the key factors to that lead to a series of negative feedback resulting in altered IVD structure and progressive disc degeneration. Image adapted from Colombini (2008).

1.7. IVD Biochemical Consequences

IVD degeneration is thought to be initiated in the NP tissue where the most profound effects are apparent in this region (Pearce et al., 1987).The biochemical consequences result from the combination of multifactoral events including age (nutrient supply), genetics, and biomechanical factors which leads to a ECM breakdown.

The changes of disc cell phenotype amplify an imbalance in proteinase synthesis from an anabolic metabolism to a catabolic metabolism breaking down proteoglycan macromolecules and collagens (Le Maitre et al., 2004, Pockert et al., 2009). The loss of the key proteoglycan aggrecan leads to NP dehydration collagen type I is synthesised instead of type II (Le Maitre et al., 2007b, Sive et al., 2002). The AF tissue experiences tears within its structure resulting in the loss of disc height removing tension from the collagen fibres of the AF thus destabilising the disc segment and limiting mobility. The breakdown of the AF and the loss of aggrecan leads to disc innervations and pain (Johnson et al., 2006, Freemont et al., 1997). It should be pointed out that not all disc degeneration results in pain; one study has shown through MRI scanning that 64% of 98 asymptomatic subjects showed signs of disc degeneration, but experienced no low back pain (Jensen et al., 1994).

1.8 Current Treatments-for Low Back Pain and IVD Degeneration

LBP treatments vary between healthcare systems, but most available treatments include medical management, physical therapy, maintaining physical activity level, cognitive behavioural therapy, and counselling (Bogduk, 2004, Lebovits et al., 2009). Medical management is probably the most popular course practitioners utilise which includes analgesics (over the counter or prescription pain killer such as non steroid anti-inflammatory drugs, steroidal anti-inflammatory drugs, and opiods), muscle relaxants, and antidepressants. The second choice of treatment is physical therapy which includes regular physical exercise, and other alternatives therapies include trans-cutaneous electrical nerve stimulation and acupuncture (Thomas et al., 2006). When pain relief is not achieved, then invasive action such as spinal fusion (arthrodesis) surgery is taken to remove the degenerate or damaged disc (Schizas et al., 2010). However, replacement procedures such as whole IVD and nucleus replacement (allogenic or autogenic) are available and although progressive improvements have been shown, it has disadvantages in tissue immunogenicity and disc dysfunction (Diwan et al., 2000, Ruan et al., 2007). Another approach is the use of prosthetic devices to replace parts of or the whole IVD. Current prosthetics on the market

include PDN (IVD nucleus replacement; Raymedica Inc.), whole IVD replacement including Charite (DePuy Spine Inc.) and ProDisc (Synthes Spine Inc.), Flexicore (Spinecore/Stryker Spine, Allendale, NJ), and Maverick (Medtronic Sofamor Danek, Minneapolis, MN) (Errico, 2005). Since their application, there have been varying degrees of success reported (Blumenthal et al., 2005, Bertagnoli et al., 2005, Sasso et al., 2008). with some reports of device failure and dysfunctions compared to spinal fusion surgery (Freeman and Davenport, 2006). Most treatments are advantageous only in the short term but not in the long term. Importantly, current treatments for LBP associated with IVD degeneration only target the symptoms and not the biological basis of the disease. Consequently research groups are focusing their attention towards the repair or regeneration of the damaged IVD tissue through tissue engineering (Alini et al., 2002, O'Halloran and Pandit, 2007, Vadala et al., 2013) as potential novel therapies to target the underlying aberrant cell biology.

1.9 IVD Tissue Engineering

Cartilage repair studies can inform the design of IVD tissue engineering since cartilage and IVD disc cells and matrices share many similarities (Vinatier et al., 2009). The cell biology of IVD and cartilage disc cells has been extensively studied leading to a number of strategies for IVD regeneration. The IVD cells are unique in phenotype and low in numbers so the first obstacle is cell source. The three choices considered are NP cells, chondrocytes, and mesenchyme stem cells (MSCs). Previous studies have shown attempts to extract disc cells for cell expansion however; this resulted in further degeneration of the tissue. Despite the outcomes of this approach, the concept has not been fully discarded (Nomura et al., 2001, Richardson et al., 2007, Yang et al., 2010). NP and chondrocyte cells share a common morphology and phenotype (Sive et al., 2002), even though chondrocytes show promising results in cartilage repair they would not be an ideal replacement since the amount of cells required from one biopsy, and PG synthesis from NP cells compared to chondrocytes is 27 times more creating a gelatinous tissue found in native IVD (Mwale et al., 2004). MSCs offer an alternative cell source because of easy isolation from various sources in tissue (e.g. bone morrow (BM) and adipose (AD) tissue), their differentiation capacity, and self renewal ability.

1.9.1 Co-cultures

Co-cultures systems have been used to investigate NP cells or chondrocytes with MSCs to study their interaction to induce differentiation. For an example, Richardson et al (2006b) co-culture (monolayer) human adult bone marrow-derived MSCs with human NP cells for

seven days. They reported an increase chondrocytic expression of key genes of SOX-9, collagen type II, and aggrecan. This study demonstrated the importance of cell-cell contact for differentiation and the expression of key genes by the production of key growth factors (Yamamoto et al., 2004) through possible cell adhesion or cell signalling pathway (Engler et al., 2006). Other groups have has also demonstrated this methodology with the combination of other factor such as mechanical load (Kim et al., 2009a).

1.9.2. Three Dimensional Scaffolds

Engler et al (2006) showed how MSC cell lineage specificity can be directed by matrix elasticity. For example, if a matrix is soft then it can mimic neurongenic soft tissue, stiffer matrices mimic muscle, and rigid matrices mimic bone. As such MSCs can 'feel and sense' matrix elasticity by binding and pulling against the matrix followed by a cellular mechano-transducer(s) required to generate signals based on the force that the cell generate to deform the matrix therefore transducing this information into morphological changes and lineage specification. For this reason three dimensional scaffolds or other polymeric materials have been used to drive MSC differentiation to chondrocyte-like cells. Various groups have demonstrated NP-like differentiation within various scaffolds such as alginate (Risbud et al., 2004), type II and type I atellocollagen (Sakai et al., 2005, Sakai et al., 2006), hyaluronan scaffold (Crevensten et al., 2004), hydroxybutyl chitosan (Dang et al., 2006), chitosan glycerophosphate (Richardson et al., 2008), or poly-l-lactic acid with the combination of inducing factors such as genetic transfection of MSCs to express key transcription factors for predifferentiation (Richardson et al., 2006a). All studies showed a variety of evidence in differentiation and expression or increase activity of NP markers such as aggrecan and collagen type II, increase activity in cellular signalling pathways, and increase expression of SOX-9 transcription factor.

1.9.3 Growth Factors

In terms of chondrogenesis growth factors such as transforming growth factor β (TGF-β-1 and 3), bone morhpogenetic proteins (BMP-7), fibroblastic growth factor2 (FGF-2), insulin-like growth factor 1 (IGF-1) with various combination of external chondrogenic medium supplements (Puetzer et al., 2010) have been known to promote MSC differentiation to NP-like cells(Risbud et al., 2004, Steck et al., 2005, Shen et al., 2009) . Risbud et al., (2004) demonstrates this combination of external growth factor applying TGF-β1 with other external factors (dexamethasone, ascorbate 2-phosphate, sodium pyruvate, and ITS-plus culture supplement) under hypoxic condition (2 % oxygen). Some consider oxygen tension (hypoxic conditions) as another morphogenetic factor which

promotes MSC differentiation to NP-like cells or chondrocytes through hypoxia inducible factors (HIF-1 and HIF-2) that regulate the metabolism, function, and fate of cells of the nucleus pulposus in the IVD (Malladi et al., 2006, Risbud et al., 2010b). Risbud showed MSCs differentiation to NP-like phenotype expressing key chondrogenic markers and protein/proteoglycans, but also maintained its differentiated state.

1.9.4 Mechanical Constraints

Only a few studies have reported that mechanical load on human NP cells regulate gene expression of cellular activity (Wuertz et al., 2009) and MSC differentiation (Le Maitre et al., 2008). The application of mechanical load can be used as a tool for aiding cell proliferation or MSC differentiation through artificial loading devices (Bueno et al., 2005, Kim et al., 2009a). Again this is performed with the combination of growth factors (e.g. TGF-β1 and hypoxic conditions) and cyclical loading using a bioreactor on a suitable scaffold (Li et al., 2009, Richardson et al., 2010).

1.10 Scaffolds for IVD Engineering

Ideally a tissue engineered IVD would need to mimic the native ECMs and therefore scaffold design would require suitable properties including biocompatibility, favourable three-dimensional structure, tissue adhesion, appropriate mechanical strength, injectability, and biodegradability. The use of scaffolds should also aid cell distribution, enhance differentiation and/or maintain cell phenotype, thus stimulating cells to synthesise the appropriate matrix. Currently, there are a number of groups that have focused on engineering specific IVD tissues, namely just NP or AF, or a whole (composite) IVD using a variety of scaffolds (synthetic and natural polymers) based on properties of the target tissue, cell source, and scaffold material (O'Halloran and Pandit, 2007, Nerurkar et al., 2010). Figure 1.11 illustrates a fundamental model for the long term strategy towards the design of an engineered IVD incorporating the use of bone marrow or AD derived MSCs. Established differentiation techniques would provide a route of MSC differentiation to NP-like cells and expansion (Clouet et al., 2009, Vadala et al., 2013).

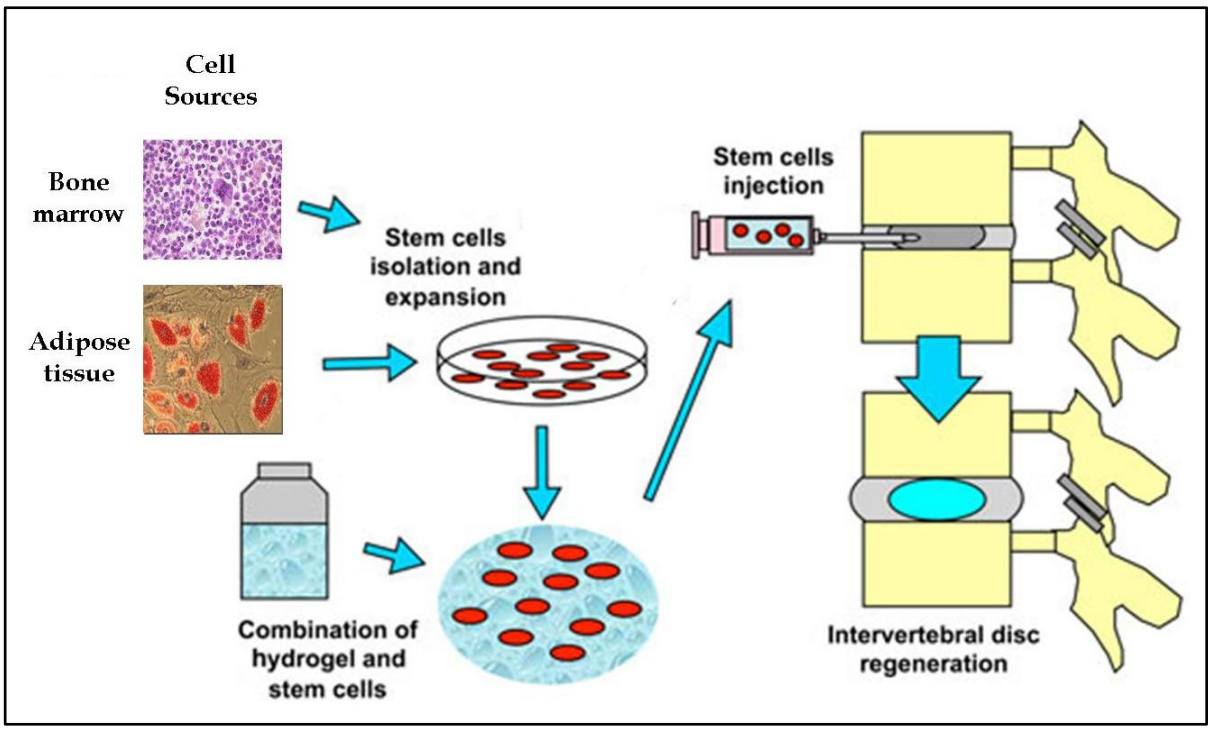

Figure 1.11. NP Tissue Engineering

An illustrated strategy to repair or regenerate NP tissue. Autologous MSCs are extracted from the patient's BM or AD tissue; MSCs are differentiated into NP like cells and expanded by various cell culturing techniques; NP-like cells are seeded on a 3D hydrogel (e.g. chitosan glycerophosphate) scaffold to maintain differentiation; NP-like cells and hydrogel arranged and loaded by less invasive injection and solidifies to body temperature into the IVD for repair/regeneration. Image modified from Vadala et al, (2013) .

1.11 IVD Nucleus Pulposus Tissue Integrity

Cell based tissue engineering/regenerative therapies offer a huge potential through the implantation of cells to repair and produce a tissue with similar characteristics to the native IVD. However, to date few studies have focused on understanding the structure/organisation of the matrix formed either following cell seeding of cells in appropriate biomaterials or following implantation into native tissue (Ng et al., 2003, Aladin et al., 2010, Kopesky et al., 2010). Indeed, ensuring that the structure and organisation of the molecules in the matrix recapitulates the ultrastructure of the native IVD will be vital for such techniques to be clinically successful. Given the predominant role aggrecan has in the IVD matrix and the extensive changes in aggrecan synthesis and degradation that occur during disc degeneration it will thus be necessary to evaluate the quality of aggrecan produced by any cell type seeded in biomaterials used for in an IVD repair/regeneration therapy.

1.12 Atomic Force Microscopy

The atomic force microscope (AFM) is a high-resolution scanning probe microscope (SPM) which scans with a solid probe across a surface (Binnig, 1982, Binnig et al., 1986). This solid probe known as a cantilever (100–400 μm long) often made of silicon or silicon nitride (Si_3N_4) and mounted with a extremely sharp tip which is on the order of a few nanometers (Tortonese, 1997). Contact mode is the conventional operational mode where the tip is moved in close proximity to the surface and presses down with a small loading force. The surface is raster scanned and controlled by piezoelectric scanner in either horizontal (x and y) or vertical (z) dimension. AFM is based on the interaction forces between the tip and surface (i.e. sample). These forces include Van der Waals, electrostatic, capillary-adhesive, and double layer forces. Depending on the force between the tip and surface, this will lead to a deflection of the cantilever based on Hooke's law. These deflections result from the amount force the cantilever encounters over the surface and the magnitude of these deflection are captured by a laser beam which reflects off the back of the cantilever in an angular direction. The changing reflected laser beams as the tip moves over the surface are captured and converted into electrical signals by a photodiode. The resulting signal produces a topographical image of the sample surface in full three-dimensional resolution (figure 1.12).

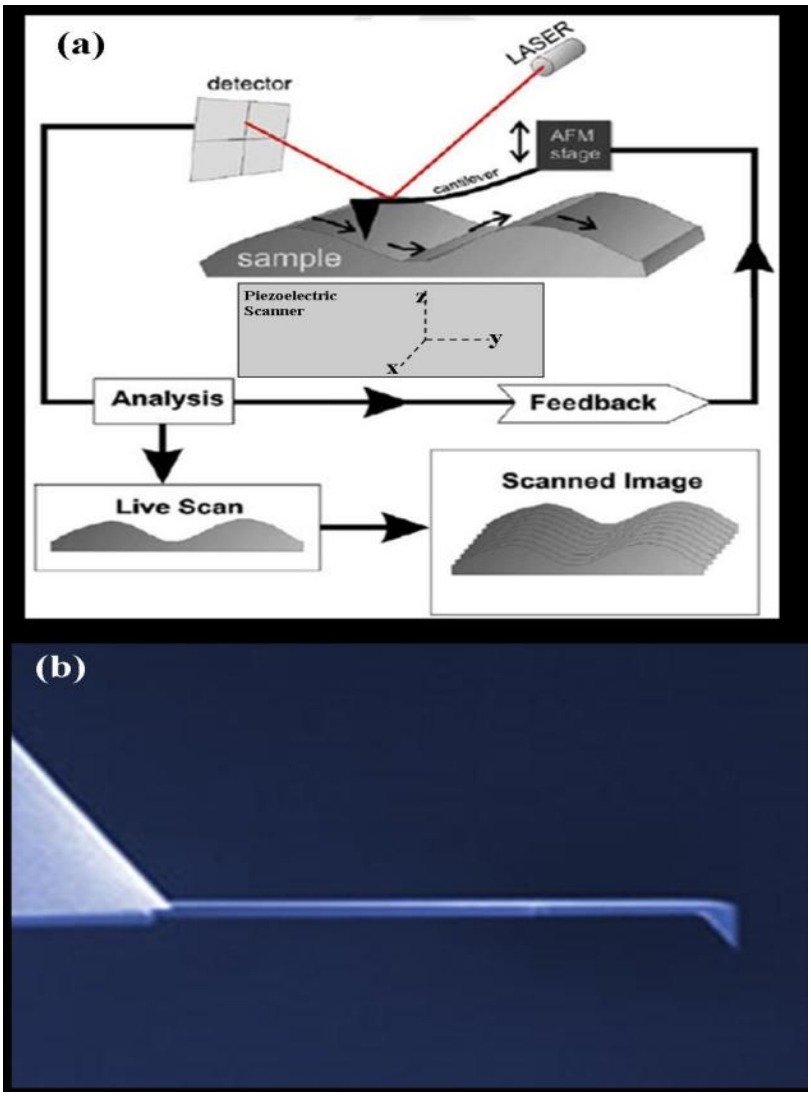

Figure 1.12. Schematic Set-up of an Atomic Force Microscope.
(a) The basic principle of AFM contact mode. By maintaining a constant tip-sample separation and using Hooke's Law (*F = -kx* where *F* is force, *k* is the spring constant, and *x* is the cantilever deflection), the force between the tip and the sample is calculated. The distance the scanner moves in the *z* direction is stored relative to spatial variation in the *x-y* plane to generate the topographic image of the sample surface. (b) OTESPA tip/cantilever used in this study (Bruker AFM Probes). Imaged adapted from Sitterberg et al., (2010).

1.12.1 AFM modes

During this study the AFM instrumentation was upgraded to a newer MultiMode model (Bruker) as a result another AFM mode and probe was applied. The following is a brief description of the older mode, Intermittent mode (IC-AFM), and the new mode Peak Force tapping (Hodson et al., 2009, Alsteens et al., 2012).

1.12.1.1 Intermittent Contact AFM

Repetitive contact during surface probing can damage or deform soft surfaces such as biological material during contact mode. In order to overcome this problem the operation mode intermittent contact AFM (IC-AFM) or tapping mode is applied. The tip/cantilever is driven to oscillate up and down near at its resonance frequency (200-400 kHz) vertically over the surface reducing friction force (figure 1.13). As a result less lateral force is applied to the sample allowing softer material such as living cells to be imaged.

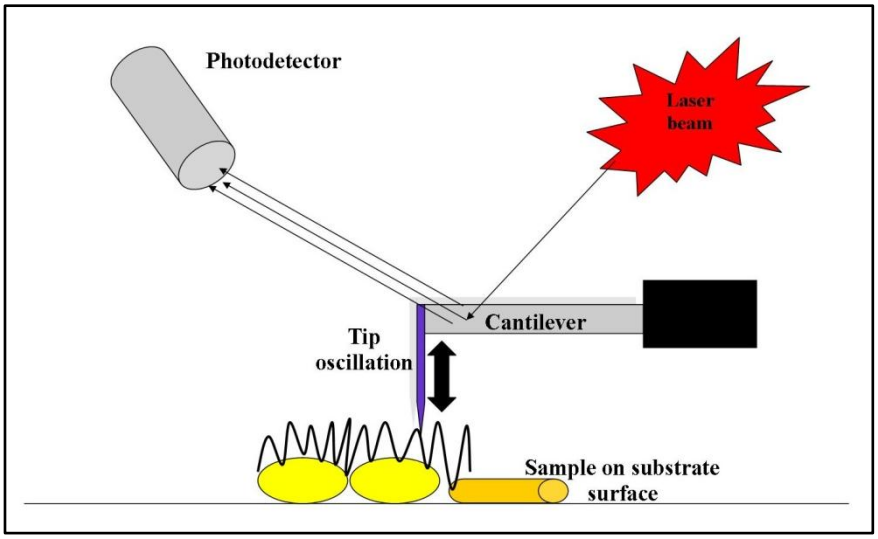

Figure 1.13. IC-AFM (Tapping Mode)

1.12.1.2 Peak Force Tapping Mode

Peak Force tapping mode (PFT) is controlled directly by using the peak force (maximum force exerted) as a feedback parameter. PFT operates similar to IC mode however it oscillates (taps) at a lower frequency (1-2 kHz) and captures a force curve each time the tip comes in contact to the surface. The process can be described in the form of one Peak Force curve cycle. This entails a sequence of events relating to the approach and withdrawal of the cantilever/tip illustrated in figure 1.14a. This starts at the approach of the cantilever/tip at a noncontact force from a discrete distance (A) followed by contact to the surface (B). The cantilever/tip gently continues to push until it reaches setpoint (Peak force) (C). Setpoint is defined as the measurement of the magnitude between the cantilever/tip and surface. At this point a topography image is produced. Point D represents cantilever/tip withdrawal which is the maximum adhesion point then returns to its original noncontact force (E). The process is repeated at every XY pixel in the image at a rate of 2000/sec (Foster, 2012). As a result a number of quantitative measurements are also calculated such as adhesion forces, Young's modulus (elasticity) (figure 1.14b).

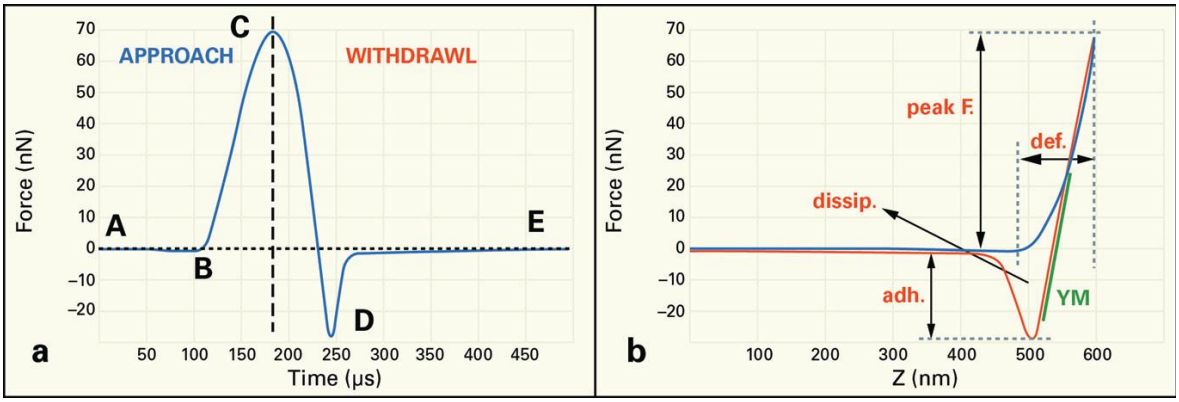

Figure 1.14 Peak Force Tapping Mode

(a) One single cycle of a Peak Force Tapping curve (b) Force vs. distance curve which quantifies a number of physical properties.[Graph copied from Foster, (2012)]

1.13 Studying Aggrecan Structure at the Nanoscale

The ability of AFM to probe the fundamental properties of sample surfaces and create three-dimensional micrographs and topographical imaging with nanometre resolution has made it an essential tool for exploring nanomechanical and structural properties in biomacromolecules and cells (Fotiadis et al., 2002, Engler et al., 2006, Stolz et al., 2009, Hodson et al., 2009).

Studying proteoglycan structure is not a new concept (figure 1.15). There have been extensive studies that have investigated proteoglycan aggregates (hylauronic acid, link protein, and aggrecan) structure from bovine AC using the same aggrecan separation and purification techniques to visualise proteoglycan by quantitative electron microscopy (EM) to measure and identify proteoglycan structure and their differences in composition and sedimentation behaviour among proteoglycan populations (Rosenberg et al., 1970, Buckwalter and Rosenberg, 1982, Buckwalter, 1983, Buckwalter et al., 1984, Buckwalter and Rosenberg, 1988, Buckwalter et al., 1994). To date, there are a number of recorded studies of electron microscopy work on IVD proteoglycans (Buckwalter et al., 1985, Buckwalter et al., 1989, Buckwalter et al., 1994). These past achievements with EM have given researchers a better understanding of the overall aggregate moiety at the microscale. However despite these achievements with EM, the graphical resolution of the aggrecan structure especially fine detail with GAG chain arrangement (number, spacing, dimensions, and conformation) was often found to appear as collapsed bundles, making determination difficult (Ng et al., 2003).

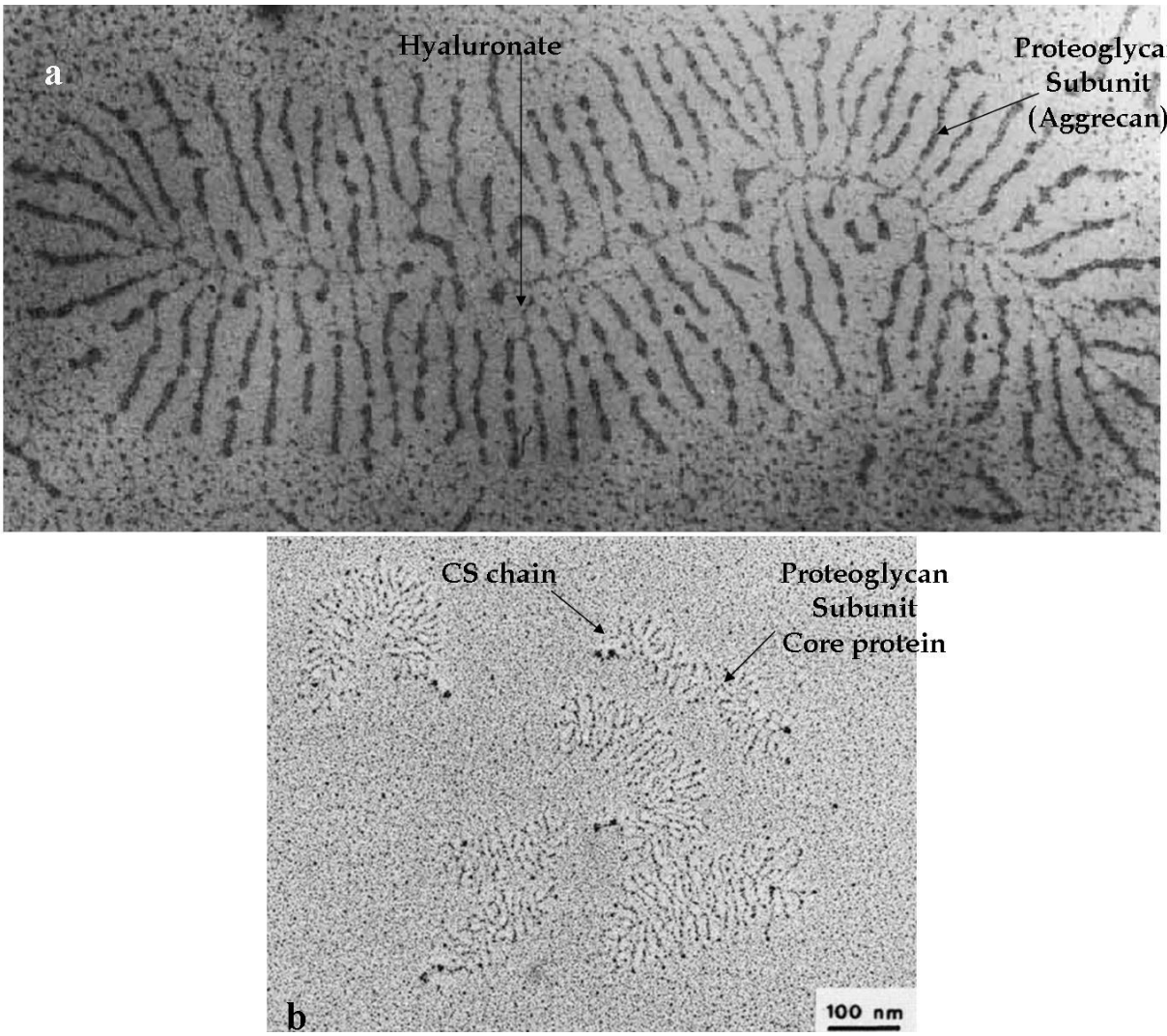

Figure 1.15. Electron Microscope Imaging of Proteoglycan Aggregates and Aggrecan Monomers

(a) Electron micrograph image of an aggregate from A1 fraction extracted from bovine foetal epiphysis cartilage (x 60,000). (b) Electron micrograph image of aggrecan monomers from bovine nasal cartilage with core protein and GAG chains after glycerol spraying/rotary shadowing. Images modified from Morgelin et al., (1989) and Buckwalter et al., (1994)

Atomic force microscopy (AFM) provides an alternative approach for visualisation of the aggrecan structure at the nanometre scale by offering high-resolution imaging. An attractive advantage of AFM over electron microscopy and other methods is the non-destruction of samples and surfaces, and yields a high signal-noise ratio for imaging. Sample preparation is simple and rapid requiring no extensive chemical fixation and staining which could produce potential image artefacts (Graham et al., 2010).

The use of AFM to investigate aggrecan's structure has been described by various research groups in the past (Ng et al., 2003, Yeh and Luo, 2004, Harder et al., 2010, Kopesky et al., 2010, Lee et al., 2010, Lee et al., 2013). One particular study by Ng et al. (2003) has extensively explored in detail this concept from bovine foetal and mature cartilage to

established aggrecan structure via AFM imaging. They reported distinct resolution of the N-terminal globular domains (G1) and visualisation of individual CS-GAG chains from bovine cartilage aggrecan. They introduced new quantitative data to measure aggrecan core protein contour length, end to end length, persistence length, CS-GAG chain length, and KS-GAG chain length. As a result they were able to quantify the comparison of immature and mature aggrecan in bovine cartilage. Figure 1.16 is a collection of AFM images from last ten years consisting of different size aggrecan monomers isolated from different sources.

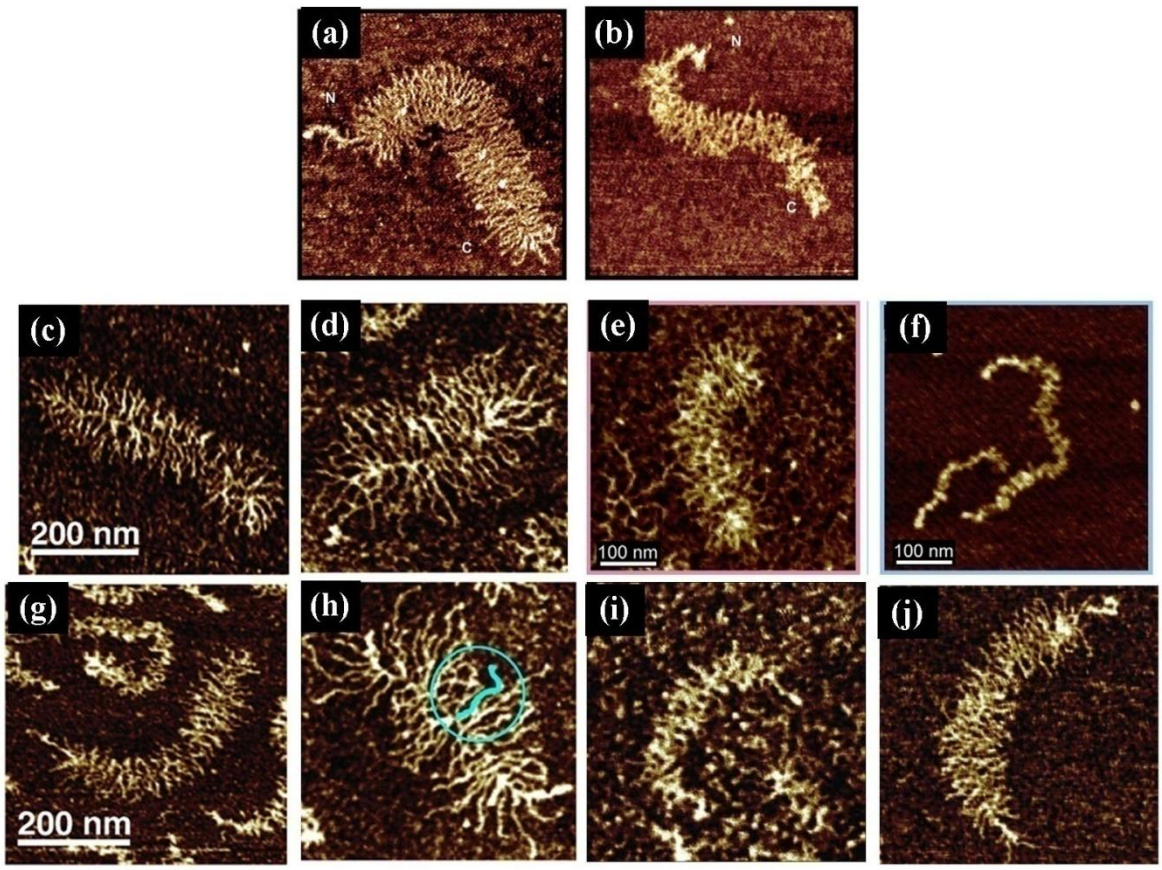

Figure 1.16. Montage of Aggrecan.

AFM height images of aggrecan monomers from the last ten years. All AFM imaging were performed in air. (a) Foetal bovine epiphyseal cartilage. (b) Mature bovine nasal cartilage. (c) Mature equine chondrocyte isolated from peptide hydrogel cultured with TGF-β1 (d) Mature equine BM MSCs isolated peptide hydrogel cultured with TGF-β1 (e) Mature equine BM MSCs isolated peptide hydrogel cultured with TGF-β1. (f) Mature equine AC. (g) Foetal equine chondrocyte isolated peptide hydrogel cultured with TGF-β1. (h) Foetal equine BM MSC isolated peptide hydrogel cultured with TGF-β1. (i) Mature human AC. (j) New born human AC. N= n-terminal and C= c-terminal of aggrecan. [Images a-b copied from Ng et al. (2003); Images c-d and g-h copied from Kopesky et al., (2010); Images e-f copied from Lee et al., (2010); Images i-j were copied from Lee et al., 2013.

Kopesky et al., (2010) utilise this methodology of measuring aggrecan dimensions and applied them to tissue engineering with the use of bone marrow stromal cells (BMSC) and 3D hydrogels. They reported the use of equine BMSC and chondrocytes (foetal and adult) isolated from animal-matched bone marrow and cartilage, and encapsulated them in a KLD12 self-assembling peptide hydrogel under chondrogenic media conditions with TGF-

β1. After 21 days of culturing, both foetal and adult BMSC and chondrocytes survived and proliferated on the hydrogel with high viability. Chondrogenesis depended on age and both foetal and adult BMSC produced more sGAG and collagen forming a mechanically functional ECM (neo-tissue) with higher mechanical stiffness compared to foetal and adult chondrocytes. Size exclusion chromatography results revealed the proteoglycan extracted from both BMSC and chondrocytes was predominantly aggrecan. AFM analysis showed CS-GAGs chain length on aggrecan was significantly longer than chondrocytes independent of age. They suggested BMSC-produced aggrecan had a phenotype of young tissue and produced a superior cartilage-like neo-tissue compared to foetal and adult chondrocytes with self-assembling peptide hydrogels. This study was followed up by Lee et al., (2010) where adult equine BMSC were seeded onto a peptide hydrogel to induce chondrogenic differentiation and aggrecan produced was extracted for AFM analysis to measure their core protein contour length and GAG chain length. Their nanomechanics as described by Dean et al.,(2005) and Dean et al.,(2006) were measured by high resolution force microscopy using microcontact printing (Wilbur JL, 1996). Results revealed adult equine BMSC derived aggrecan was longer in both core protein and GAG chain length compared to adult equine cartilage making them biomechanically superior.

A more recent publication from the same group have reported their findings of human aggrecan structure from one new born and two adults isolated from AC (Lee et al., 2013). They reported the age-related nanostructure (CP length and GAG chain length) of aggrecan were significantly different between 38 year old adult to a newborn. They also investigated the nanomechanics as previously described (Dean et al., 2005) and found that adult aggrecan was weaker in compression than to new born aggrecan. The study had the opportunity to investigate the effects of GAG chain length has on aggrecan nanostructure (29 year old) based on a previous EM study by Morgelin et al.,(1989) which found that aggrecan with longer extended GAG chain length influence CP length. The current study showed that CP length (decreased) was significantly different in deglycosylated aggrecan compared to glycosylated aggrecan which showed the effects on GAG biosynthesis with age.

1.14 Hypothesis

Proteoglycan separation protocols for aggrecan have allowed early electron microscope studies to visualise and quantify proteoglycans aggregates and proteoglycan subunits (aggrecan) from animal and human tissue. AFM analysis has allowed a more in-depth

detail of ultrastructure of aggrecan revealing that CS-GAG chains influence aggrecan mechanical and compressive properties. Current knowledge of directing MSC differentiation to chondrocyte-like cells similar to NP phenotype together with the combination of 3D scaffold such as hydrogels create an opportunity to tissue engineer an appropriate IVD tissue. However, before NP tissue engineering can be fully realised the quality of aggrecan from engineered IVD needs to be studied. To date there have been no reports detailing the ultrastructure of human IVD aggrecan from nucleus pulposus tissue and how its ultrastructure and nanomechanical properties may alter with degeneration or the ultrastructure of aggrecan within "engineered" IVD tissues and whether the aggrecan produced is the most appropriate to form a functional IVD tissue.

Studies have shown aggrecan synthesised from seeded hydrogel scaffolds form foetal like ultrastructure making them biomechanically superior. Therefore in this study it was hypothesised that IVD disc cells (adult mature human NP cells in particular) seeded into a hydrogel would synthesise aggrecan with a ultrastructure similar or enhanced to that found in NP tissue and that media conditions would influence structure.

1.15 Aims

In order to test this hypothesis this project had the following aims, to;

- Establishing a working protocol to extract and purify aggrecan molecules from IVD tissue and cell seeded constructs for subsequent AFM imaging.
- Quantify the morphology of aggrecan derived from bovine NP tissue, and NP cells cultured in standard and chondrogenic media.

Chapter 2

General Methods

2.0 General Methods

The following methods were routinely performed throughout the study for aggrecan extraction/isolation, aggrecan detection, AFM imaging, and data analysis of aggrecan ultrastructure. Materials and reagents were obtained from Sigma Aldrich, Dorest, UK unless otherwise stated. All AFM equipment and materials were obtained from Bruker unless otherwise stated.

2.1 Isolation of Aggrecan from Bovine NP tissue (D1 and D1D1 Fractions) and Aggrecan Detection.

Figure 2.17 is an overview of the experimental design to obtain a D1 or D1D1 fraction to isolate aggrecan molecules. In some experiments extraction was followed by a single purification step by centrifugation (D1) whereas in other experiments this D1 fraction was further purified with a second centrifugation step (D1D1).

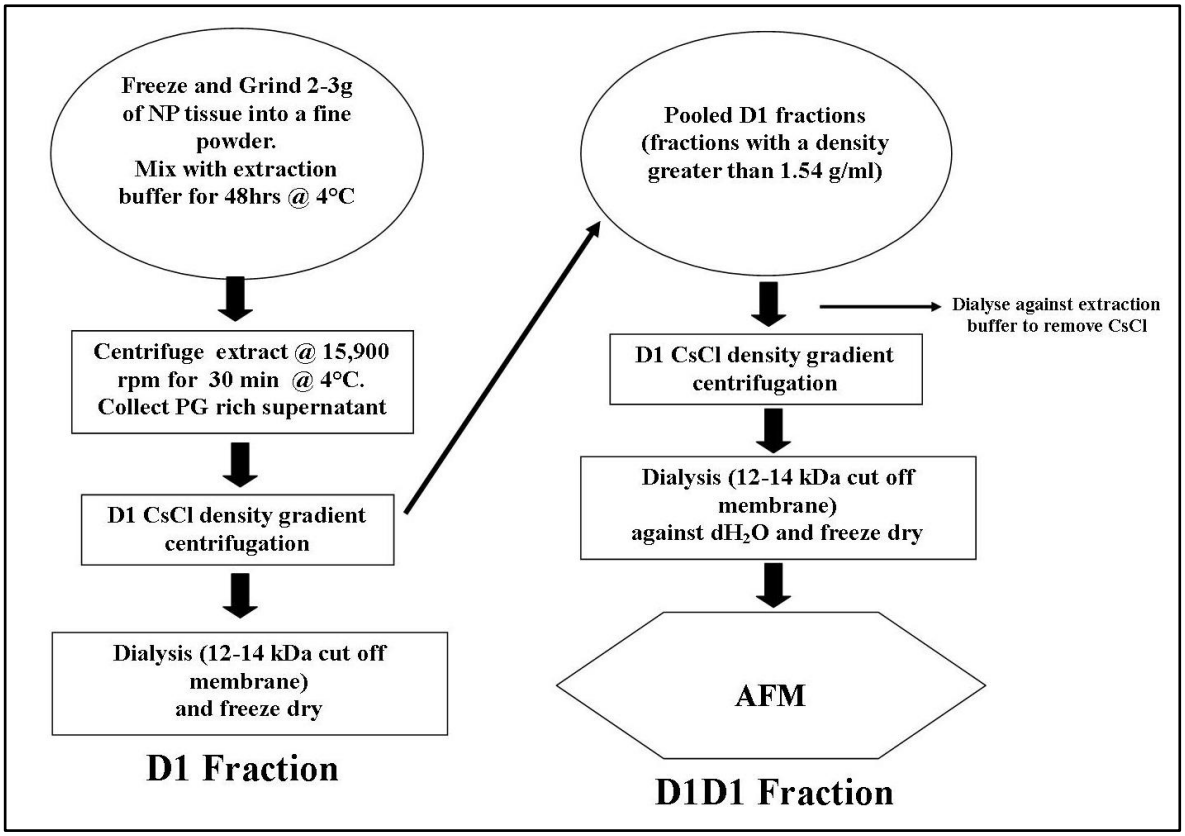

Figure 2.17 Experimental design for aggrecan isolation from bovine NP tissue

2.1.1 Aggrecan Extraction from Bovine NP Tissue

Two grams of nucleus pulposus tissue from bovine (age range 18-36 months caudal (tail) discs) (Staffordshire Meat Packers LTD, Stoke-on-Trent) were dissected into 2 mm cubes and stored at -80°C. Subsequently the tissue was thawed and then pulverised into a fine powder with a Retsch MM301 Ball Mill with the cup and ball cooled to -20°C for one hour prior to use. The cup and ball was then placed in liquid nitrogen (LN_2) with the tissue for

15 minutes. The LN_2 was carefully drained off and the cup and ball with the tissue were closed and secured for milling for 3 minutes. The resultant powdered tissue was then placed into a 50 ml falcon tube and the wet powdered tissue weighed. Twelve millilitres of extraction buffer (4M guanidine-HCl plus Protease Complete Tablets, pH 7.2 (Roche)) was added to every 1 gram of wet powdered tissue, then mixed for 48h on a tube roller at 4°C (Struglics and Larsson, 2010). The tissue-guanidine-HCl mixture was centrifuged (Sovall RC-5B centrifuge with a fixed angle SS34 rotor) in a 50 ml Oakridge tube (Nalgene) at 15,900 rpm for 30min at 4 °C collecting the supernatant (Struglics and Larsson, 2010).

2.1.2 Dissociative CsCl Density Gradient Centrifugation

The protocol below is a detailed account on the amount of CsCl (Melford, UK) required for a 13.5 ml Quick Seal centrifugation tube (Beckman Coulter) under dissociative conditions (4M GuHCl) at a starting density of 1.58 g/ml to isolate aggrecan enriched D1 fractions (Roughley and White, 1980, Lee et al., 2010). It should be noted that two centrifuge tubes are required for balancing purposes during centrifugation.

2.1.2.1 CsCl Preparation and D1 Fraction Isolation

A 50 ml falcon tube was placed on a balance and tared. The following is the amount (g) of CsCl which was required to give a starting density of 1.58 g/ml. The equation below was used to calculate the precise amount of CsCl required in each centrifugation tube:

$$\chi = \alpha[\{1.347\rho\} - \{0.0318M\} - 1.347] \text{(Equation 1)}$$

Where:

- Þ= final density of solution to be centrifuged in g/ml: **1.58 g/ml**
- α = final volume of solution to be centrifuged in ml: **13.5 ml**
- M= molarity of GuHCl of sample: **4M**
- X= the amount (g) of CsCl to be added: **8.83g**

Once calculated the amount of CsCl (8.83g) was placed in the 50 ml falcon tube. The PG supernatant was added up to the final weight (e.g. 1.58 g/ml x 13.5 ml = **21.33 g**) drop by drop with Pasteur pipette. It should be noted that if the final weight is not reached by the PG supernatant then additional extraction buffer was used:

$$\text{Final weight (g)} = Þ \times \alpha \qquad \text{(equation 2)}$$

The PG supernatant with CsCl was sealed with parafilm and mixed for one hour at 4°C. The PG supernatant with CsCl was transferred into a 13.5 ml Quick Seal centrifugation tubes via a 10 ml syringe and 19G needle, and heat sealed followed by ultracentrifugation (L-90K ultracentrifuge with a fixed angled Ti 70.1 rotor(Beckman Coulter)) at 56,000 rpm

for 72 h at 4°C. Eleven fractions were carefully collected as 1 ml fractions using a 1 ml syringe and transferred into 2ml tubes. Each fraction was weighed to measure its density (g/ml). Fractions greater than 1.54 g/ml were selected as D1 fractions and pooled together for dialysis overnight against 1M NaCl and then with water for 48 hrs followed by freeze drying (Roughley and White, 1980, Lee et al., 2010).

2.1.2.2 D1D1 Fraction Isolation

Bovine NP tissue was subjected to two dissociative CsCl gradient density centrifugations to give a D1D1 fraction for Chapter 3 experiment. After the first centrifugation (D1 fraction as described above), fractions greater than 1.54 g/ml were selected as D1 fractions and pooled together for dialysis against extraction buffer overnight to remove CsCl (section 2.1.3 for more details). Fresh CsCl was added and the sample subjected to a second dissociative CsCl gradient density centrifugation as previously described. Fractions greater than 1.54 g/ml were selected as D1D1 fractions and pooled together for dialysis overnight against 1M NaCl (Fisher Scientific) and then with water for 48 hrs followed by freeze drying.

2.1.3 Membrane and Sample Preparation for Dialysis and Freeze Drying

The following protocol is a standard dialysis protocol. Dialysis membrane (12-14 kDa MW cut off; Medicell International LTD) was boiled in deionised water for 2 minutes and 5-20 ml of sample was placed into the membrane and dialysed against high grade pure water for 48 hours. A sample (310 µl) was taken to assess protein content (BCA assay), GAG content (DMMB assay), and for dot blotting for aggrecan detection. Samples were snap frozen in LN_2 for 15 minutes and placed in a freeze dryer for 48-72 hrs. Freeze dried pellets were weighed and resuspended in high grade pure water according to their protein content, aliquoted to a concentration of 50 µg/ml and stored at -20°C for AFM analysis. In the case for alginate constructs, after freeze drying, the pellet was only stored at -20°C.

In the case of D1D1 isolation this procedure was performed. There was an additional dialysis step when preparing a second D1 centrifugation run (figure 2.17) where the dialysis membrane was prepared in the same manner and no freeze drying was involved instead sample was dialysed against extraction buffer instead of water overnight to remove CsCl and fresh CsCl added for a second D1 CsCl centrifugation run.

2.1.4 Protein and Sulphated Glycosaminoglycan Quantification

Protein content was assayed using a bicinchoninic acid (BCA) protein assay kit (Thermo Scientific) using 25 µl of BSA as a standard (0-2000µg/ml range) in triplicate. Twenty-five microlitres of sample (performed in triplicate) were loaded onto a 96 well plate and 200 µl of BCA reagent was added and incubated for 30 minutes at 37°C then read at an absorbance of 540 nm.GAG content was assayed by dimethylmethylene blue (DMMB) assay(see appendix for preparation) using 40 µl of chondroitin sulphate C sodium salt as a standard (7-500 µg/ml range). Forty microlitres of sample (performed in quadruplicate) were loaded onto a 96 well plate and 200 µl of DMMB solution was added to each well and mixed for 30 seconds and read at an absorbance of 540 nm with MultiSkan plate reader (Thermo Scientific). For lower volumes of sample, 5µl of standard and sample were used.

2.1.5 Aggrecan Dot Blot

A polyvinylidene fluoride (PVDF) transfer membrane (Perkin-Elmer) was cut into a 6cm x 8cm square and pre-treated with a 100 % methanol (10 sec), deionised water (5 min), and Tris buffer saline (50 mM Tris and 150 mM NaCl, pH 7.6) plus 0.1% vol/vol Tween 20 (TBS-T). In a 0.5 ml Eppendorff tubes, 5 µl of poly-l-lysine (0.01% solution) plus 10 µl of sample was mixed and 5 µl of the mixture was dotted onto the membrane surface to allow the fully glycosylated proteoglycans to bind onto the PVDF membrane. For aggrecan detection, 5µl of 10 µg BSA negative control, 5 µl of poly-L-lysine (PLL) as a blank and 2 µl of bovine aggrecan (AC) as a positive control (2 µl plus 10 µl of PLL) were included. The membrane was allowed to fully dry at 37°C for 30-45 minutes. The membrane was again rehydrated with methanol (10 sec), deionised water (5 min), and TBS-T. The membrane was washed and mixed with 20 ml of blocking buffer (5% non-fat milk powder + TBS-T) overnight at 4°C.

The membrane blot was briefly washed with TBS-T then transferred to 20 ml of blocking buffer (2% non-fat milk powder + TBS-T) containing aggrecan antibody (MCA1454G mouse anti-human aggrecan at 1/2000 dilution (AbDSerotec)) for two hours at room temperature. The membrane was washed with TBS-T for 10 minutes followed by 2 x five minute washes with the same buffer followed by 20 ml of blocking buffer (2% non-fat milk powder + TBS-T) containing the secondary antibody (anti-mouse IgG (goat) HRP-labelled 1/10,000 dilution (Perkin-Elmer)) for one hour at room temperature. Again the membrane was washed with TBS-T as mentioned before. The solution was quickly drained and 2 ml of enhanced chemiluminescence (ECL-Plus) substrate (Perkin Elmer) was

pipetted onto the membrane surface evenly and left for one minute. The membrane was transferred to a sealing film and heat sealed. The membrane blot was transferred in a cassette with film (Hyperfilm blue (5x7 inch); GE Healthcare) for an exposure time of 15-25 seconds or 1-3 minutes. The film was placed in 100 ml of developer (1/10 dilution; Kodak) for 3 minutes then washed in water then placed in 100 ml of fixer (1/5 dilution: Agar Scientific) followed by a second wash of water. The film was then left to air dry for one hour and digitally scanned by an Epson flatbed scanner.

2.2 Surface Characterisation of APTES-mica

After having extracted and isolated aggrecan and demonstrated its presence by blotting, the next step was to image the aggrecan ultrastructure. Before doing so it was necessary to characterise the AFM substrate to support aggrecan absorption and sufficiently flatten onto the surface to enable imaging by surface topography mapping.

2.2.1 Mica Preparation for Surface Roughness Analysis

Mica sheets (Agar Scientific) were cut to size and adhered with nail varnish onto a 15 mm diameter specimen discs (Agar Scientific) to dry overnight. The mica surface was cleaved by peeling off the top layer of mica with adhesive tape. Sixty microlitres of APTES (0.01% v/v) (Acros Organics) were deposited at different time points (1, 5, 15, 20, 30, and 60 min) onto freshly cleaved mica followed by three gentle washes of 400 µl distilled H_2O. The sample was allowed to air dry in a dust-free environment for 1.5-2 hrs.

2.2.2 AFM Imaging (Intermittent Contact Mode)

Each surface was scanned by tapping mode in air using a Bruker Multimode AFM instrument with a Nanoscope IIIa controller, an E scanner, and an OTESPA probe with a spring constant of 42 N/m and a radius of curvature of 7 nm. AFM height images were captured at a scan rate of 1.49 Hz and a scan size of 1µm x 1µm (512 x 512 pixels). All images were taken in triplicate at three different positions on the surface for each time point including freshly cleaved blank mica. AFM height Images were first order flattened by Nanoscope software and exported as ASCII files. RMS roughness analysis (set parameters: box size dimensions start at 5 and end at 105 box size dimensions, 5 step size in pixel, and iteration at 19) of APTES was carried out with Microsoft Visual Basic 6.0 routines that incorporated the following equation as detailed previously (Sherratt et al., 2004):

$$\mathrm{RMS} = (\sum (\mathrm{Z_i} - \mathrm{Z_{ave}})^2 / N)^{0.5} \qquad (Equation\ 3)$$

Where:

- Z_{ave} = the average Z-value (height value in nm) within a given area
- Z_i = the current Z-value
- *N*= the number of points within the given area

The box size was converted to box dimensions (nm) by multiplying by the value calculated which is nanometre per pixel (1.95312 nm per pixel= (1µm scan size/512 pixels) x 1000). The box dimension values were plotted against mean RMS value for each APTES incubation time point.

2.2.3 Contact Angle Assessment for APTES-mica Surface

The purpose was to measure the contact angle (θ) which is defined as the angle formed between the liquid-solid and liquid-vapour interface. A surface is defined as hydrophilic (i.e. wettable) when the angle of the droplet is less than 90° whereas a droplet greater than 90° is hydrophobic or nonwettable (Sherratt et al., 2004).

APTES surface preparation for substrate hydrophilicity assessment was similar to that previously described with the exception that 120µl of APTES (0.01% v/v) was applied onto freshly cleaved mica sheets that were cut into a square instead of a circular shape to ensure all edges were straight for photographic purposes. The time point with the lowest surface roughness (30 minutes) was employed with three gentle washes of 400 µl distilled H_2O. Excess liquid was removed from the surface by capillary action at the edge with filter paper, and the sample was allowed to air dry in a dust-free environment for 1.5-2 hrs. Ten microlitres of deionised water or column buffer (0.2 M Na acetate, pH 5.5) were carefully place on the edge of the mica sheet and a side view of each drop was photographed within one minute in triplicate. The hydrophobicity / hydrophilicity of APTES-mica was quantified by measuring the drop contact angle (θ) with aid of ImageJ (Schneider et al., 2012) rectangular tool to determine the height (*H*) and width (*W*) of the drop (Sherratt et al., 2005, Kielty et al., 2007):

$$\theta = (\tan^{-1}\left[\frac{2H}{W}\right]) \times 2 \qquad (Equation\ 4)$$

2.3 Imaging the Ultrastructure of Aggrecan

2.3.1 AFM Sample Preparation for Tissue Extracted Aggrecan

Mica sheets were cut and adhered to SPM specimen discs. The mica surface was cleaved by peeling off the top layer of mica with adhesive tape. Sixty microlitres of APTES (0.01% v/v) were added on the freshly cleaved mica surface for 30 minutes then followed by three gentle washes of 400 µl distilled H_2O. Excess liquid was removed from the surface by capillary action at the edge with filter paper, and the sample was allowed to air dry in a dust-free environment for 1.5-2 hours before aggrecan deposition. Dilutions of aggrecan were prepared from the stock solution (50ug/ml) to give concentrations of 1.25, 0.625, 0.3125, and 0.1562 µg/ml (protein content). Fifty microlitres of the appropriate dilution was placed on the APTES-mica surface and left for 15 minutes prior to being washed gently with four washes of 400 µl distilled H_2O. Excess liquid was removed from the surface by capillary action at the edge with filter paper, and the sample was allowed to air dry for 1.5-2 hours.

2.3.2 AFM Imaging of Aggrecan Ultrastructure

2.3.2.1 Intermittent Contact Mode

AFM imaging was performed as previously described with the same instrument and probe tip. The same imaging software WSxM (version 5.0) was also used for illustration purposes. However, height images of aggrecan were captured at a scan rate of 1.0Hz at a 2 µm x 2 µm scan size (512 x 512 pixels).

2.3.2.2 Peak Force Tapping Mode

A new AFM instrument was utilised later in the study where immobilised aggrecan was scanned by Peak Force tapping mode in air using a MultiMode 8 AFM instrument (ScanAsyst) with a Nanoscope V controller, an E scanner, and ScanAsyst Air probe (spring constant=0.4 N/m; radius of curvature= 2 nm). Height images of aggrecan were captured overnight at a scan rate of 0.488 Hz at a 8 µm x 8 µm scan size (2048 x 2048 pixels). Further details of AFM imaging settings (table 7.5) are listed in the appendix.

2.4 Measuring Aggrecan Ultrastructure

Past studies have quantified aggrecan core protein contour length of aggrecan molecules isolated from bovine and human tissue as well as hydrogel constructs (Ng et al., 2003, Kopesky et al., 2010, Lee et al., 2010, Lee et al., 2013). Although imaging software differed from the current study, the same morphological characteristics were the same. In terms of GAG brush length, previous analysis has been limited to one study by Ng et al.,

(2003) where aggrecan was obtained from bovine AC. Aggrecan GAG chain length has been another parameter that has been measured in previous studies (Ng et al., 2003, Kopesky et al., 2010, Lee et al., 2013). However, this approach has its limitation as the GAG chains can overlap and shorter chains can be difficult to distinguish. Therefore measurements of selected GAG chain could overestimate chain length on a single aggrecan molecule (Ng et al., 2003, Kopesky et al., 2010, Lee et al., 2010, Lee et al., 2013). Here, a novel approach, adopted from previous studies of fibrillin and microfibril ultrastructure (Sherratt et al., 2007, Sherratt et al., 2005) was utilised where the mean GAG brush width was determined on a single aggrecan molecule based on AFM height imaging.

Figure 2.18 is a detailed account of the image processing undertaken for one single AFM height image and the inlay at the bottom is general schematic representation of full-length aggrecan structure found in bovine and humans tissue showing which morphological parameters were measured in this study; aggrecan core protein contour length, GAG brush width, and GAG brush length.

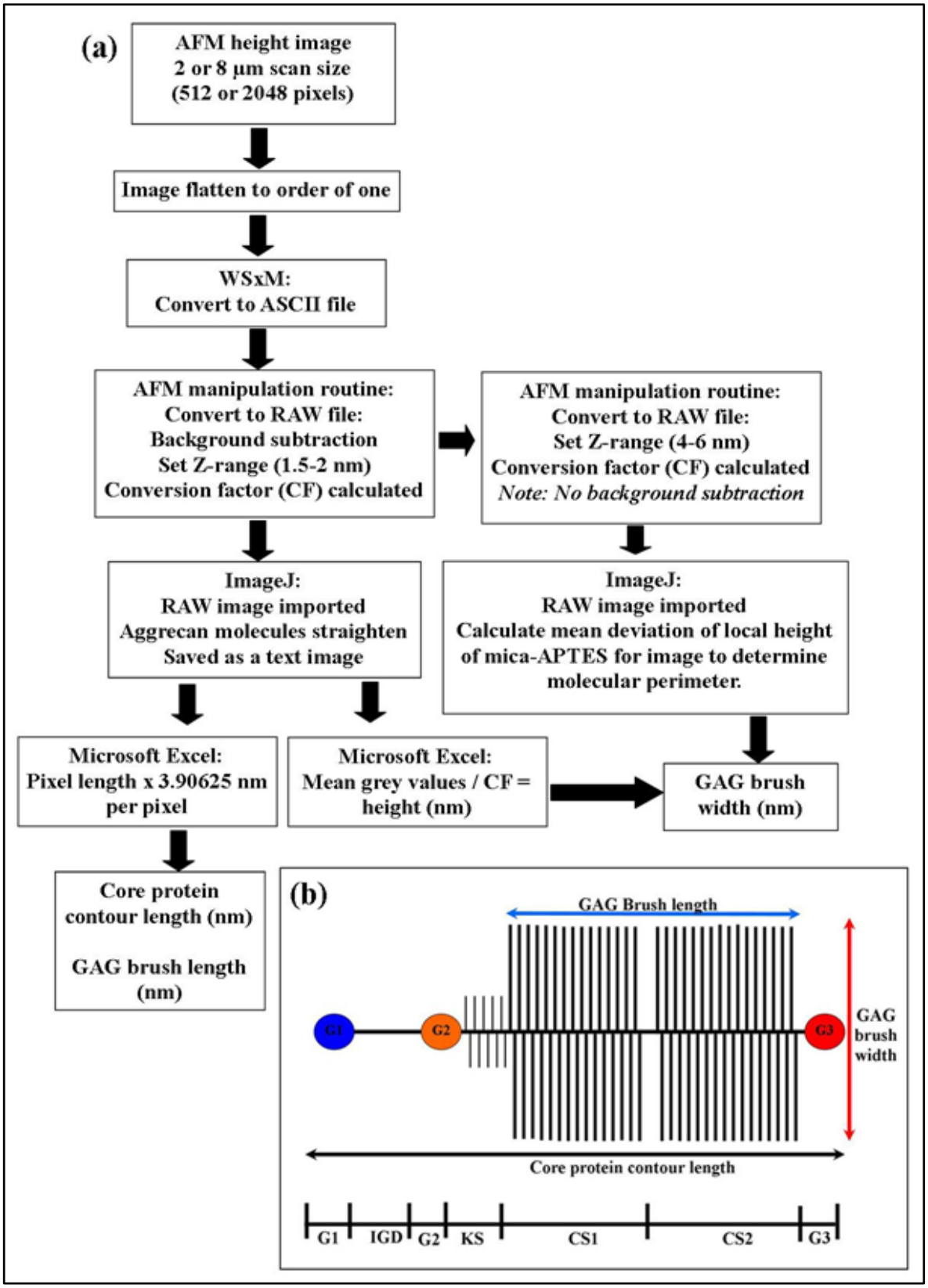

Figure 2.18 AFM Image Processing for Quantification of Aggrecan Morphological Parameters.

(a) An overview of AFM imaging processing from AFM height images to RAW files to quantifying aggrecan morphological parameters. (b) The bottom inlay illustrates the selected aggrecan morphological parameters for quantitative analysis: core protein contour length, GAG brush length, and GAG brush width. G1= globular domain 1, IGD= interglobular domain, G2= globular domain 2, KS= keratan sulphate II, CS1= chondroitin sulphate domain 1, CS2= chondroitin sulphate domain 2, and G3= globular domain 3.

2.4.1 Imaging Processing from AFM Height Images to RAW Files

Selected images were first order flattened by Nanoscope software (version 8.0) and saved as an ASCII file with WSxM (version 5.0). The ASCII file was then converted to a RAW image file as previously described by Sherratt et al., (2005).

2.4.2 Measurement of Aggrecan Core Protein Contour Length and GAG Brush Length

JPEG images of their RAW file counterpart were used to allocate each individual aggrecan molecule a unique aggrecan number for every AFM height image on PowerPoint slides. Converted RAW files were imported onto ImageJ where the CP length and GAG brush length were measured by using the Straighten plug-in function (Kocsis et al., 1991, Sherratt et al., 2005). Aggrecan molecules were selected by tracing a line and points along the core protein length from end to end (figure 2.19a). The resulting straightened image was saved as a text image file. During straightening ImageJ displays the pixel length value for CP length and GAG brush length in the text image file which in turn was converted to nanometres by multiplying pixel length value by 3.90625 nanometres per pixel. Nanometres per pixel was calculated below:

Each height image was scanned at 2 µm (2000 nm) at 512 pixels therefore to calculate nanometres per pixel:

Nanometres per pixel = scan size (nm) / 512 pixels. *(Equation 5)*

It should be noted that later in the study AFM images were scanned at 8 µm x 8 µm (2048 x 2048 pixels) where the nanometres per pixel still equated to 3.90625 unless otherwise stated.

2.4.3 Measuring GAG Brush Width

As previously mentioned straightened aggrecan molecules were saved as a text image and copied onto a Microsoft Excel spreadsheet and the mean gray values were converted to height in nanometres (figure 2.19):

Height in nanometres = mean gray value / conversion factor (CF). *(Equation 6)*

The converted data was plotted as a surface contour map (figure 2.19b and c) which allowed visual selection of the GAG brush domain to measure GAG brush length (pixel length x 3.90625 nanometres per pixel) and the GAG brush width (figure 2.19c and d).The mean height (nm) was plotted against the transverse distance (nm) as depicted in figure

2.19d. In order to distinguish between the substrate surface and the aggrecan molecule, the mean deviation of local substrate surface height (nm) was determined; this was used as a cut off point to define the molecular perimeter (figure 2.19d) in order to calculate GAG brush width (see figure 7.48 in appendix for further details).

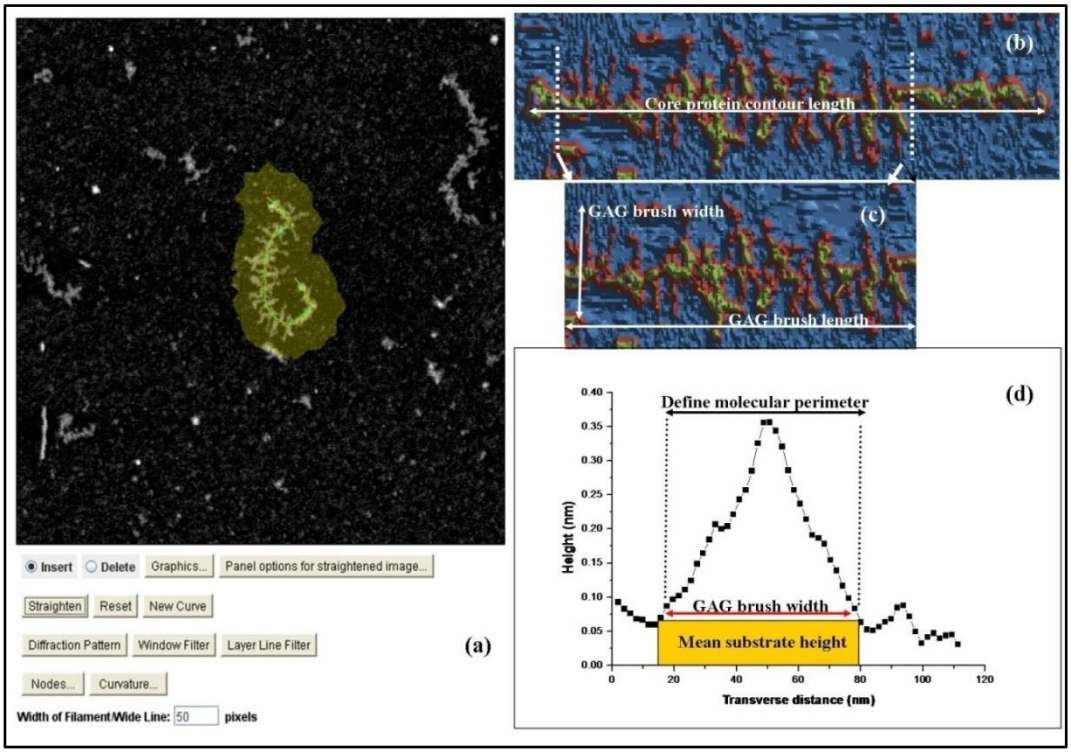

Figure 2.19. Calculating Aggrecan Morphological Parameters.

(a) ImageJ Straighten Plug-in function allowed the selection of individual aggrecan monomers for straightening. (b) Selected aggrecan molecule image was straightened, rotated 90° to the right (not shown), and saved as a text image. (c) The text image was copied to Microsoft Excel and plotted as a surface area graph where the GAG brush region is selected. GAG brush length was measured in the same manner as core protein contour length. (d) The mean height (nm) is plotted against the transverse distance (nm) with the molecule perimeter defined (indicated in yellow) to calculate the GAG brush width.

2.5 Statistical Analysis

All data was managed by Microsoft Excel and statistical data for aggrecan dimensions (Chapter 3 and 5) and alginate beads area (mm^2) (Chapter 4) were expressed as relative frequency distribution which was generated by OriginPro 8.5. Aggrecan dimensions were reported as mean ± SEM in text and figures generated by OriginPro8.5 Peak Analyser (Fit peaks (pro) function) to indentify aggrecan subpopulations (peaks) and to calculate the mean value and SEM with a built-in Gaussian goodness of fit function for each subpopulation identified. All graphs and histograms were generated by GraphPad Prism (version 6.02). Non-parametric data was determined by Sharpio-Wilk test and statistical testing for aggrecan dimensions and alginate bead size was performed either with an unpaired t-test (parametric) or Mann-Whitney test (nonparametric) by GraphPad Prism.

The correlation of coefficient was calculated by linear regression (R^2) or by Spearman's ranking correlation (r) with nonparametric data.

2.6 Gene expression

Quantitative real-time polymerase chain reaction (q-RT-PCR) was used as an additional method to confirm if aggrecan gene expression was evident during cell culturing in alginate in both standard and chondrogenic media. NP cells have been described as chondrocyte-like cells (Trout et al., 1982), but differ to articular chondrocytes (Mwale et al., 2004). However NP cells do express the chondrocyte ECM genes (aggrecan (ACN), type II collagen (COL2), type I collagen (COL1), and versican (VCN)) (Sive et al., 2002, Minogue et al., 2010).

2.6.1 Gene Expression Analysis

2.6.1.1 RNA Extraction

Alginate beads that were broken down and stored at -80°C were thawed and centrifuged at 12,000g for 15 minutes at 4 °C to remove debris. The supernatants were transferred to a clean 1.5 ml tubes where 100 µl of bromochloropropane (BCP) was added, vortexed for 20 seconds, and incubated at RT for 3 minutes. This was followed by another centrifugation at 12,000g for 15 minutes at 4 °C. The top aqueous phase was transferred to a clean tube where GlycoBlue (2 µl), isopropanol (250 µl), and high salt precipitation solution (HSPS; 0.8M sodium citrate and 1.2M NaCl) (250 µl) were added. Samples were inverted 10 times to mix followed by a 10 minute incubation at RT. The resulting mixture was centrifuged at 12,000g for 20 minutes at 4 °C. After centrifugation a small blue pellet was seen at the bottom of the tube. Without disturbing the pellet the supernatant was carefully removed and 1 ml of ice cold 75% ethanol was added. The solution was gently pipetted up and down and centrifuged at 12,000g for 5 minutes at 4 °C. The ethanol was carefully removed without disturbing the pellet and the pellet left to air dry. The pellet was then resuspended in 21.2 µl of TE (10mM Tris and 1mM EDTA, pH 8.0) buffer.

A further purification step was employed to remove alginate contaminants from the RNA samples. Saturated butanol was added (500 µl) to the RNA samples and mixed then centrifuged at 12,000g for 1 minute. The upper organic layer was removed leaving a thin layer on the top of the aqueous phase. The same procedure was repeated with 500 µl of diethyl ether. The diethyl ether was carefully removed by leaving the sample open under a

fume hood for 10 minutes at 37^{o}C. The RNA sample was quantified using a Nanodrop (Thermo Scientific).

2.6.1.2 Reverse Transcription of RNA

A High Capacity cDNA Reverse Transcription Kit was used according to manufacturer's instructions (see appendix for further details) to transcribe RNA to cDNA. A 20 µl reaction contained 10 µl of reaction mixture and 10 µl of RNA sample (200 ng/ µl) in each tube. Samples were subjected to a four step incubation using a thermal cycler. The concentration of the end product was approximately 100ng/µl in 20µl of cDNA.

2.6.1.3 Quantitative Real Time Polymerase Chain Reaction

Gene expression was analysed utilising q-RT-PCR. The list of genes and primer sequences along with their individual probes are listed in table 5.2. A 10 µl reaction mixture was required that contained a PCR universal master mix and predesigned primer/probe sets for each target gene. All PCR reactions were performed on an ABI StepOnePlus real-time PCR machine. Levels of gene expression were quantified by the 2-$\Delta\Delta^{CT}$ method (Livak and Schmittgen, 2001) and were normalised to the average of two housekeeping genes (GAPDH and MRPL19) for each target gene.

Table 2.1 Primer and Probe Sequences used in the RT-PCR Analysis

Target gene	**Forward primer**	**Reverse primer**	**Probe**	**Gen Bank accession no.**
GAPDH	CTCCTCTGACTTCAACAG	CGTTGTCATACCAGGAAA	CACCCACTCCTCCACCTTTGA	NM_001256799
MRPL19	CCACATTCCAGAGTTCTA	CCGAGGATTATAAAGTTCAAA	CAAATCTCGACACCTTGTCCTTCG	NM_014763
Aggrecan	GGCTTCCACCAGTGTGAC	GTGTCTCGGATGCCATACG	TGACCAGACTGTCAGATACCCCATCCA	NM_001135
Type I α collagen	TCAGCTTTGTGGATACGC	CTGGGCCTTTCTTACAG	CAGTAACCTTATGCCTAGCAACATGC	NM_000089
Type II collagen	CAGTGGTAGGTGATGTTC	GGCTTCCATTTCAGCTATG	CCAACACTGCCAACGTCCAG	NM_033150
Versican	TCCCTCACTGTGGTCAAG	GTGTGTACCTGCTGGTTG	AAACACAACCCCATCCACAGTCAGT	NM_004385

Chapter 3

Optimisation of Methodology to Image and Analyse Aggrecan Ultrastructure by Atomic Force Microscopy.

3.1 Introduction

The extraction and purification of aggrecan was required in order to study its ultrastructure with AFM. The following techniques used in this investigation are routinely applied in aggrecan isolation and are adapted for this study. Bovine caudal (tail) discs, are considered to be a useful model of normal human IVDs (Demers et al., 2004), were employed due to the scarcity of healthy human mature NP tissue.

3.2 Aims

- To optimise an extraction and purification protocol for the isolation of aggrecan from bovine IVD.
- To determine the optimum surface conditions for aggrecan immobilisation for AFM imaging
- To develop image analysis protocols to quantify aggrecan ultrastructure.

3.3 Experimental design

3.3.1 Aggrecan isolation

Aggrecan from bovine caudal disc (NP tissue) was extracted by 4M GuHCl and mixed for 48 hrs followed a D1D1 CsCl density gradient centrifugation for purification. Aggrecan was confirmed by immunoblotting (dot blotting), DMMB, and BCA assays.

3.3.2 AFM imaging

APTES-mica surface were characterised by RMS surface roughness analysis and contact angle for hydrophilicity to ensure the immobilisation of aggrecan for AFM imaging. AFM imaging was conducted in air and by Intermittent mode (IC-AFM) or also known as Tapping mode with an OTESPA probe (radius of curvature = 7nm; spring constant= 42 N/m). AFM images were scanned as 2 µm x 2 µm (1 µm x 1 µm scan size for RMS roughness analysis) (512 x 512 pixels) size images and processed into RAW files.

3.3.3 Quantification of aggrecan dimensions

RAW files were open in ImageJ and the molecules straightened then saved as a text image file. The text image file was pasted onto an Excel spreadsheet where aggrecan dimensions (CP length, GAG brush length, and GAG brush width) were quantified for each aggrecan molecule (n= 300).

3.3.4 Statistical analysis

All aggrecan dimensions were expressed as distributions and plotted as a histogram. Aggrecan dimensions were reported as mean ± SEM. Correlation (R^2) for protein and

GAG concentrations to fraction number (density) was calculated by linear regression. Full details for all procedures were located in Chapter 2.

3.3 Results

3.4.1 D1D1 fractions isolated from bovine NP tissue

The first aim of this study was to adapt existing procedures to optimise methodology for the extraction and purification of aggrecan from caudal discs with 4M GuHCl and D1D1 CsCl density gradient centrifugation. As a result eleven fractions were collected with a range of increasing density from 1.36 (top fraction) to 1.86 g/ml (bottom fraction). As expected, the density of each fraction gradually increased down the centrifugation tube and gradients at the bottom of the tube contained the molecules of interest such as aggrecan molecules with a higher density compared to non-glycosylated proteins. D1D1 fractions were defined as fractions with a density greater than 1.54 g/ml which included the six bottom fractions.

3.4.2 GAG and protein quantification

Figure 3.20 is graphical representation of concentrations of sGAG and protein found for each D1D1 fraction (represented as fractions 5-11) including the top fractions (1-4) isolated from bovine NP tissue. After fraction 6 there was a high increase of protein concentration than sGAG which was ten times more ranging from 3 to 800 µg/ml. According to figure 3.20 protein concentration correlated (R^2=0.78) with density whereas sGAG concentration was low in comparison however with a correlation (R^2=0.65) with density ranging from 10 to 90 µg/ml.

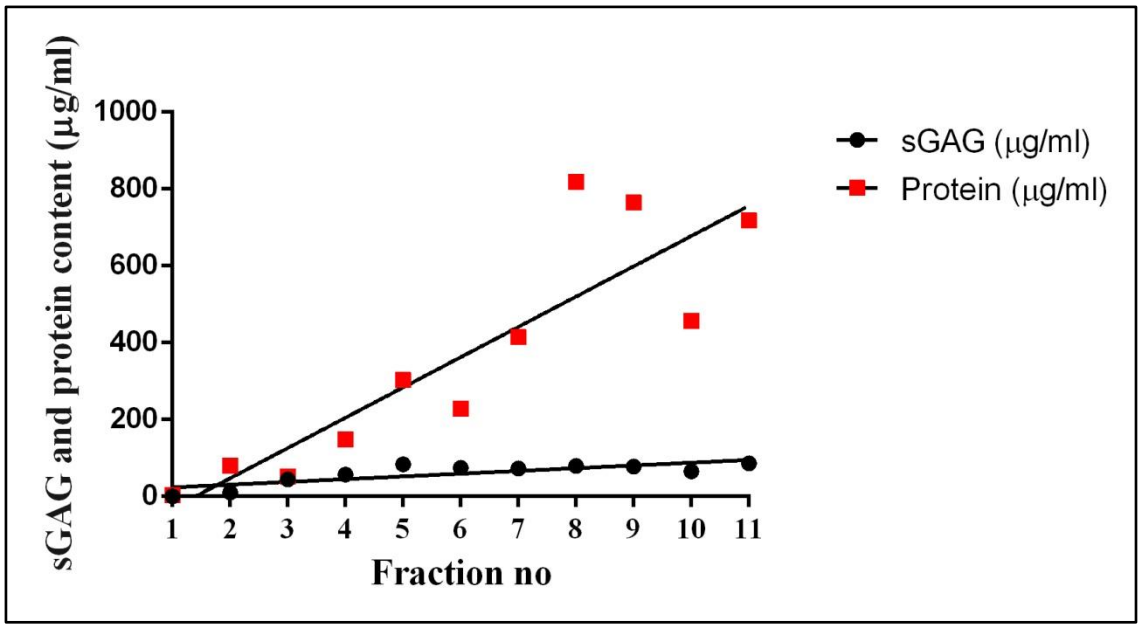

Figure 3.20. D1D1 sGAG and Protein Level in Top Gradient Fractions and D1D1 Fractions.

3.4.3 Immunodetection of aggrecan in the D1D1 Fraction obtained from Bovine NP Tissue

An aggrecan dot blot, utilising a commercially available antibody, was used to specifically detect the presence of aggrecan in the isolated density gradient fractions. The aggrecan antibody specifically targets the bovine/human non-glycosylated N-terminal region of the core protein (CP) containing G1-IGD-G2 domain. Glycosylated aggrecan was bound to the PVDF blotting paper with the aid of positively charged PLL which acted as a binding substrate to negatively charged aggrecan molecules since proteoglycans do not readily bind to the PVDF membranes. A D1D1 fraction (pooled fraction 5-11) isolated from bovine NP tissue was probed for aggrecan detection and was found to be positive since the antibody is indicative to aggrecan according to figure 3.21.

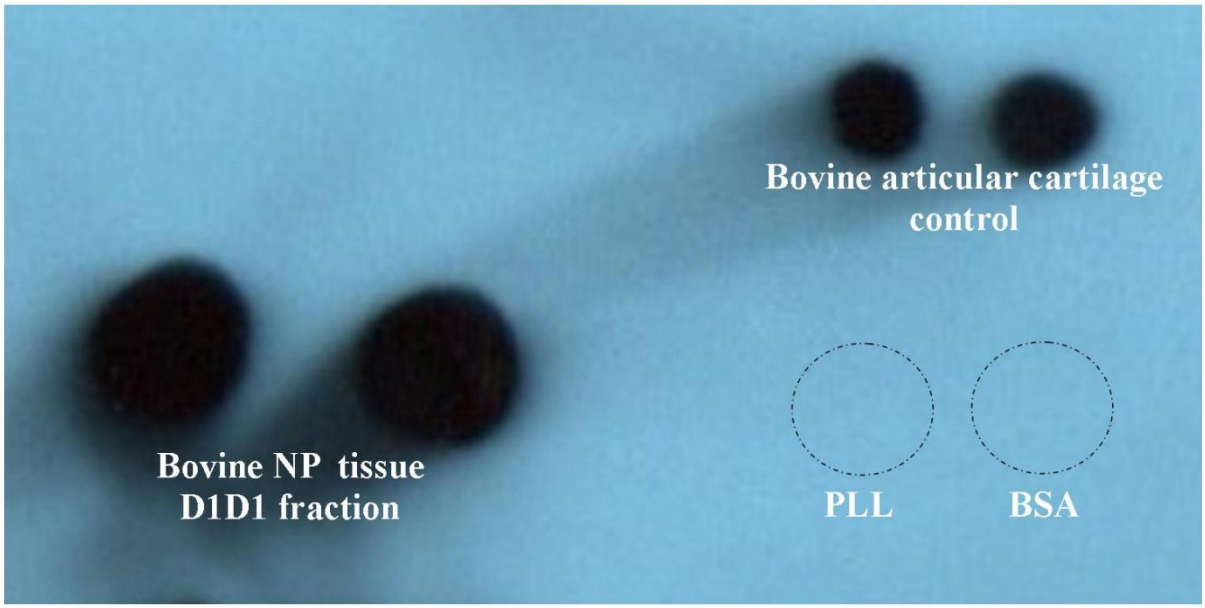

Figure 3.21. D1D1 Fraction Aggrecan Dot Blot.
(left) D1D1 fraction isolated from bovine NP tissue (dotted in duplicate). (top right) Positive control - Commercial available aggrecan from bovine AC (2µg). PLL= blank; BSA= Negative control (0.3µg).

3.4.4 Assessment of Surface roughness of APTES-mica

Before aggrecan can be immobilised for AFM imaging, the APTES-mica surface must be characterised to ensure that the topography and surface chemistry is sufficiently capable of binding to mica and low in surface roughness. Blank mica was used as a control to demonstrate its featureless and atomically flat appearance without APTES deposition (figure 3.22a) whereas following deposition of mica to APTES for one minute, the mica surface was patchy in appearance with an increase in surface topography. However, following 5 minutes of APTES deposition there were no patches but a consistent covering over the mica surface (figure 3.22a and b).

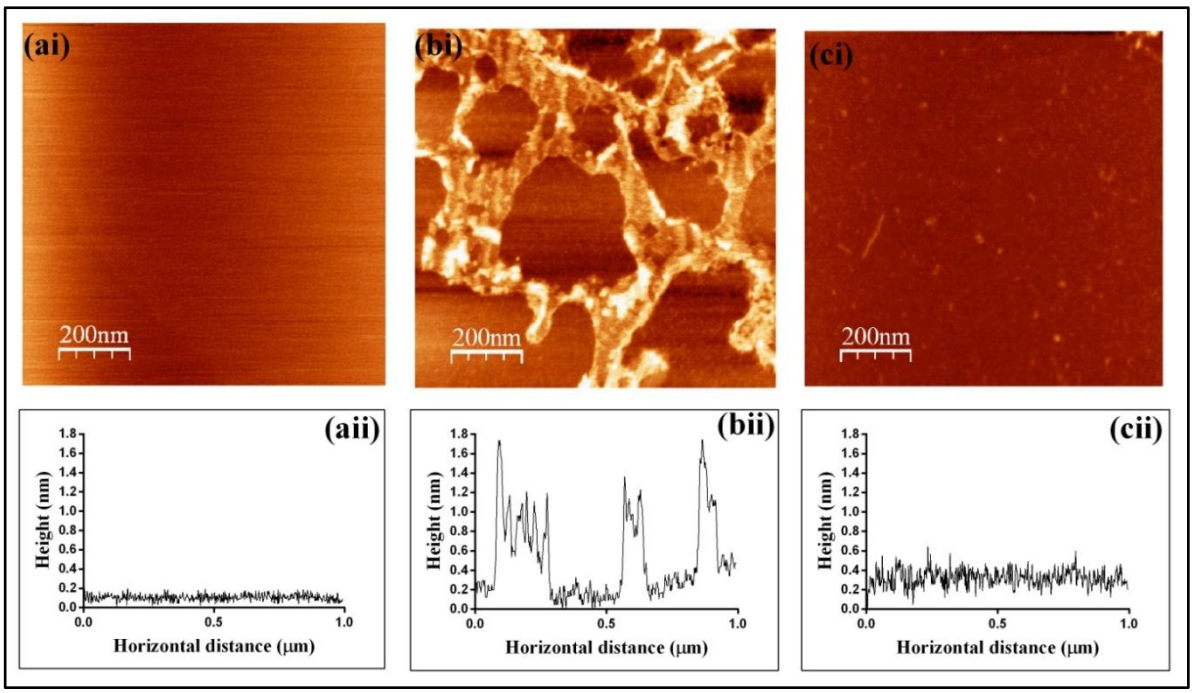

Figure 3.22. AFM Height Images of Blank Mica and APTES-mica Surfaces.
1μm x 1 μm scans. (ai) Blank mica surface (aii) Mica surface profile. (bi) APTES-mica surface at 1 minute binding time (bii) 1 minute surface profile (ci) APTES-mica surface at 5 minute binding time. (cii) 5 minutes surface profile.

Time points where APTES was deposited on cleaved mica for a further 15, 20, 30, and 60 minutes showed the same appearance (images not shown) with the surface topography similar in appearance. Due to the limitation with imaging alone, quantification of the surface roughness was required. Quantifying surface roughness was performed by determining the root mean square (RMS) roughness value of each deposition time point however a 1 μm x 1 μm scan size was used instead of a 2 μm x 2 μm scan size as detailed previously (Sherratt et al., 2004). Figure 3.23 summarised the RMS surface roughness of APTES-mica at different deposition time points (1, 5, 15, 20, 30, and 60 minutes). Surface roughness was the highest at one minute (0.24 nm ± 0.16 nm), but decreased after five minutes (0.11 nm ± 0.13 nm), however RMS surface roughness values for longer depositions time (15 (0.08 ± 0.002 nm), 20 (0.08nm ± 0.001 nm), 30 (0.07 nm ± 0.005 nm), and 60 (0.08 nm ± 0.02 nm) minutes) decreased indicating no define changes to surface roughness after 15 minutes according figure 3.23.

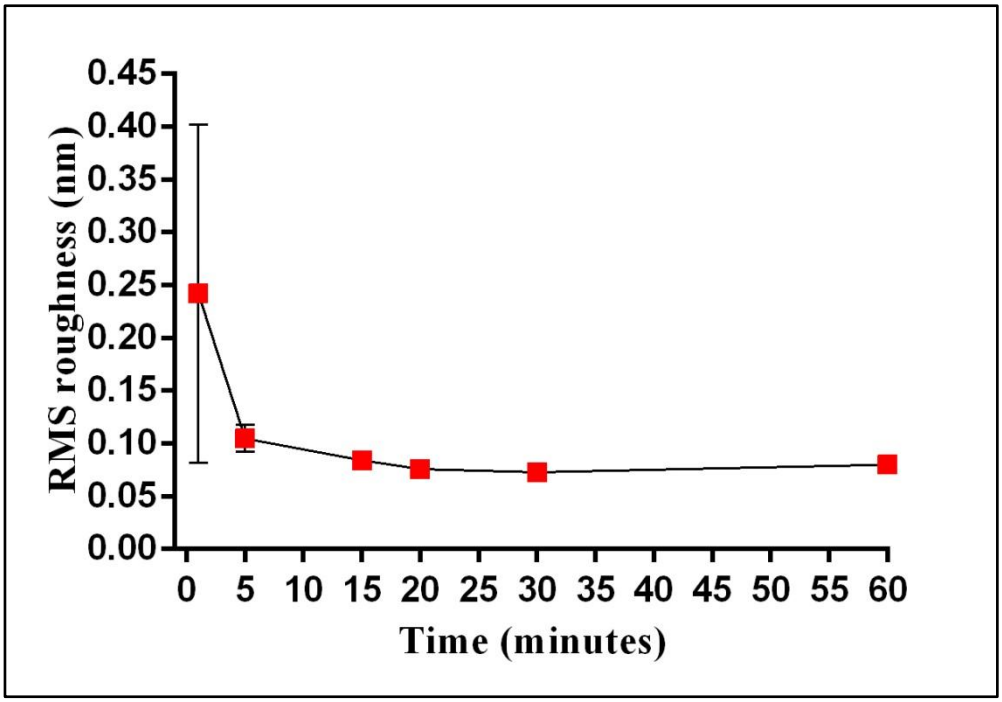

Figure 3.23. Summary of RMS Surface Roughness of APTES-mica.
Summary of RMS roughness values for each APTES deposition time point on mica (1, 5, 15, 20, 30, and 60 minutes). All data is represented as mean ± SEM.

3.4.5 Assessment of the APTES-mica Surface Chemistry

Having shown evidence that coating APTES onto mica results in a low surface roughness (0.07-0.08 nm) after 15 to 60 minutes of deposition time, it was necessary to determine if the surface chemistry was suitable with aggrecan. Mica alone has a negative surface charge once exposed to water and this would repel aggrecan molecules due to their negatively charged CS chains. The deposition of APTES chemically modified mica to leave exposed amine groups on the mica surface that binds to the negatively charged aggrecan molecules.

The surface chemistry of the APTES-mica surface was investigated where a side view image of a 10 µl (deionised water or column buffer) droplet was deposited onto the APTES-mica surface base as described in previous studies (Sherratt et al., 2004, Kielty et al., 2007). Based on previous studies (Ng et al., 2003, Lee et al., 2010, Lee et al., 2013) it was reported that 30 minute deposition time was applied onto mica, and the lowest surface roughness (0.07 ± 0.005 nm) was found at 30 minutes therefore this time point was selected for this experiment. Figure 3.24 depicts side view images of droplets of either deionised water (figure 3.24b) or column buffer (figure 3.24c) onto freshly cleaved mica alone or with mica exposed to APTES for 30 minutes. Freshly cleaved mica on its own produced no visible droplet with either deionised water (image not shown) or column buffer and hence the contact angle was not measurable. However, droplets were observed on the APTES-mica surface with both deionised water and column buffer. The contact

angle values for both deionised water (22 ± 2.8°) and column buffer (21 ± 2.6°) were found to be almost identical with both contact angles values less than 90° demonstrating that the APTES-mica surface was found to be hydrophilic.

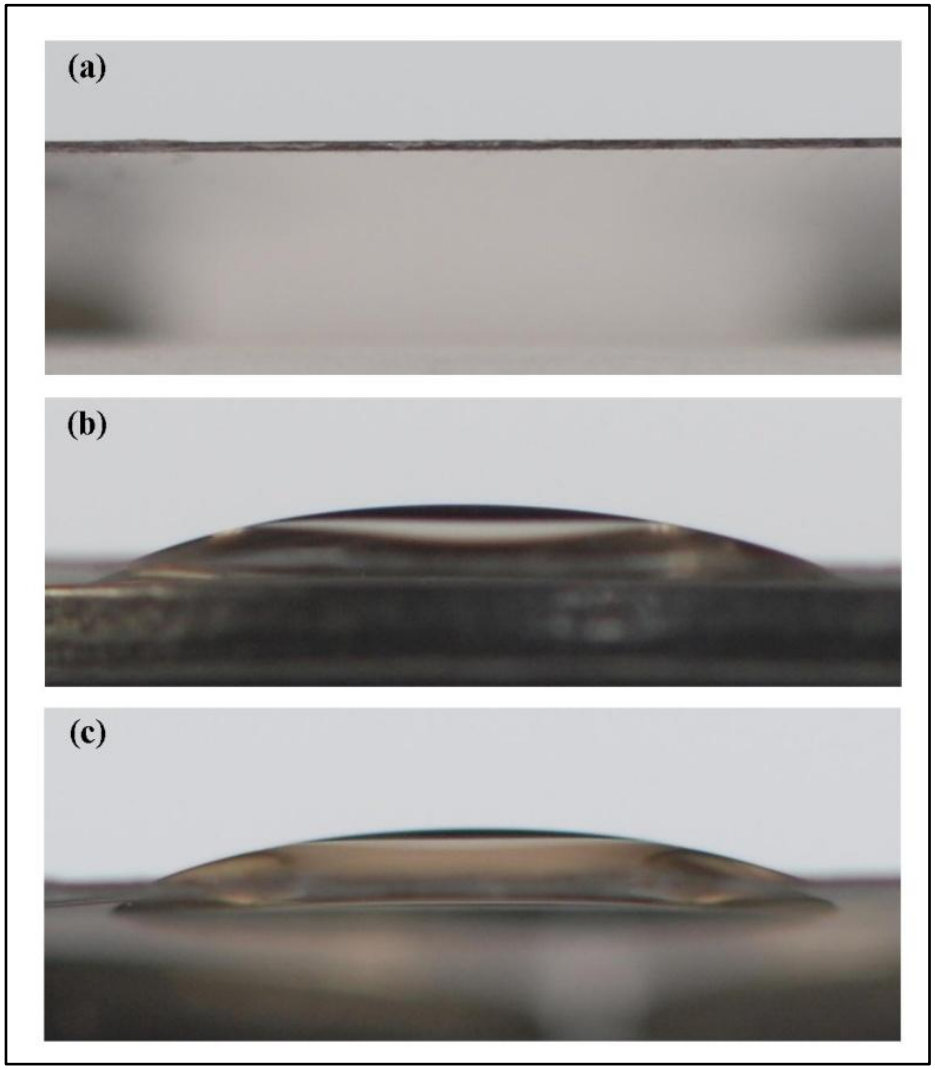

Figure 3.24. The Hydrophobicity/Hydrophilicity of the APTES-mica Surface.
(a) Column buffer on blank mica. (b) APTES-mica at 30 minutes with deionised water; θ= 22 ± 2.8 °. (c) APTES-mica at 30 minutes with column buffer; θ= 21 ± 2.6°. All data is represented as mean ± SEM.

3.4.6 AFM Imaging of Isolated Aggrecan

Mica was chemically modified with 0.01% APTES for 30 minutes prior to washing. Once the surface was dry, aggrecan molecules were immobilised onto the APTES-mica surface where the negatively charged CS chains bind to the surface by electrostatic interaction to exposed immobilised protonated amine groups on the APTES-mica surface. The immobilised aggrecan molecules were visualised in air by intermittent tapping mode AFM (figure 3.25). The height images of aggrecan displayed a central linear core with numerous side chains. Such a structure is characteristic of aggrecan which typically has a core protein-sGAG brush (bottle brush) structure when bound to a APTES-mica surface (Ng et

al., 2003). At the ends of the core protein, a non-glycosylated N-terminal region (containing G1-IGD-G2 domains) and C-terminal region (G3 domain) were observed in a proportion of the aggrecan monomers. The GAG brush region could be seen with a variety of short or extended GAG chains as shown in figure 3.25b and c.

Two types of aggrecan molecules were observed: i) full-length monomers which have both globular domains present on both ends (figure 3.25b and c) that were found in low abundance and ii) non-intact monomers of which three variants were observed. Non-intact aggrecan was observed as i) an aggrecan monomer with a partial brush region with only one globular domain end (figure 3.25d), ii) as fragments with only a small sections of the CS GAG brush and no globular domains visible (figure 3.25e), and iii) intact brush region with no or one globular domain end on either N or C terminal end (figure 3.25a and f).

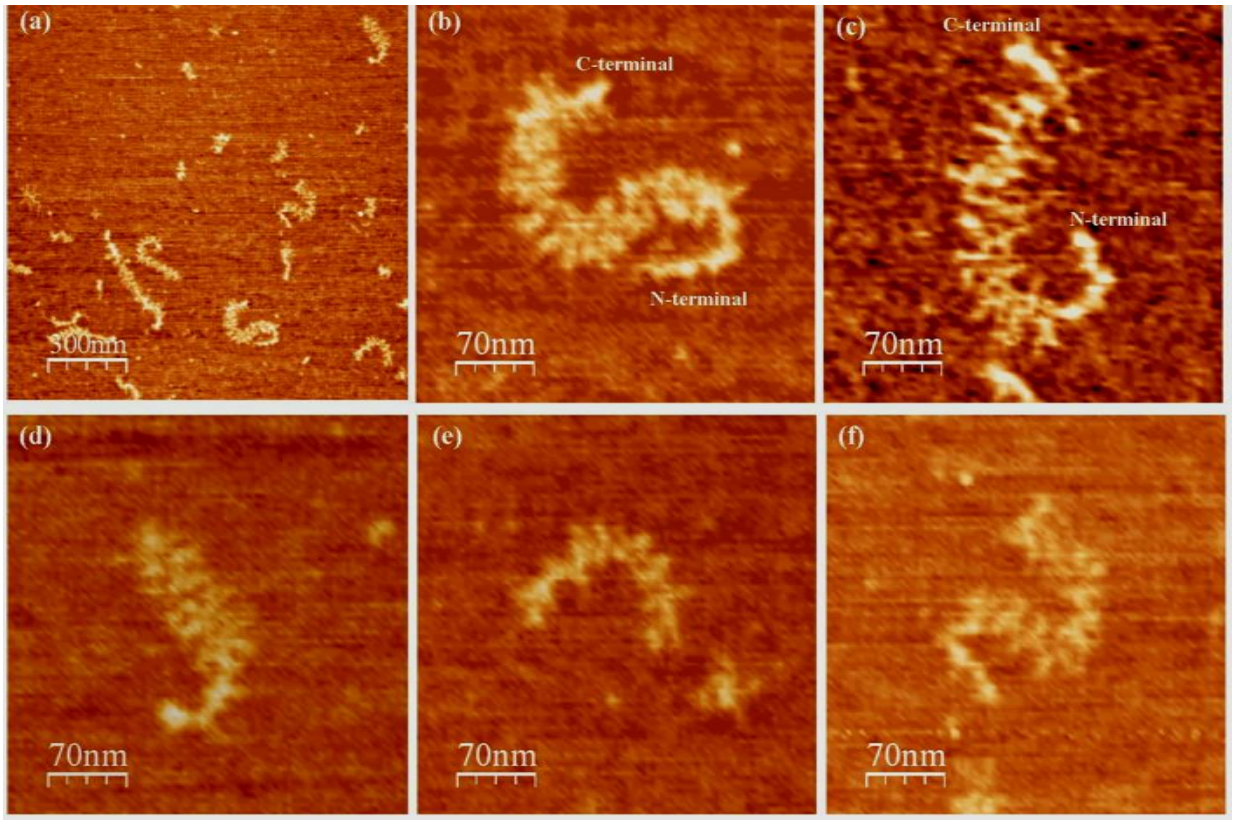

Figure 3.25. Full-Length and Non-intact Aggrecan Molecules Found in Bovine NP Tissue.
AFM height images. (a) General aggrecan population from bovine NP tissue bound to APTES-mica surface [Height scale= 1.5 nm)]. (b-c) Full-length aggrecan monomers with N and C-terminals globular domains. (a, d-f) Non-intact population: (d) Partial CS brush region with one globular end. (e) Cleaved and degraded aggrecan fragment with no globular terminal ends (a and f) Aggrecan monomer with only one or no globular domain end [Height scale= 1.0 nm].

3.4.7 Aggrecan Core Protein Length

A key morphological parameter for aggrecan is the core protein length which was quantified from the contour length measured on AFM images. The following are the terminologies used throughout this chapter for defining different aggrecan populations when interpreting aggrecan dimension data. The term general aggrecan species refers to all aggrecan molecules observed, non-intact refers to the aggrecan species minus the full-length aggrecan species, and full-length aggrecan species referred to those monomers that were observed with N-terminal and C-terminal globular domains present (Ng et al., 2003).

The CP length for general and non-intact species indicated the frequency distribution for aggrecan was bimodal (figure 3.26a and b). The positions of the two peaks in both general (215 ± 2 nm, 371 ± 6 nm) and intact species (217 ± 2 nm, 363 ± 5 nm) with identical CP length range (100-500 nm) indicate the presence of two separate/distinct populations with differing CP lengths. Full-length aggrecan monomers (Figure 3.26c) were low in abundance (5% of cohort measured similar to other studies which found only 5-14 % full-length monomers from their total population (Lee et al., 2010, Lee et al., 2013). CP length in full-length monomers were longer in length (429 ± 0.9 nm) with a range from 390-470 nm compared to the general and non-intact species where CP length ranged 120-470 nm. .

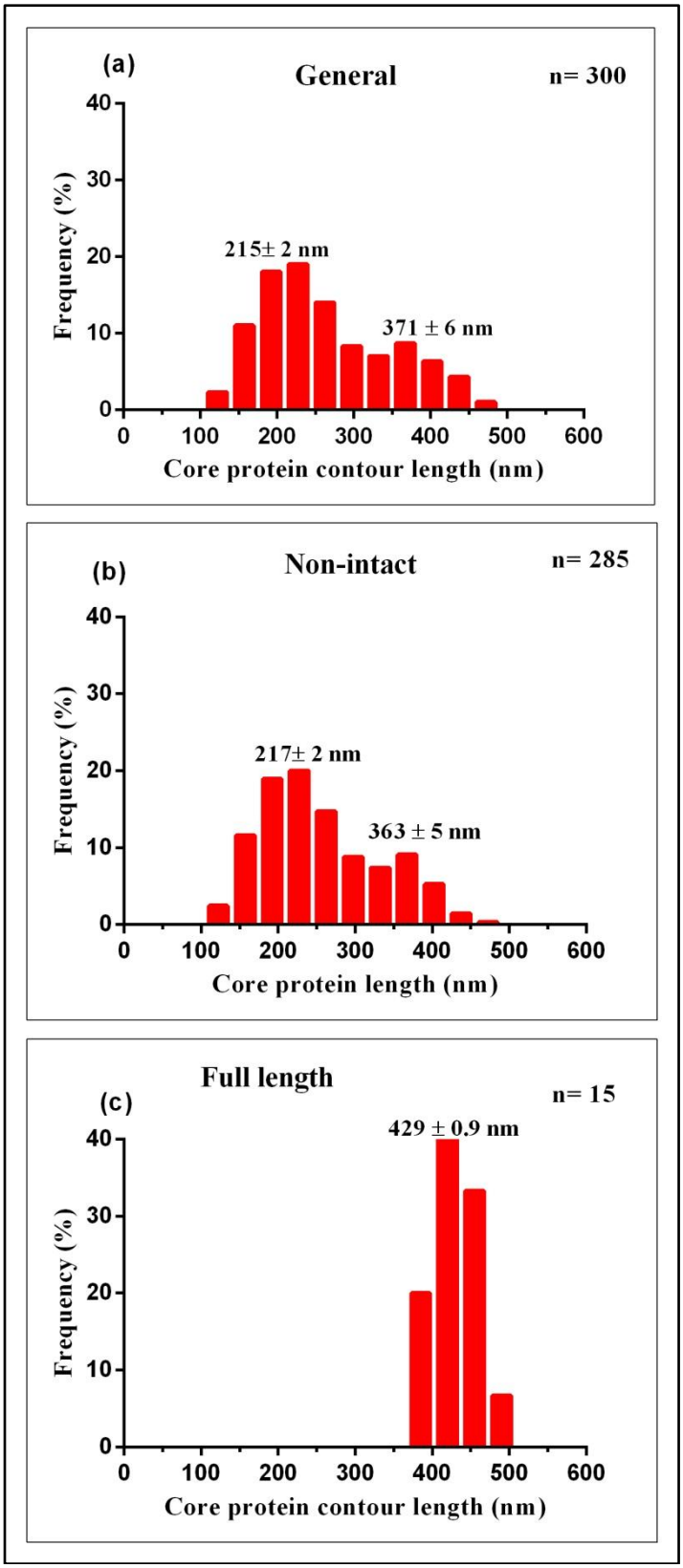

Figure 3.26. Aggrecan Core Protein Contour Length Quantification for Aggrecan Extracted from Bovine NP Tissue.

(a) Bovine NP tissue contour length of aggrecan general species (n= 300; 215 ± 2nm and 371 ± 6 nm). (b) Bovine NP tissue contour length of aggrecan non-intact species (n= 285; 217 ± 32nm and 363 ± 5 nm). (c) Bovine NP tissue aggrecan full-length species contour length (n= 15; 429 ± 0.9 nm). All data was represented as mean ± SEM.

3.4.8 Aggrecan GAG Brush Length

The GAG brush length here is defined as the total length of the glycosylated regions along the aggrecan core protein between the G2 and G3 domains. Figure 3.27a and b depict the GAG brush length of the aggrecan general and non-intact species and again show bimodal distributions indicating the presence of two distinct populations with differing brush lengths. The aggrecan general (166 ± 6 nm, 299 ± 10 nm) and non-intact (165 ± 6 nm, 303 ± 14 nm) species showed similar mean GAG brush length values and same range from 50 to 350 nm. The full-length aggrecan species (figure 3.27b) was found to be unimodal with a longer GAG brush length (277 ± 2 nm) compared to both general and non-intact species ranging from 190-340 nm.

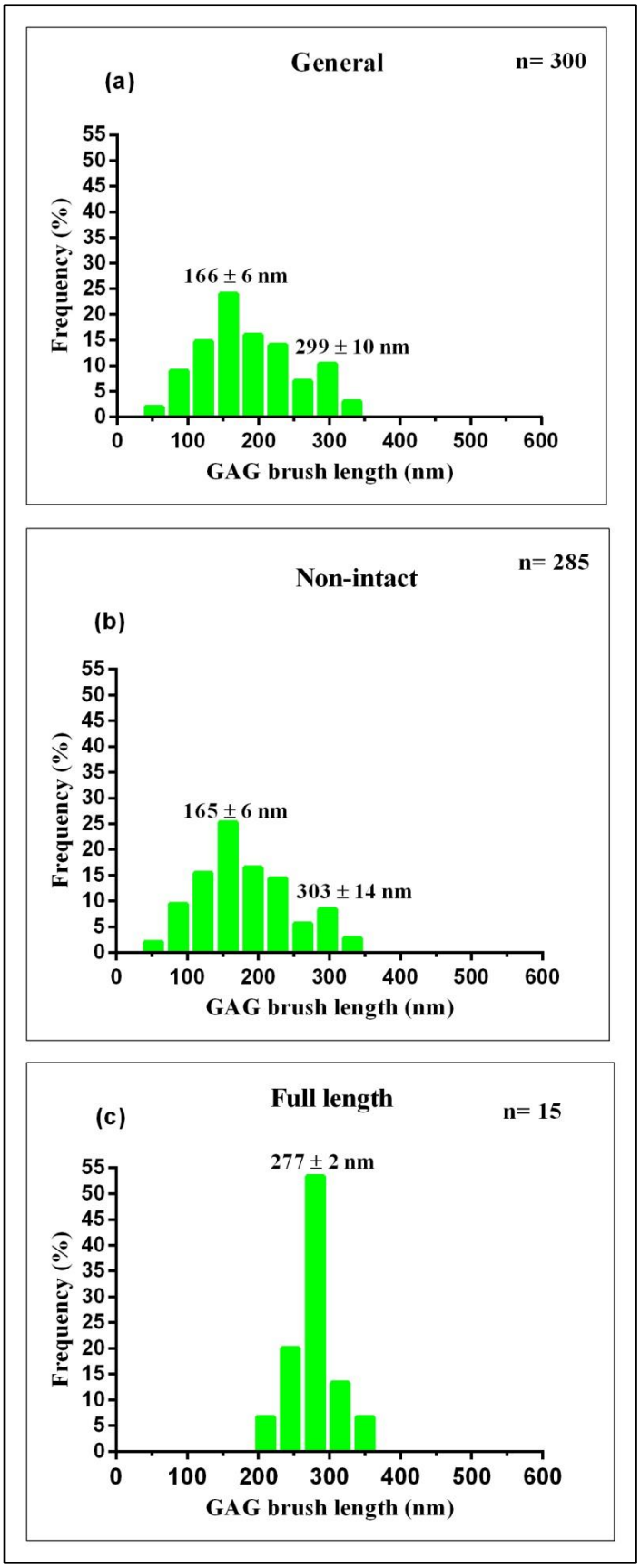

Figure 3.27. Aggrecan GAG Brush Length Quantification for Bovine NP Tissue.
(a) GAG brush length of aggrecan general species (n= 300; 166 ± 6nm and 299 ± 10nm). (b) GAG brush length of aggrecan non-intact species (n= 285; 165 ± 6nm and 303 ± 14nm). (c) GAG brush length of aggrecan full-length species (n= 15; 277 ± 2 nm). All data was represented as mean ± SEM.

3.4.9 Quantification of Aggrecan GAG Chain Width

Individual GAG chain contour length measurements were not possible due to the dense packing and overlapping of most individual GAG chains. Instead, the width of the brush region was calculated from width length of the mean transverse height distance obtained from AFM height imaging. The GAG brush width distributions of the general aggrecan and non-intact species were unimodal and their GAG brush width size range (20-80 nm) was identical (figure 3.28a and b). The data showed that even though the predominant mean GAG brush width was 37 ± 2 nm there was a wide variety of brush width sizes present. The full-length species showed a bimodal distribution with two peaks at two mean values at 40 ± 12 nm and 59 ± 12 nm (figure 3.28b) however there was no change in GAG brush width range (30-80 nm).

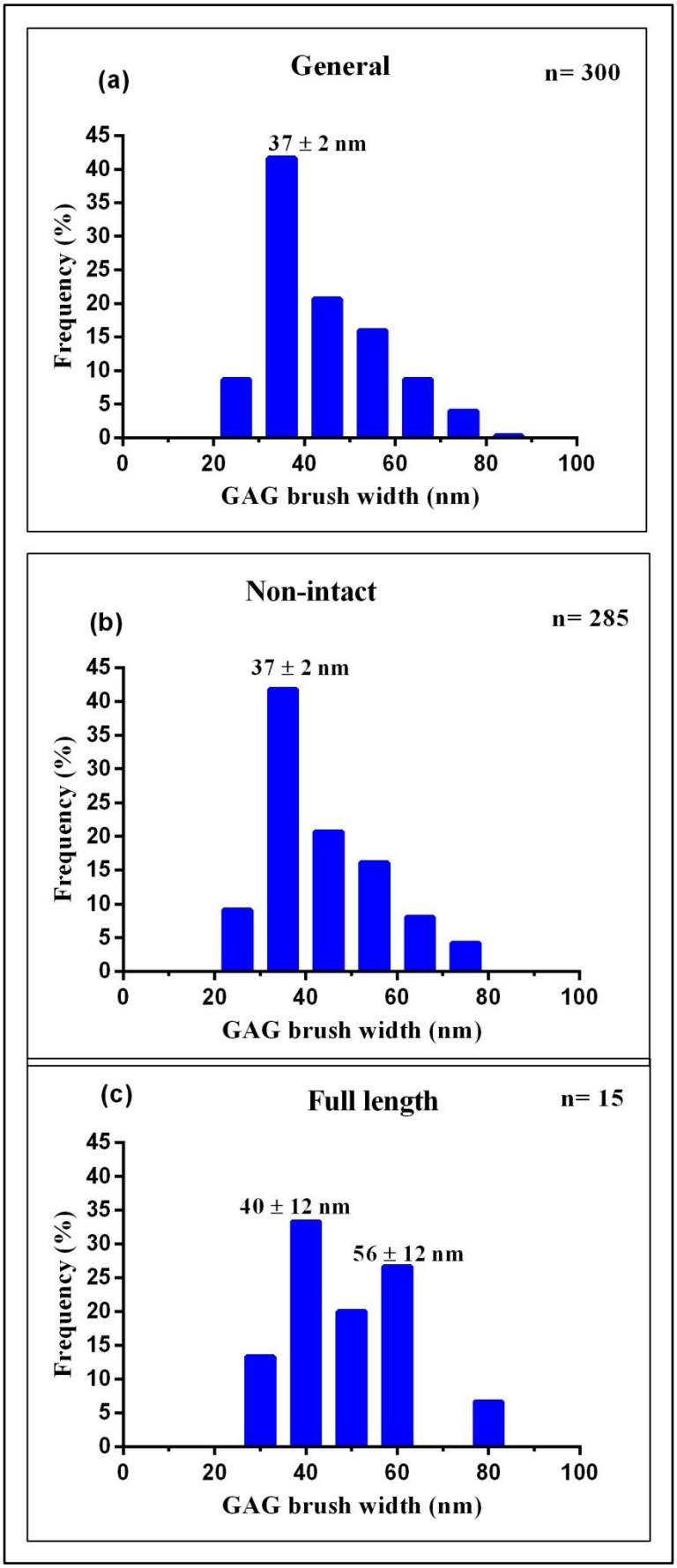

Figure 3.28. Aggrecan GAG Brush Width Quantification for Bovine NP Tissue.
(a) GAG brush width of the aggrecan general species (n= 300; 37 ± 2 nm). (a) GAG brush width of the aggrecan non-intact species (n= 285; 37 ± 2 nm) (c) Bovine NP tissue GAG brush width of the aggrecan full-length species (n= 15; 40 ± 12 nm and 56 ± 12 nm). All data was represented as mean ± SEM.

3.5 Discussion

The objective of this chapter was i) to optimise a procedure to isolate aggrecan from bovine nucleus pulposus tissue ii) to determine the optimum conditions for aggrecan immobilisation for AFM imaging, and iii) to develop and adapt existing image analysis protocols to quantify aggrecan ultrastructure.

3.5.1 Aggrecan Isolated From Nucleus Pulposus Tissue

A D1D1 CsCl density gradient separation technique was optimised for aggrecan isolation for this chapter. Isolated D1D1 fractions were further studied to confirm the presence of aggrecan using DMMB and BCA assays and immunoblotting (dot blotting). Additional validation/confirmation for the presence of aggrecan in the D1D1 fractions was undertaken visualising the actual aggrecan structures by AFM imaging. Aggrecan was successfully isolated using the above methods as previously described from other studies (Ng et al., 2003, Lee et al., 2013).

3.5.2 The APTES-mica Surface is Suitable for AFM Imaging of Aggrecan Molecules

There are a number of studies that have used APTES as a binding substrate to immobilise aggrecan onto mica (Ng et al., 2003, Kopesky et al., 2010, Lee et al., 2010, Lee et al., 2013). Despite the number of studies in the past that have applied APTES to immobilise other polyanion molecules (i.e. DNA) no study has shown any surface roughness quantification for mica with APTES at a 0.01% (v/v) concentration (Lyubchenko et al., 1993, Tanigawa and Okada, 1998, Ng et al., 2003).

However an adapted methodology (Sherratt et al., 2004, Sherratt et al., 2005) was used to quantify the RMS surface roughness of APTES-mica. This methodology has been used in past studies to quantify the root mean square (RMS) surface roughness of glass and poly-L-lysine bound to mica. The objective was to ensure that the APTES-mica substrate surface was no greater than 0.99 nm for AFM imaging (Ng et al., 2003). This is important since aggrecan molecules are reported to be ~1 nm in height (Tanaka, 1978, Ng et al., 2003), therefore a low surface roughness is required to avoid distorted imaging or morphology. The data here showed deposition of 0.01% APTES for 30 minutes to chemically modified mica with a low surface roughness of 0.07 nm fell well within the accepted range of 0.99 nm.

The contact angle assessment was needed to characterise the surface chemistry in order to demonstrate that APTES-mica was hydrophilic for immobilisation of aggrecan. Again the methodology was adapted from a previously studies that characterised chemically modified

mica and glass surfaces (Sherratt et al., 2005, Kielty et al., 2007). Water (Chapter 3) and column buffer (Chapter 4 and 5) were used since isolated aggrecan was resuspended in both solvents during sample preparation for AFM imaging. It was to ensure that both solvents readily bound to APTES-mica during aggrecan immobilisation. The evidence presented in this chapter has shown that the APTES-mica was a suitable surface for aggrecan immobilisation for subsequent AFM imaging.

3.5.3 Comparison of CP Contour and GAG Brush Length to Other Studies.

Isolation of aggrecan was possible by following previously published protocols (Roughley and White, 1980, Ng et al., 2003, Sivan et al., 2006, Lee et al., 2010). As a result immobilising aggrecan molecules onto APTES-mica and imaging their ultrastructure by AFM was successful. This has allowed aggrecan dimensions to be quantified by existing imaging software. The following are details of the comparison between the current study findings and other publications for CP and GAG brush length.

There are a limited number of AFM imaging studies that have published their findings of CP length of aggrecan monomers and those that have, utilised aggrecan extracted from cartilage. (Ng et al., 2003, Yeh and Luo, 2004, Kopesky et al., 2010, Lee et al., 2010). To date, however, there are no published findings of aggrecan dimensions from bovine IVD tissue. Our findings have found aggrecan CP contour length from bovine NP tissue at two mean distributions of 215 ± 2 nm and 371 ± 6 nm whereas aggrecan extracted from bovine mature nasal cartilage had contour CP length (full length) of 352 ±88 nm (Ng et al., 2003), and those from equine AC Lee et al.(2010) had CP length of 220 ± 142 nm (total population) and 475 ± 2 nm (full-length aggrecan) (table 3.1). Importantly, the study by Lee et al., (2010) showed their aggrecan CP length (general population) was a bimodal distribution, similar to this study and only identified a small cohort of (n= 20) of full-length aggrecan monomers (table 3.1). Lee et al., 2010 and Kopesky et al., 2010 comment about the different CP lengths were due to proteolytic degradation or catabolic processing of the CP which is due to proteolytic enzymes. CP length measured from bovine NP tissue was found to be more similar with equine AC (Lee et al., 2010) instead of bovine AC (Ng et al., 2003). This was due to the fact that Ng et al., (2003) reported their findings on mainly full-length aggrecan monomers (n= 141) compared to the findings of this study where full-length monomers were low in abundance (n= 15).

GAG brush length has only been measured in one previous study where aggrecan was extracted from mature bovine nasal cartilage tissue (Ng et al., 2003). They showed that GAG brush length (from full-length aggrecan monomers only) measured 268 ± 73 nm compared to our findings at 277 ± 2 nm for full-length monomers.

3.5.3.1 Aggrecan Core Protein and GAG Brush Length Cleavage.

The general aggrecan species consisted of a variety of aggrecan monomers with different CP lengths which may represent degraded or fragmented products, or partially degraded monomers with one or both globular ends cleaved or nonexistent (i.e. non-intact species). This may be due to matrix homeostasis/remodelling in tissue which leads to degradation of aggrecan. No specific enzymatic investigation was performed in this study, however a number of enzymes have been reported to be present within the disc which are able to degrade aggrecan. Aggrecan degradation may result from the action of matrix metalloproteinases (MMPs) and aggrecanases known as A Disintegrin-like And Metalloproteinase domain with Thrombo-Spondin Type I motif (ADAMTS), cathepsin D and L, and calpain which cleave specific amino acid sequences at the IGD, CS1, and CS2 domains along the aggrecan core protein (Sztrolovics et al., 1997, Tortorella et al., 1999, Roberts et al., 2000, Ariga et al., 2001, Pockert et al., 2009, Fukuta et al., 2011). Such degradation would produce aggrecan molecules of different sizes (Jahnke and McDevitt, 1988, Buckwalter, 1995). In general, aggrecanases and MMPs cleave at N (G1 and IGD domains) and C (CS2 and G3 domains) terminal sides. MMPs cleave at three positions; at the IGD domain, one near G2, and two (depending on the number of VNTRs present) in the CS1 domain. Aggrecanases target one position in the IGD domain while the other four target the CS2 domain. Figure 3.29a summaries the current knowledge of MMPs and aggrecanases core protein cleavage sites which may point to the variation of core protein and GAG brush lengths (figure 3.29b).

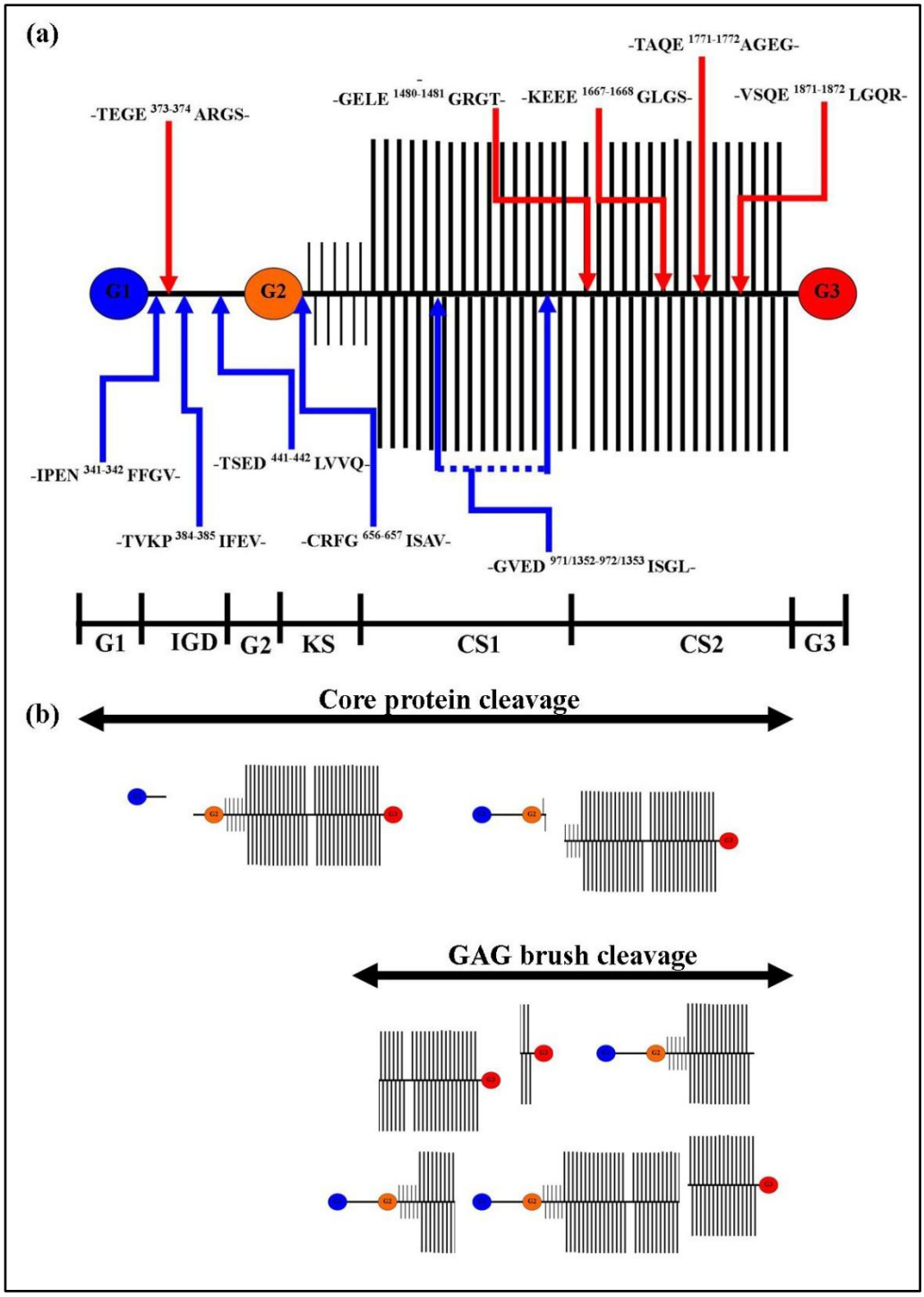

Figure 3.29. MMPs and Aggrecanases Cleavage Sites.

(a) Schematic representation of aggrecan cleavage sites of aggrecanases (red) and MMPs (blue). (b) Truncated aggrecan molecules from MMP or aggrecanase enzymatic activity on core protein and GAG brush region. Box sequences for aggrecanases cleavage site denoted for bovine core protein. G1= globular domain 1, IGD= interglobular domain, G2= globular domain 2, KS= keratan sulphate II, CS1= chondroitin sulphate domain 1, CS2= chondroitin sulphate domain 2, and G3= globular domain 3. [Adapted from Struglics et al., (2006) and Huang and Wu (2008)] (Struglics et al., 2006). Note: Aggrecanase cleavage sites between human and bovine are similar however, differ in homology (Tortorella et al., 2000).

Of the cohort of monomers (300 in total) analysed only 5% were found to be full-length aggrecan monomers. This could be due to four possibilities; the data reported in this study

accurately reflects the aggrecan population in the tissue. The aggrecan isolated from bovine NP tissue contained a subpopulation of cleaved molecules (non-intact species) only (Lee et al., 2013). There was a possibility that the extraction and purification steps during isolation could damage aggrecan molecules (Stevens et al., 1979). As a result, only damaged aggrecan molecules absorbed to the APTES-mica surface.

Full-length aggrecan represents monomers that are intact and have not undergone proteolytic cleavage, with both N and C terminals globular domain ends (Ng et al., 2003) visible by AFM imaging. In the population analysed the CP length varied although all globular domains were visible suggests that no proteolytic cleavage to the CP had occurred, and that other factors may influence CP length. For example, a number of studies have described particular phenomena where the number and length of GAG chains present on the monomer may influence CP length (figure 3.30). This is thought to be due to repulsive intra- and intermolecular electrostatic double layer interactions of GAG chain domains (Morgelin et al., 1989, Ng et al., 2003, Lee et al., 2013).

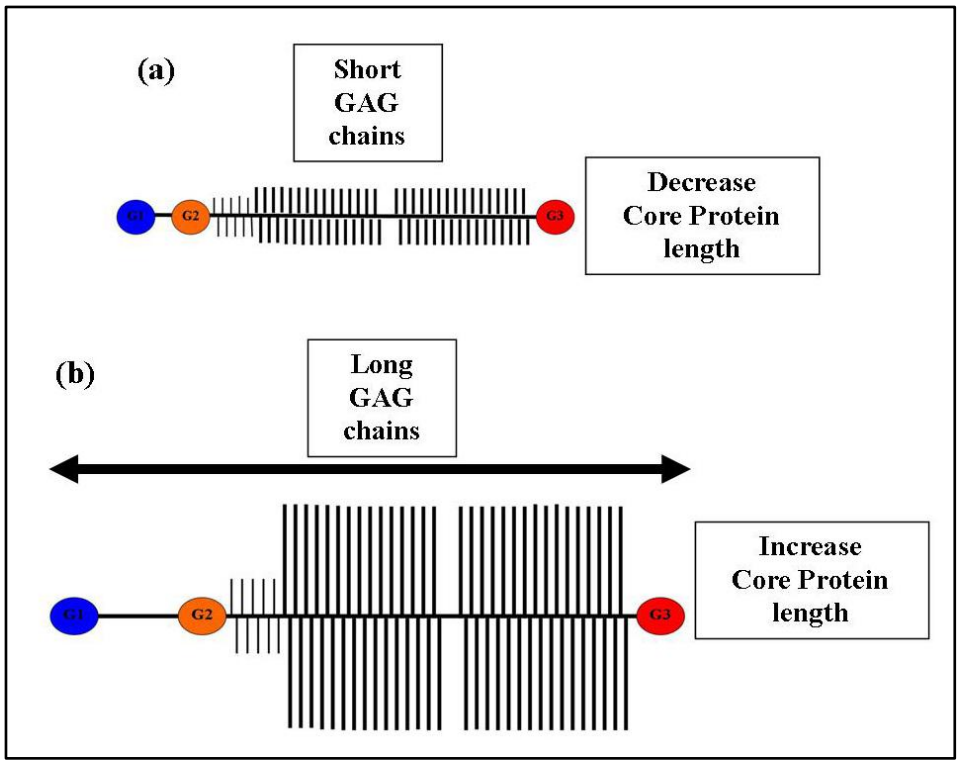

Figure 3.30. GAG chain length influences CP contour length
(a) Aggrecan molecule with short CS GAG chains with short CP length. (b) Aggrecan molecule with long CS GAG chain length influences CP length.

3.5.4 GAG Brush Width

GAG chain parameters in this study were measured differently since direct measurement of the GAG chain length was limited due to GAG chain overlapping and density. The

advantages of the current method was that the entire GAG brush region could be selected for all aggrecan molecules whereas other studies only measured selected number of GAG chain lengths. The second advantage is that the entire GAG chains can be measured in less time. This is especially advantageous when measuring large numbers of aggrecan molecules.

3.5.4.1 GAG Brush Width Variations

The findings in this study showed that GAG brush width distribution in general and non-intact species were unimodal and full-length species were bimodal, however all three species showed a variety of GAG brush widths. The current literature doesn't specify or describe variable GAG brush width within IVD aggrecan monomers. However there are three possible suggested explanations that are described in the literature which could explain this phenomenon.

The first is the most likely of three is the nutrient supply of the IVD may play a role. The NP cells in tissue rely on diffusion of nutrients such as glucose and oxygen from capillaries from adjacent vertebra where the nearest blood vessels can be 8mm away (Brodin, 1955b, Diamant et al., 1968, Mobasheri, 1998, Urban, 2002). The IVD microenvironment has a low oxygen content (1-5%) which has an effect on glucose transport and metabolism, and disc cells must obtain a critical concentration greater than 0.5 mmol/L of glucose to maintain viability (Ishihara and Urban, 1999, Urban et al., 2004). The NP cells are subjected to a gradient of nutrient availability (low levels of glucose and oxygen) from the outer to inner IVD. Low levels of glucose and oxygen in tissue could affect chondroitin sulphate (CS) synthesis. CS is a disaccharide consisting of the uronic acid; glucuronic acid (GluA) and the amino sugar known as D-*N*-acetyl-galactosamine (GalNAc) (Dudhia, 2005, Lamari and Karamanos, 2006). The synthesis of GluA requires the presence of oxygen and glucose in order for UDP-glucose dehydrogenase to convert uridine diphosphate glucose or UDP-glucose to UDP-GluA (Spicer et al., 1998, Campbell et al., 2000). If a low or high level of glucose and oxygen tensions is present then CS biosynthesis might be affected (Scott and Haigh, 1988).

NP cells expressing a variety of enzymes that deal with CS GAG chain polymerisation. The current literature describes a number of glycosyltransferases that polymerise CS chains; chondroitin synthase-1, 2, 3(ChSy-1, ChSy-2, ChSy-3), chondroitin polymerizing factor (ChPF), and chondroitin GalNAc transferase-1 and 2(ChGn-1 and ChGn-2) are associated with chondroitin sulphate GAG chain polymerisation in humans (Little et al.,

2008, Victor et al., 2009, Mikami and Kitagawa, 2013). They are required to be expressed in combination to achieve polymerisation activity (Kitagawa et al., 2001, Kitagawa et al., 2003, Izumikawa et al., 2007, Izumikawa et al., 2008). The existence of multiple polymerising enzymes expressed in different relative abundance synthesise GAG chains of different length (Kitagawa et al., 2003, Izumikawa et al., 2007, Izumikawa et al., 2008, Little et al., 2008).

The third is probably the least likely. Agonists such as hormones and growth factors can stimulate signalling pathways leading to GAG elongation in proteoglycans (Schonherr et al., 1993, Dadlani et al., 2008, Kopesky et al., 2010).The limited passage of these hormones and growth factors to the IVD could affect GAG chain length.

3.5.4.2 GAG Brush Width Findings and other AFM Imaging Studies

Only one study has commented on GAG brush width in bovine nasal cartilage from AFM imaging (Ng et al., 2003) which was found to be 47 ± 12nm (full-length only) whereas the findings of this study showed in both general species and full length to be unimodal in distribution with 36-40 nm as the predominate GAG brush width in both general and full-length species. Since then no other study that has reported aggrecan GAG brush width in this way. However, GAG brush width still relates to GAG chain length bearing in mind that GAG brush width is a mean value calculated on a single aggrecan molecule as a whole unit. Therefore the findings in this study to GAG brush width could be related to other studies that have measured GAG chain length. Variations of GAG chain length has been reported in other species tissue (bovine and equine AC) which are equivalent to the variation reported in this study (Ng et al., 2003, Kopesky et al., 2010, Lee et al., 2010).

3.6 Conclusion

The most common techniques for aggrecan isolation have been adapted and optimised for this study and successfully isolated aggrecan for subsequent AFM imaging. Adapting previous protocols for AFM sample preparation made it possible to immobilise aggrecan on APTES-mica which was found suitable for AFM imaging in air. The use of pre-existing imaging analysis software to quantify aggrecan dimensions has enabled this study to characterise aggrecan ultrastructure from bovine NP tissue. It was found that aggrecan molecules exist predominantly as non-intact species with varying CP length, GAG brush length, and GAG brush width. The variation of CP and GAG brush lengths are possibly due to degradation and varying GAG brush widths could be possibly due to a combination

of inter-linked biological factors. The lengths of the aggrecan CP and GAG brush domains were comparable to previous studies however GAG brush width was limited to comparison to other studies. Overall, the aggrecan isolation method, aggrecan immobilisation, AFM imaging and quantification of aggrecan dimensions has provided a template for future work to investigating aggrecan molecules in tissue or other materials/environment such as 3D cell culturing.

Chapter 4

Modified Aggrecan Isolation Procedure from Alginate Constructs for AFM Imaging

4.1 Introduction

The following chapter has incorporated the methodology from Chapter three to isolate and image newly synthesised aggrecan from alginate constructs. Using existing procedures for cell seeding and alginate bead formation this methodology was complimented with ultracentrifugation (CsCl density gradient centrifugation) under dissociative conditions. Unfortunately, ultracentrifugation alone was not sufficient to purify aggrecan from alginate fragments. Another common method for aggrecan purification was size exclusion chromatography (SEC). SEC is a technique that separates molecules based on their size. SEC is a common method of separating small and large molecules such as alginate fragments and aggrecan. It was necessary to purify aggrecan molecules from residue alginate fragments that were still present after ultracentrifugation in order to image aggrecan molecules by AFM. Previous studies have demonstrated the use of D1 CsCl density gradient centrifugation to isolate aggrecan from hydrogel constructs (Kopesky et al., 2010, Lee et al., 2010). The amount of aggrecan synthesis in alginate constructs is less than tissue which is enriched with proteoglycan therefore a D1 CsCl density gradient centrifugation was sufficient.

4.1.1 Alginate

Hydrogels are defined as cross-linked polymeric networks containing hydrophilic groups that promote swelling due to interaction with water (Lee and Mooney, 2001). They have been used as scaffolds for tissue engineer application and model extracellular matrices for biological studies (Lee and Mooney, 2001, Discher et al., 2009). Alginate is a widely used hydrogel in the study of tissue engineering (TE). The current uses of alginate in TE are as a tissue bulking agent, drug delivery carrier, carrier for cell therapies, and as a model for extracellular matrix (ECM) (Augst et al., 2006). Alginate is a widely used material found in food and medical applications (Sun and Tan, 2013). As a biomaterial it has a number of advantages such as being biocompatible and non-immunogenic, possible due to the their hydrophilic character (Shapiro and Cohen, 1997). Another attractive advantage is alginate's gentle gelling behaviour that allows the encapsulation of various molecules or cells with no or minimal damage (Klock et al., 1997). However, there are some disadvantages with alginate as it doesn't readily degrade naturally in mammals and some cell types do not naturally adhere to alginate (Smetana, 1993, Lansdown and Payne, 1994).

Alginic acid, which is derived from brown algae, is composed of two monomers called β-D-mannuronic acid (M) and α-L-guluronic acid (G). The introduction to high concentrations salts (e.g. NaCl) to alginic acid forms alginates (Haug, 1962). Alginate polymer chains contain three different polymeric block repeats (figure 4.31) which are homopolymeric M-block (M-M-M), homopolymeric G-block (G-G-G), and heteropolymeric MG-block (G-M-G-M) (Draget et al., 1997).

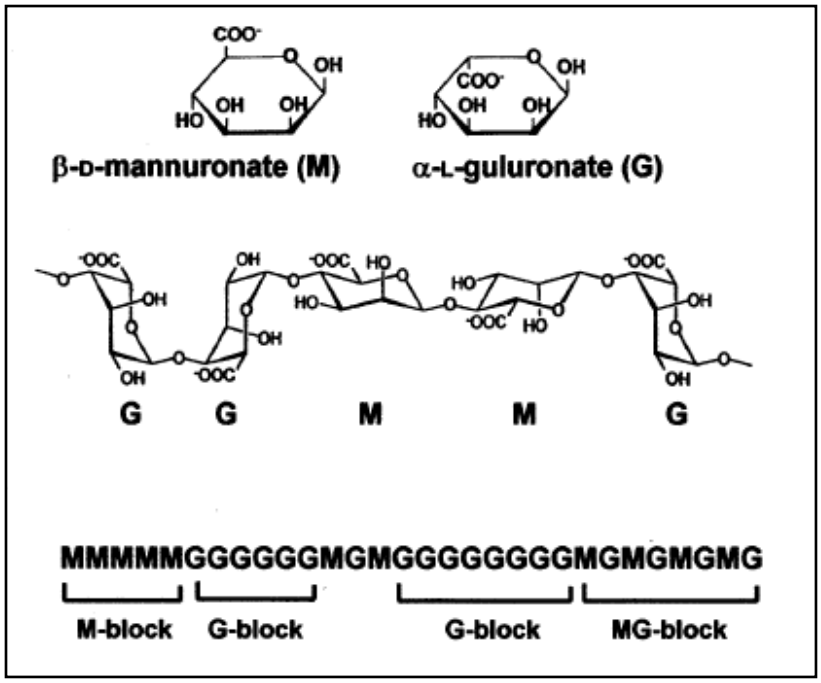

Figure 4.31. Alginate Structure. Copied from Draget et al (1997)

Alginate gelation takes place in the presence of $CaCl_2$ where Ca^{2+} ions (figure 4.32b) have a specific and strong interactions between long stretches of G blocks inducing an interchain association and the formation of the gel junction zones by Ca^{2+} ions connecting polymer chains pairs forming a structure known as an egg-box model described in figure 4.32a (Grant et al., 1973, Morris et al., 1978, Martinsen et al., 1989, Draget et al., 1997, Sikorski et al., 2007).

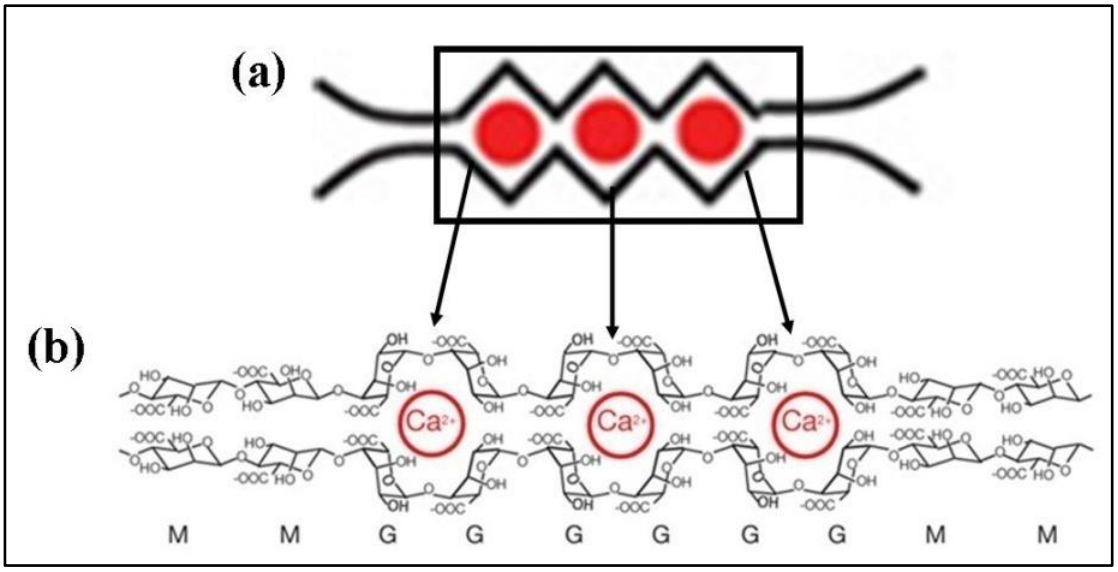

Figure 4.32. Alginate Polymer Formation by Ionic Crosslink through Calcium Ions
(a) Alginate egg-box model. Calcium ions indicted in red (b) Full alginate structure containing G and M blocks with Ca^{2+} ions cross linking two alginate chains. Image modified from Sun et al., (2012).

4.1.2 Cellular Immobilisation with Alginate

Alginates beads have been used as an *in vitro* model to mimic a 3D microenvironment for cell culturing in order to maintain cell phenotype compared to cell monolayers. Past studies have immobilised different cells types or biological agents in alginate constructs such as organelles (Kierstan and Bucke, 1977), enzymes (Kierstan and Bucke, 1977), yeast cells (Kierstan and Bucke, 1977, Cheetham et al., 1979), bacteria (Ohlson et al., 1979), plant cells (Brodelius et al., 1979), animal cells (Nilsson and Mosbach, 1980), islet cells (Lim and Sun, 1980) and articular chondrocytes (Benya and Shaffer, 1982, Guo et al., 1989, Hauselmann et al., 1992, Grandolfo et al., 1993, Hauselmann et al., 1994, Mok et al., 1994, Kolettas et al., 1995, van Susante et al., 1995, Hauselmann et al., 1996) which share a common morphology and phenotype to NP disc cells (Sive et al., 2002, Richardson et al., 2010). The first published study on canine disc cells cultured in alginate microspheres was by Maldonado and Oegema (1992) to investigate their cellular metabolism up to 14 days. Since then other studies have used AF or NP disc cells from other species in order to investigate their responsive cellular functions such as genetic expression, matrix production, disc cell morphology, and mechanical load to understand the IVD cellular biology (Chiba et al., 1997, Hutton et al., 1999b, Melrose et al., 2000, Wang et al., 2001, Horner et al., 2002, Gaetani et al., 2008, Korecki et al., 2009, Chou and Nicoll, 2009, McCanless et al., 2011). Alginate is commonly used in cell encapsulation for cell differentiation and studying extracellular matrix (Ma et al., 2003, Melrose et al., 2000). The purpose of this chapter was to study the aggrecan molecules synthesised from cell seeded in alginate constructs with AFM. Before this can take place a modified aggrecan

isolation techniques was needed. Isolation procedures adapted from the previous chapter were modified with the addition of size exclusion chromatography to remove residual alginate fragments that would interfere with AFM imaging. Bovine NP cells were used as a model because of their availability and their fast expansion in culture.

4.2 Aims

- To assess the variability of manually produced alginate bead sizes to ensure there was no high variation between individual alginate beads which may affect aggrecan synthesis.
- To modify aggrecan isolation from alginate beads with the addition of size exclusion chromatography to separate aggrecan molecules from residual alginate fragments for AFM imaging.

4.3 Experimental design

4.3.1 Alginate Bead Preparation for Size Determination

The purpose for this experiment was to monitor the size variability between individual alginate beads that were produced manually. A high alginate bead size variability will affect cell density and this in turn may influence matrix production, importantly aggrecan synthesis.

1.2% alginate solution (0.15M NaCl + 25 mM HEPES solution (Singh et al., 2011)) was prepared from alginic sodium salt mixed with NaCl and HEPES with low heat (40°C) for 3 hours. Once the solution was cooled to room temperature, the pH was adjusted to pH 7.4 then autoclaved. For cell culturing purposes solutions, 0.15M NaCl and 102 mM $CaCl_2$ were autoclaved for sterilisation.

Alginate solution (1 ml) was transferred to a 5 ml syringe and slowly injected drop by drop with a 21G needle into a 50 ml falcon tube filled with 102 mM of $CaCl_2$ where the needle was in close proximity to the calcium solution by gently turning the tube to break the surface tension to form a tear shape. The resulting beads were mixed on a roller for a further 10 minutes and washed three times with 0.15 M NaCl for 3 minutes each. This was performed in triplicate.

Afterwards, the 0.15M NaCl was discarded. Each separate 50 ml falcon with 1 ml of alginate beads (50-70 beads) were placed and distributed into three separate six well plates with 3 mls of 102 mM $CaCl_2$ in each well. The beads were moved to the centre of the well

where each well was photographed (courtesy of the Photographic Unit, University of Manchester). ImageJ was used to calculate the area (mm^2) of each alginate bead (See appendix figures 7.49 and 7.50 for more details).

4.3.2 Bovine NP Cell Expansion

Bovine NP cells were harvested from bovine caudal (tail) discs (age range 18-36 months) (Staffordshire Meat Packers LTD, Stoke-on-Trent) and stored in a cell bank provided by Regenerative Medicine, Centre for Tissue Injury and Repair. Further details on extracting bovine NP cells are found in Minogue et al., (2010).

One millilitre of bovine NP (~$1x10^6$) cells were immediately placed in a T-75 cell culture flask containing 12 ml of standard media (sterile filtered with a 0.2 µm filter into a autoclaved 500 ml Duran bottle) which consisted of Dulbecco's Modified Eagle Medium (DMEM + high glucose+ L-alanyl-glutamine), 10% foetal calf serum (FCS), 1% penicillin, streptomycin, and amphotericin B solution, L-ascorbate acid (25 µg/ml), and sodium pyruvate (1 mM). Once the NP cells reached 70-90% confluence the media was removed and cells washed twice with 10 ml of PBS. The cells were trypsinised with 5 ml of trypsin for 5 min at 37°C. The flask was gently tapped to detach cells. The detached cells were split into three T-150 cell culture flasks containing 25 ml of warm media. The media was removed and changed every 2-3 days.

4.3.3 Cell Encapsulation into Alginate Beads

Once the bovine NP cells reached 80% confluence, cells were trypsinised and counted with a haemocytometer and adjusted to 6 x 10^6 cells/ml in 1.2 % alginate solution. The procedure for alginate bead formation was repeated as previously described. The beads were transferred via a sterilised spatula to a 6-well plate with 5 ml of warm media and incubated at 37°C with 5% CO_2 for 21 days. The media was changed every 2-3 days.

4.3.4 Isolation of Aggrecan from Alginate Constructs

Figure 4.33 depicts the modified procedures for isolating aggrecan from alginate constructs. All procedures were similar except the alginate beads were dissolved in EDTA-citrate buffer prior to GuHCl extraction.

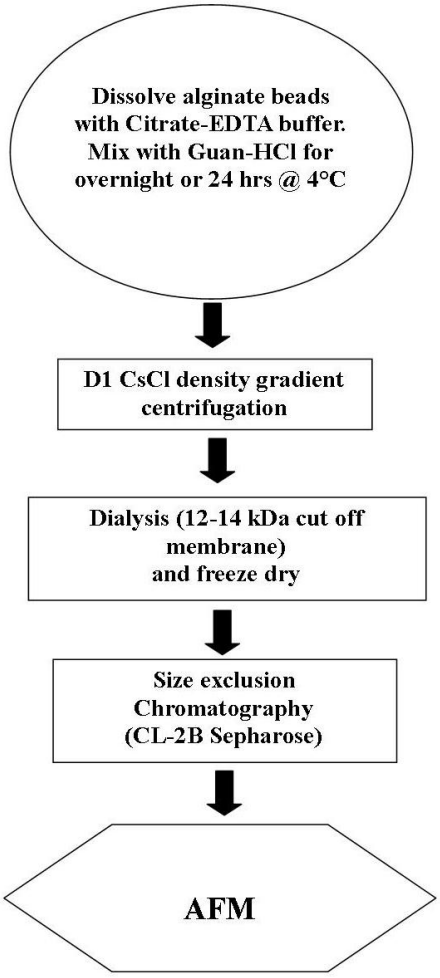

Figure 4.33. Aggrecan Isolation from Alginate Beads

Alginate beads were transferred by a sterilised spatula into a 15 ml falcon tube. Alginate beads were depolymerised by 0.5 ml of citrate-EDTA buffer (55 mM sodium citrate, 30 mM EDTA, 0.15 NaCl, pH 6.0) and incubated for 5 minutes at 37°C. Ice-cold extraction buffer (4.2M guanidine-HCl plus Protease Complete Tablets (Roche) pH 7.2) (11.5 ml) was added and mixed for overnight or 24 hours at 4°C. The resulting mixture was designated as the cell-alginate extract.

4.3.4.1 Dissociative CsCl Density Gradient Centrifugation (D1 fraction)

Procedures for a D1 CsCl density gradient centrifugation were detailed in Chapter 2 located at section 2.1.2.1 CsCl preparation and D1 fraction isolation.

4.3.5 Aggrecan Dot Blot

Procedures for aggrecan immunoblotting were detailed in Chapter 2 located at section 2.1.5 Aggrecan dot blot.

4.3.6 Size Exclusion Chromatography for Separating Alginate from Aggrecan Molecules

Size exclusion chromatography (SEC) was applied (Hauselmann et al., 1992, Mok et al., 1994, Sivan et al., 2006) where freeze dried pellet (D1 fraction) was resuspended in cold running buffer (1 mg/ml in 2ml) and size-fractionated (elution speed 0.5 ml/min) at room temperature by a Sepharose CL-2B column connected to an AKTA prime plus purification system (GE Healthcare). Protein was measured by an absorbance of 280 nm for each 1 ml eluted fraction resulting in a total of 70 fractions collected.

4.3.7 AFM Sample Preparation and Imaging

Procedures for sample preparation and AFM were detailed in Chapter 2 located at section 2.3.1 AFM sample preparation for tissue and section 2.3.2 General AFM imaging of aggrecan ultrastructure.

4.3.8 Statistical Analysis

Further details for data and statistical analysis were listed in Chapter 2 located at section 2.5 statistical analysis.

4.4 Results

4.4.1 Alginate beads size variability

Figure 4.34 depicts distributions of alginate bead area (mm^2) which were unimodally distributed for all plates. Plates 2 and 3 (figure 4.34c and d) showed a similar mean value of 3.8 ± 0.01 mm^2 and 3.8 ± 0.05 mm^2 and size range where plate 2 varied between 2.5-5.0 mm^2 and plate 3 fell within a similar range (2.0-5.0 mm^2). Plate 1 (figure 4.34b) had the lowest value at 3.5 ± 0.05 μm^2 however fell into the same range as plate 2 and 3. Statistical test (figure 4.34e) showed no difference between plate 2 and 3 ($p= 0.8097$) whereas plate 1 was found to be significantly different between plate 2 and 3 ($p<0.001$). Data indicated by figure 4.34b-d showed that manually produced alginate beads were consistent in size and variability was minimal as indicated by figure 4.34e.

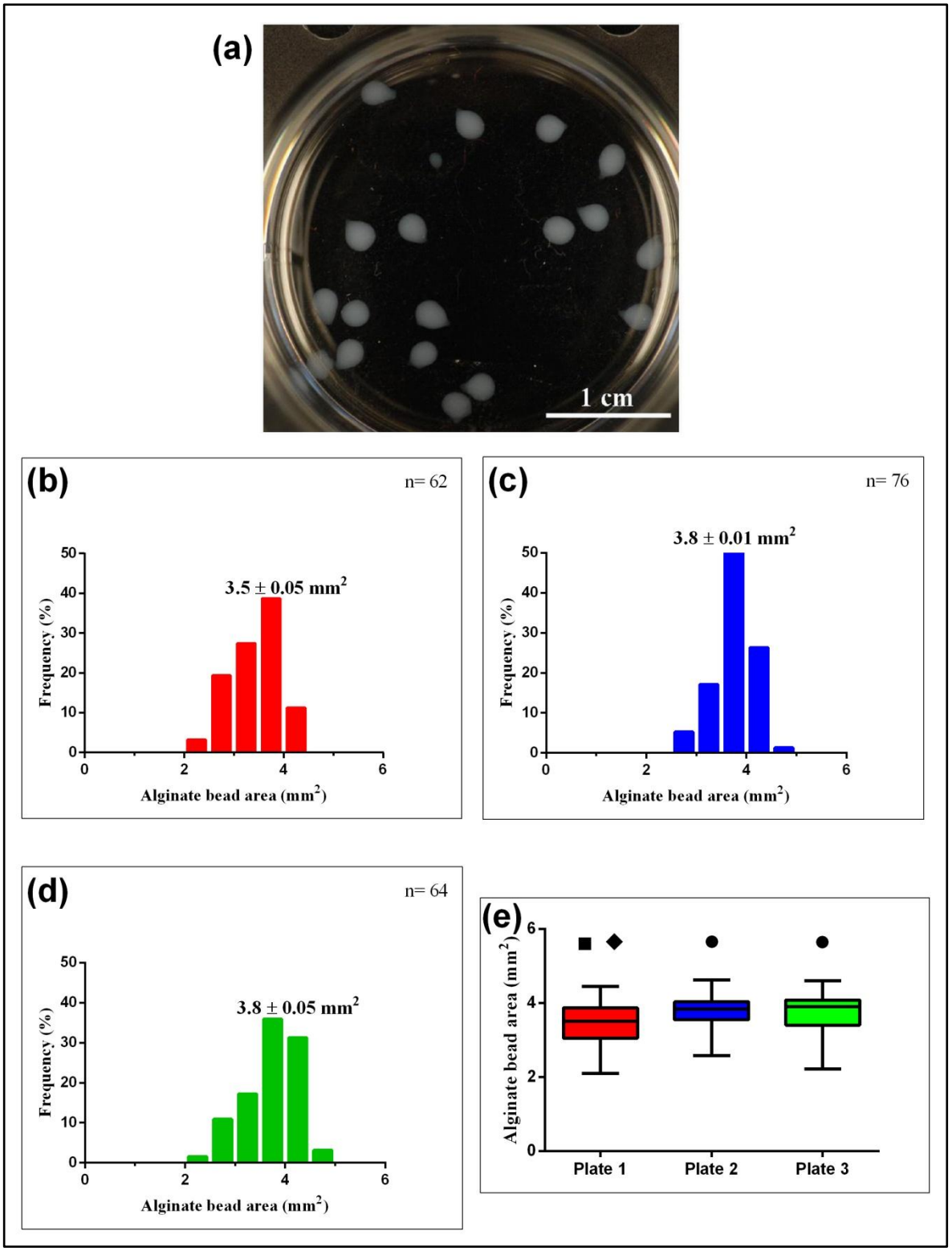

Figure 4.34. Alginate Bead Size.

One millilitre of alginate beads were injected into individual tubes of 102 mM $CaCl_2$ and placed in separate 6-well plates. The above graphs represent frequency count of bead area (mm^2) for each plate. (a) A well of tear shaped alginate beads. (b) Plate 1 (c) Plate 2 (d) Plate 3 (e) Box and whisker plots of alginate bead size (mm^2) of plate 1, 2, and 3. ●= vs. Plate 1 ($p< 0.0001$) by Mann-Whitney test; ■= vs. Plate 2 ($p< 0.0001$) by Mann-Whitney test; ♦= vs. Plate 3 ($p< 0.0001$) by Mann-Whitney test. All data was represented as mean ± SEM.

4.4.2 NP Cells Synthesise Aggrecan in 3D Alginate Cultures

Figure 4.35 show that alginate cell culture was positive for aggrecan on dot blots incubated with anti-aggrecan bovine/human antibody as previously observed in bovine NP tissue. It should be noted that the anti-aggrecan bovine/human antibody was indicative of aggrecan from tissue however it was also found indicative of aggrecan derived from alginate constructs.

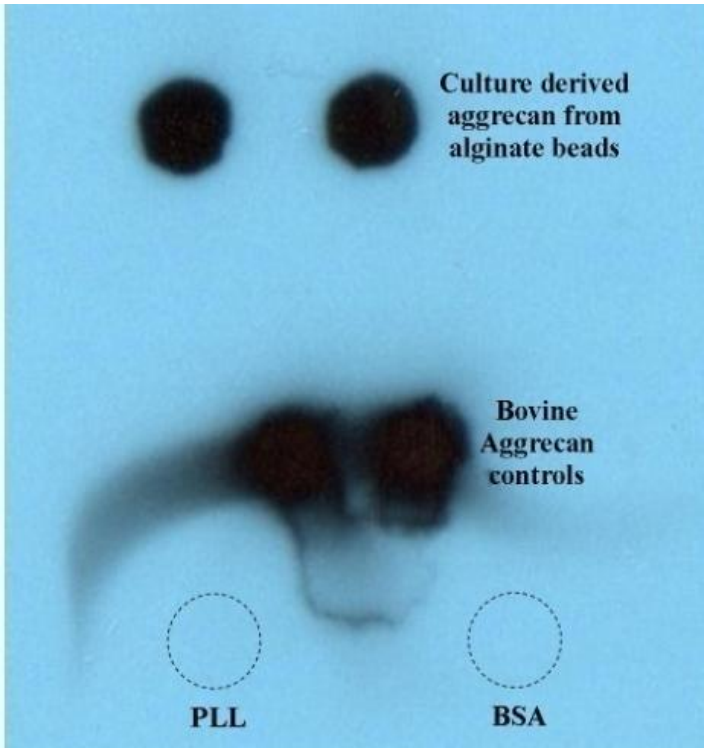

Figure 4.35. Aggrecan Dot Blot

Bovine aggrecan extracted from bovine NP cells cultured alginate beads for 21 days under standard media conditions. Dot blot was done in duplicate to confirm the presence of aggrecan synthesised in alginate beads. All samples except BSA were bound to PVDF blotting paper via PLL. Aggrecan control sample= bovine AC (2 µg) (Sigma). PLL= poly-L-lysine (blank); BSA= bovine serum albumin (negative control; 0.3µg).

4.4.3 Aggrecan Obtained by Size Exclusion Chromatography

D1 fraction (pooled fractions and freeze dried) isolated from NP cell-seeded alginate beads were chromatographed on a Sepharose CL-2B column under non-reducing conditions. An elution profile (figure 4.36a) was produced from the resulting eluted 70 fractions as two peaks; a high molecular weight peak (V_0) and a low molecular weight peak (V_t), and the area between Vo and Vt known as Vi (intermediate molecular weight peak). AFM height images (figure 4.36b-g) of fractions from V_0, Vi, and V_t presented a population of different sized alginate molecules where V_0 (figure 4.7b and c) contained high molecular weight long linear alginate polymers exceeding 1 µm in length whereas V_t (figure 4.36f and g) contained short linear fragments. Vi contained a intermediate size alginate fragments for

fraction 34 with high abundance (figure 4.36d) however aggrecan molecules were observed in fraction 36 as illustrated in figure 4.36e.

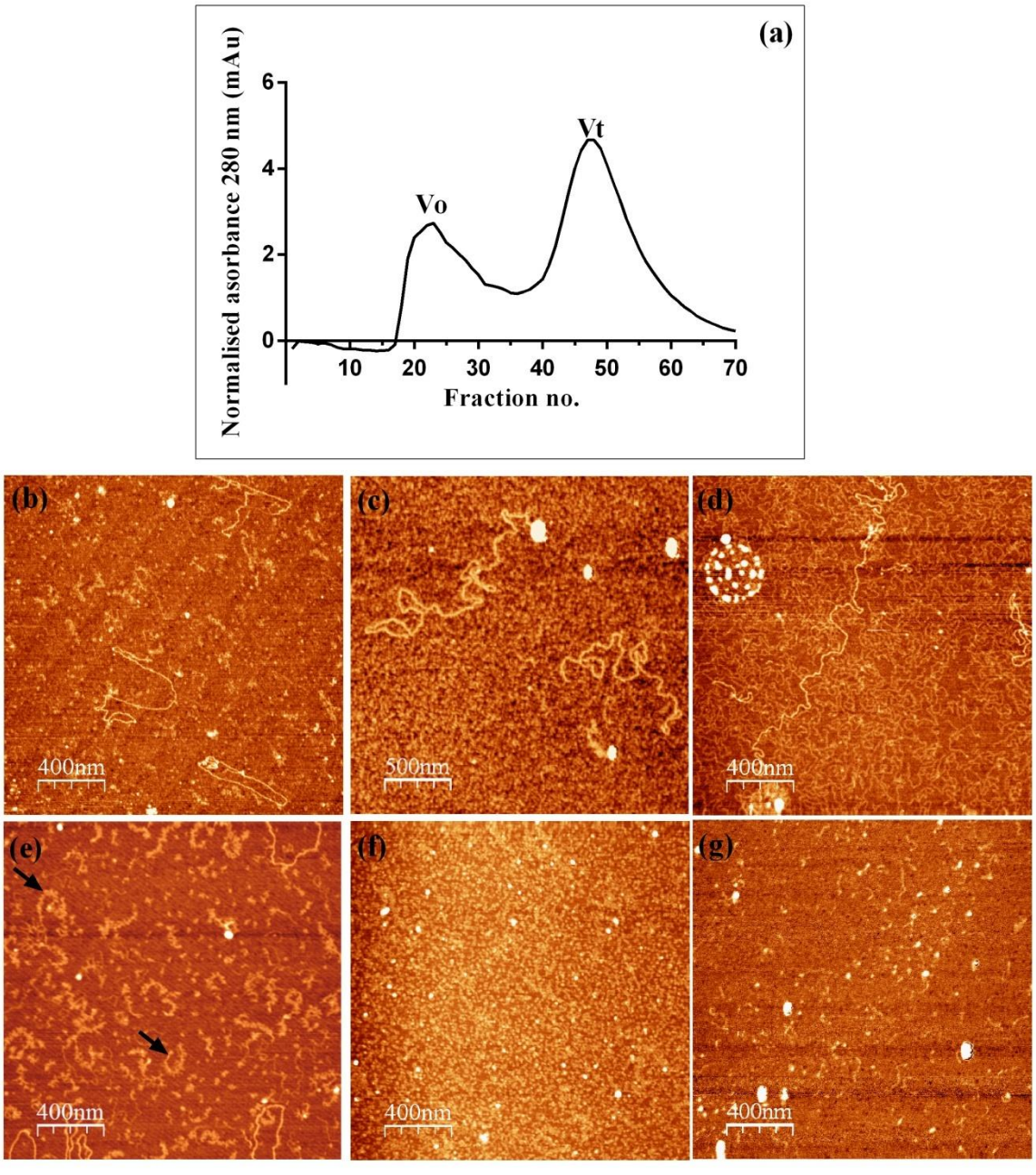

Figure 4.36. Isolation of Aggrecan from Alginate.
(a) Size exclusion chromatography elution profile. V_o represent the high molecular weight molecules containing the large alginate fragments and V_t represents low molecular molecules containing smaller. (b) Fraction 19 (Vo) (c) Fraction 23 (Vo). (d) Fraction 34 (Vi) (e) Fraction 36 (Vi). Aggrecan molecules indicated by black arrows. (f) Fraction 49 (Vt). (g) Fraction 57 (Vt). [Height scale=2.0 nm]

4.4.4 Aggrecan Synthesised by NP Cells in 3D Culture can be Imaged by AFM

AFM imaging revealed similar aggrecan molecules as previously observed from bovine NP tissue (figure 4.37a and b). A CP structure was observed along with side chains resembling a bottle structure (figure 4.37b). In some aggrecan structures a globular domain

was distinguishable as indicated in figure 4.37b. Aggrecan was found to be in a abundance whereas alginate was found in low in abundance. Alginate was found sufficiently distinct in appearance to ensure that aggrecan and alginate were not confused with each other.

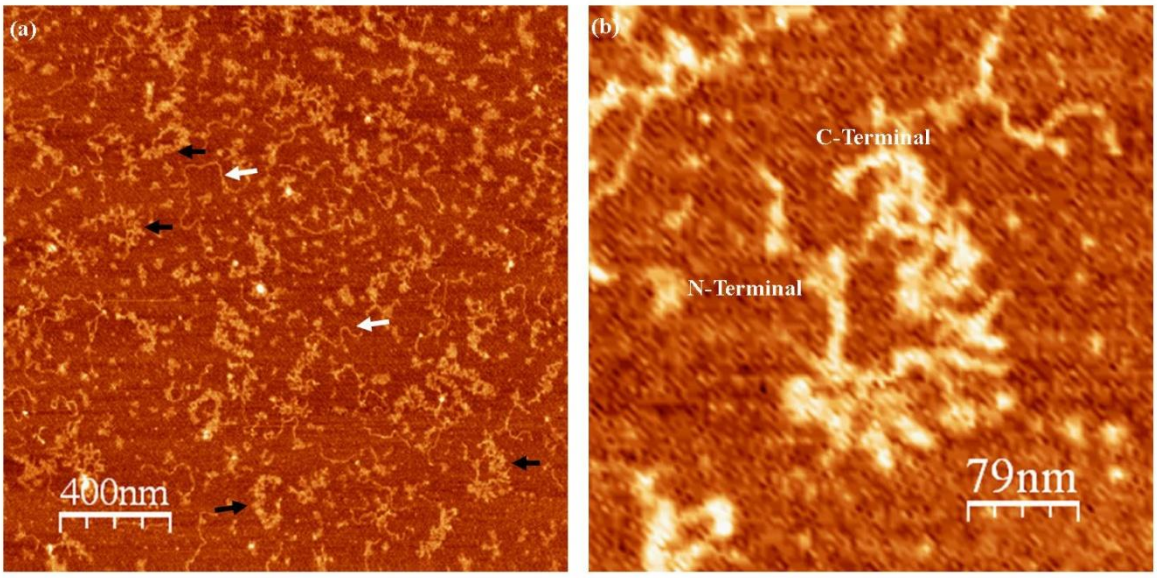

Figure 4.37. Aggrecan Isolated from Bovine NP Cells Embedded in Alginate Beads
Intermittent tapping mode AFM height images. (a) Size fractionated aggrecan population (fraction 36; black arrows) from 21 day cell culture with small alginate fragments (white arrows)which appear as thin long linear structures around the surrounding APTES-mica surface (2µm x 2µm scan). [Height scale =2.0 nm] (b) Culture derived full-length aggrecan monomer with N and C-terminals. [Height scale= 1.0 nm]

4.5 Discussion

4.5.1 Manual Formation of Alginate Beads Lead to Low Size Variability

Alginate beads in this study were produced manually and not by mechanical automation which could lead to a variation in alginate bead size. High variation in alginate bead size could influence the amount of cells that are seeded in each bead. The variation of cell density could dictate cellular proliferation and extracellular matrix production due to the nutrient and oxygen gradient within the alginate bead microenvironment. Size distribution between all plates were unimodal and plate 2 and 3 (3.8 ± 0.01 mm^2 and 3.8 ± 0.05 mm^2) showed no difference in size ($p=8097$) whereas there was some variation according to plate one (3.5 ± 0.05 mm$^{2;}$ $p<0.001$). Other groups have used automated methods to produce alginate beads or spheres whereas in this study manual methods were used which found that alginate bead size was relatively invariant.

4.5.2 Isolated Aggrecan from Alginate Cell Culture

Alginate fragments from SEC were still present and interfered with standard DMMB (Halle et al., 1993) and BCA assays (data not shown) therefore aggrecan quantification was not possible. This is due to the anionic COO^- groups from ά-L-guluronate of the alginate polymer chain which reacts with both assay dyes without the presence of GAGs and proteins. Evidence of the isolation of aggrecan has been reported in this section by; (1) antibody detection; (2) AFM imaging that allowed the visualisation of aggrecan bottle brush structures in detail revealing a central core protein and densely packed GAG chains confirming aggrecan isolation.

4.6 Conclusion

The application of alginate in cellular encapsulation allowed easy gel preparation independent of temperature and mimics the three-dimensional environment of tissue. Statistical analysis of alginate bead size revealed that manually processed beads were found to be relatively invariant. The encapsulation of bovine NP cells in alginate constructs cultured for 21 days showed evidence of aggrecan synthesis by immunoblotting. This was confirmed by AFM where aggrecan nanostructure moieties such as core protein and GAG chain could be seen as previously described in Chapter 3. In addition to these findings size exclusion chromatography was found sufficient in removing residual alginate fragments to allow the visualisation of aggrecan from alginate.

Chapter 5

Aggrecan Ultrastructure in Tissue Engineered NP Cell Seeded Constructs

5.1 Introduction

5.1.1 Growth factors

Transforming growth factor beta (TGF-β1, 2, and 3) are a group of growth factors known to alter IVD homeostasis by shifting cellular metabolism to an anabolic state (Masuda, 2008). In terms of disc cells they are known to increase proteoglycan synthesis (Thompson et al., 1991, Risbud et al., 2006, Abbott et al., 2012). In general, this is due to the stimulating signal pathways for GAG biosynthesis (or GAG elongation) (Schonherr et al., 1993, Little et al., 2008). Past studies have reported that TGF-β increases proteoglycan synthesis (Risbud et al., 2006) however only a limited number of studies have actually looked at the ultrastructure of proteoglycans (aggrecan) when cells are cultured with TGF-β (Kopesky et al., 2010, Lee et al., 2010). In this chapter human NP cells were seeded in alginate constructs and cultured for 21 days in standard or chondrogenic media with TGF-β3. Using previous aggrecan isolation techniques from Chapter 3 and 4, aggrecan molecules were separated for AFM imaging and compared to aggrecan derived from bovine NP tissue.

5.1.2 Gene expression

Quantitative real-time polymerase chain reaction (q-RT-PCR) was used as an additional method to confirm if aggrecan gene expression was evident during cell culturing in alginate in both standard and chondrogenic media. NP cells have been described as chondrocyte-like cells (Trout et al., 1982), but differ to articular chondrocytes (Mwale et al., 2004). However NP cells do express the chondrocyte ECM genes (aggrecan (ACN), type II collagen (COL2), type I collagen (COL1), and versican (VCN)) (Sive et al., 2002, Minogue et al., 2010).

5.2 Hypothesis

As mentioned before, studies have shown aggrecan synthesised from seeded hydrogel scaffolds form foetal-like ultrastructure making them biomechanically superior. Therefore in this study it was hypothesised that IVD disc cells (adult mature human NP cells in particular) seeded into a hydrogel would synthesise aggrecan with a ultrastructure similar or enhanced to that found in NP tissue and that media conditions would influence structure.

5.3 Aims

- Assess the ultrastructure of aggrecan derived from human NP cells seeded in alginate beads and cultured in standard media conditions to analyse whether the aggrecan was similar in structure to that isolated from native tissue.
- Assess the ultrastructure of aggrecan derived from human NP cells seeded in alginate beads and cultured in media with transforming growth factor beta 3 (TGF-β3) to assess whether growth factors influence the ultrastructure of aggrecan .
- To compare the aggrecan ultrastructure from native NP tissue to aggrecan from alginate constructs.

5.4 Experimental design

5.4.1 Human NP Cell Expansion

Non-degenerate human IVD tissue from one male donor aged 36years (table 5.2) was collected at the time of post-mortem examination (within 18 hours of death), with the consent of relatives of the deceased (Ethic no.: 05/MRE04/3). Human NP cells were harvested as previously described (Richardson et al., (2012) and stored in a tissue bank operated by Regenerative Medicine, Institute of Inflammation and Repair

Sample no	Source	Grade*	Sex	Age (years)	Disc level**
PM16	Post-mortem	2	male	36	L1/2

Table 5.2. Sample details

= Histological changes in the tissues were graded on a scale of 0–12, where 0–3 nondegenerate, 4–7 mildly degenerate, and 8–12 severely degenerate according to published criteria (Sive et al., 2002). The above sample was therefore considered as nondegenerated. *= L1/2 is the lumbar disc level of the spine and the disc level from which NP cells were extracted**

Human NP cells were thawed and transferred to a T75 vented flask under standard media conditions (see appendix). Once the NP cells reached 70-90% confluence cells were split and further expanded in T-150 vented flasks and media was changed every 2-3 days.

5.4.2 Human NP Cell Encapsulation into Alginate beads

Human NP cells were seeded in alginate beads as previously described in Chapter 4 except 4 x 10^6 cells/ml were mixed in 1.2% alginate solution for each six well plate (30-70 beads per plate). This was done in duplicate. Cells seeded alginate beads were distributed evenly in six wells and cultured in 4 ml standard media or chondrogenic media at 37^0C. Media was changed twice a week.

5.4.3 Isolation of Aggrecan from Alginate Beads for AFM Imaging and Gene Expression Analysis

A set number of alginate beads were set aside for AFM imaging (~30 beads) and gene expression analysis (20 beads). Alginate beads were dissolved (as described in Chapter 4) and aggrecan extracted from a D1 CsCl density centrifugation as previously described (Chapter 2).

Alginate beads for gene expression analysis were transferred to a 1.5 ml eppendorf tube and 450 µl TRIzol added together with 50 µl of molecule grinding resin and grounded with a micropestel. A further 500 µl of TRIzol was added to the tube and incubated at room temperature (RT) for one minute and stored at -80°C for extraction of RNA. For details of procedures for RNA extraction, reverse transcription to cDNA, and real time quantitative polymerase chain reaction were listed at Chapter 2 section 2.6.1

5.4.4 Size Exclusion Chromatography

Top peak void volume fraction was obtained from SEC (SM= F19, CM= F19, and bovine NP tissue= F20) and used for AFM imaging and immunoblotting. Fractions were refrigerated at 4°C and used within seven days. Selected fractions were aliquoted into 100 µl and stored at -80°C. Procedures for SEC were listed in Chapter 4 section 4.3.6.

5.4.5 Identifying Fractionated Aggrecan with Immunoblotting

Every fourth fraction including the top peak of Vo, intermediate (if present), and Vt from SEC were subjected to aggrecan dot blotting as described in Chapter two section 2.1.5 were quantified by BCA for protein content and a known protein concentration (2 µg/ml) was used.

5.5 Results

5.5.1 Size Exclusion Chromatography and Immunobloting

5.5.1.2 D1 Isolated Aggrecan from Bovine NP Tissue

Due to difficulties in obtaining mature normal (non-degenerate) human NP tissue, bovine NP tissue was used as an alternative. As aggrecan was extracted and purified from alginate beads seeded with human NP cells by GuHCL extraction followed by D1 CsCl density gradient centrifugation and size exclusion chromatography it was necessary for bovine NP tissue derived aggrecan to be isolated in the same manner so that data was comparable.

Figure 5.38a illustrates the SEC elution profile of bovine NP tissue (D1 fraction). The void volume (Vo) peak was observed with the highest absorbance followed by Vi. The Vo peak indicated the presence of eluted high molecular weight material whereas the Vi represented eluted intermediate molecular weight material. The Vt is known to contain small eluted molecular weight material however this peak was almost non-existence indicating a predominant presence of eluted high and intermediate molecular weight material from bovine NP tissue. In order to localise the presence of aggrecan, fractions from the Vo, Vi, and Vt positions were screened by aggrecan dot blot analysis. Figure 5.38b shows the presence of aggrecan in fractions F18 to F58 with greater dot intensity seen predominantly in Vo fractions (F18-22).

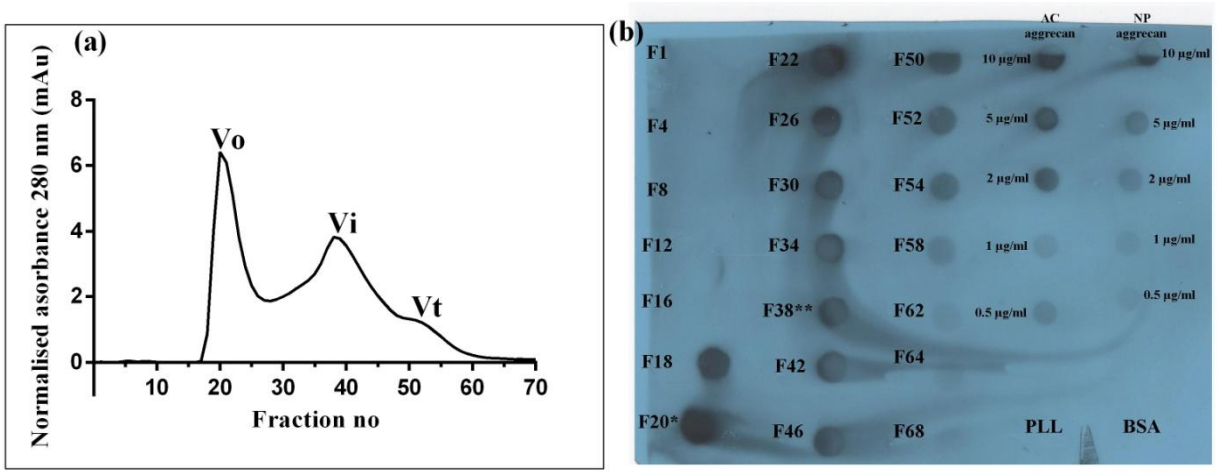

Figure 5.38. SEC and Aggrecan Immunoblotting of D1 Isolated Bovine NP Tissue
(a) SEC elution profile of bovine NP tissue (D1 fraction). (b) Aggrecan dot blot analysis containing selected eluted fractions. AC= Aggrecan control (bovine AC control); NP= Aggrecan control (bovine NP tissue extract); PLL= poly-L-lysine (blank); BSA= bovine serum album (0.3 µg) (negative control). *= Vo; **= Vi

5.5.1.3 Aggrecan Isolated from Human NP Cells Seeded in Alginate

NP cells were seeded in alginate and cultured in standard (SM) or chondrogenic media (CM) for 21 days. SEC was applied to remove residual alginate fragments from aggrecan molecules for subsequent AFM imaging. Assessment of both SM and CM SEC elution profiles (figure 5.39a and c) showed that there were a number of similarities and differences. The similarities found were that the Vo and Vt fractions eluted at the same fraction position (F19 and F52 respectively). The differences were that the SEC elution profiles of SM contained all three peaks (Vo, Vi, and Vt) whereas the profiles of the CM only produced two distinguishable peaks (Vo and Vt). In figure 5.39c, the absorbance of Vt peak for SM was higher compared to Vo indicating a higher presence of low molecular weight materials well as intermediate size material (Vi). The absorbance peak of Vo for CM was slightly higher compared to the Vt peak indicating an equal presence of large and small molecular size particles (figure 5.39c). Aggrecan dot blot analysis revealed the

presence of aggrecan was predominantly localised in the Vo region with both SM and CM fractions (figure 5.39b and d).

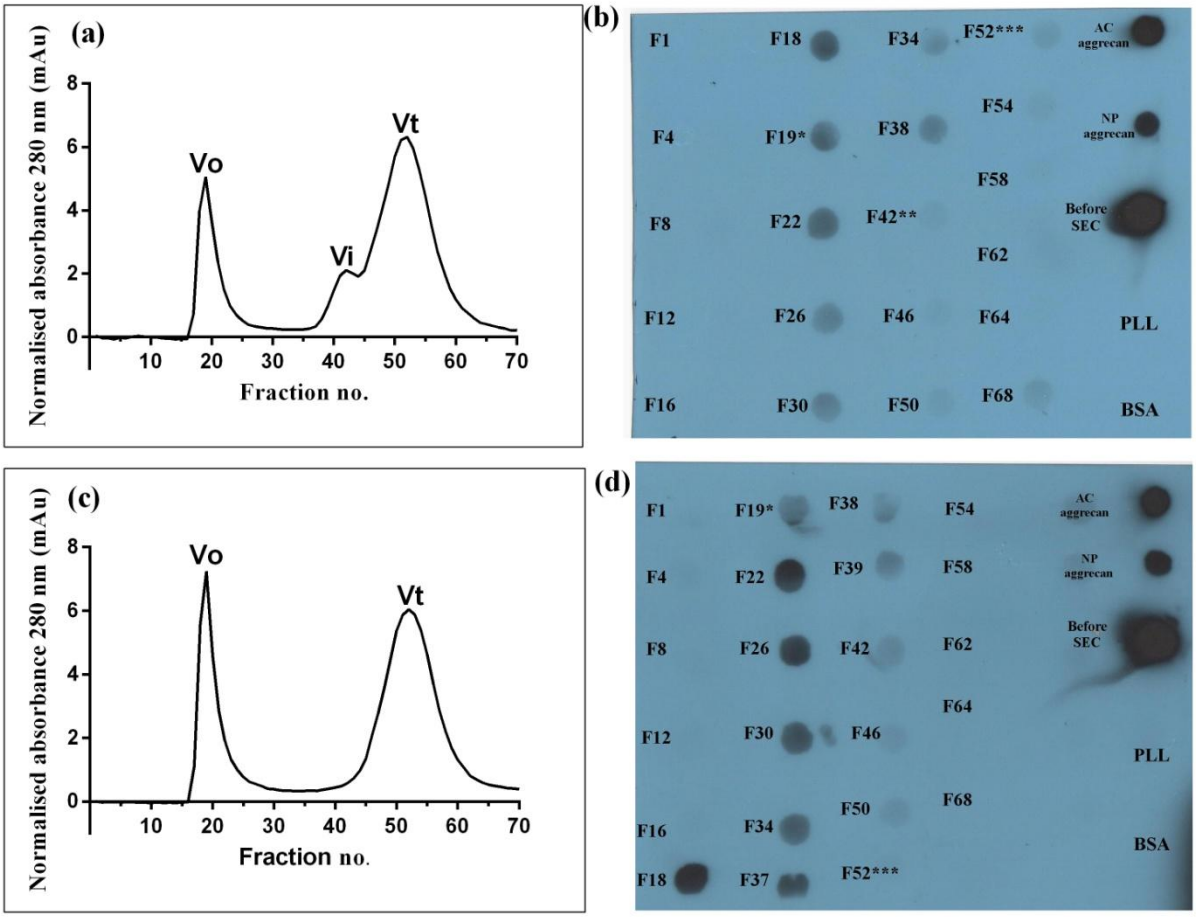

Figure 5.39. SEC and Aggrecan Dot Blot Analysis from Human NP Cells.
(a) Standard media SEC profile and (b) Standard media aggrecan dot blot analysis of selected eluted fraction from SEC. (c) Chondrogenic media SEC profile and (d) Chondrogenic media aggrecan dot blot analysis of selected eluted fraction from SEC. AC= Aggrecan control at 2µg/ml (bovine AC control); NP= Aggrecan control at 2µg/ml (bovine NP tissue extract); PLL= poly-L-lysine (blank); BSA= bovine serum album (0.3 µg) (negative control). *= Vo top peak, **= Vi top peak, and *= Vt top peak.**

5.5.2 Gene Expression

A set number of 20 alginate beads were collected from SM and CM cultures. The RNA was extracted and converted to cDNA for gene expression analysis for chondrocyte markers. Figure 5.40 depicts the results of quantitative real-time polymerase chain reaction (qRT-PCR) data of the relative gene expression of typical chondrocyte markers. All data for relative gene expression was normalised to the average of two housekeeping genes, glyceraldehyde-3-phosphate dehydrogenase (GAPDH) and mitochondrial 39S ribosomal protein L19 (MRPL19). Human NP cells cultured in CM showed a higher level of gene expression for all genes analysed compared to human NP cells cultured in SM.

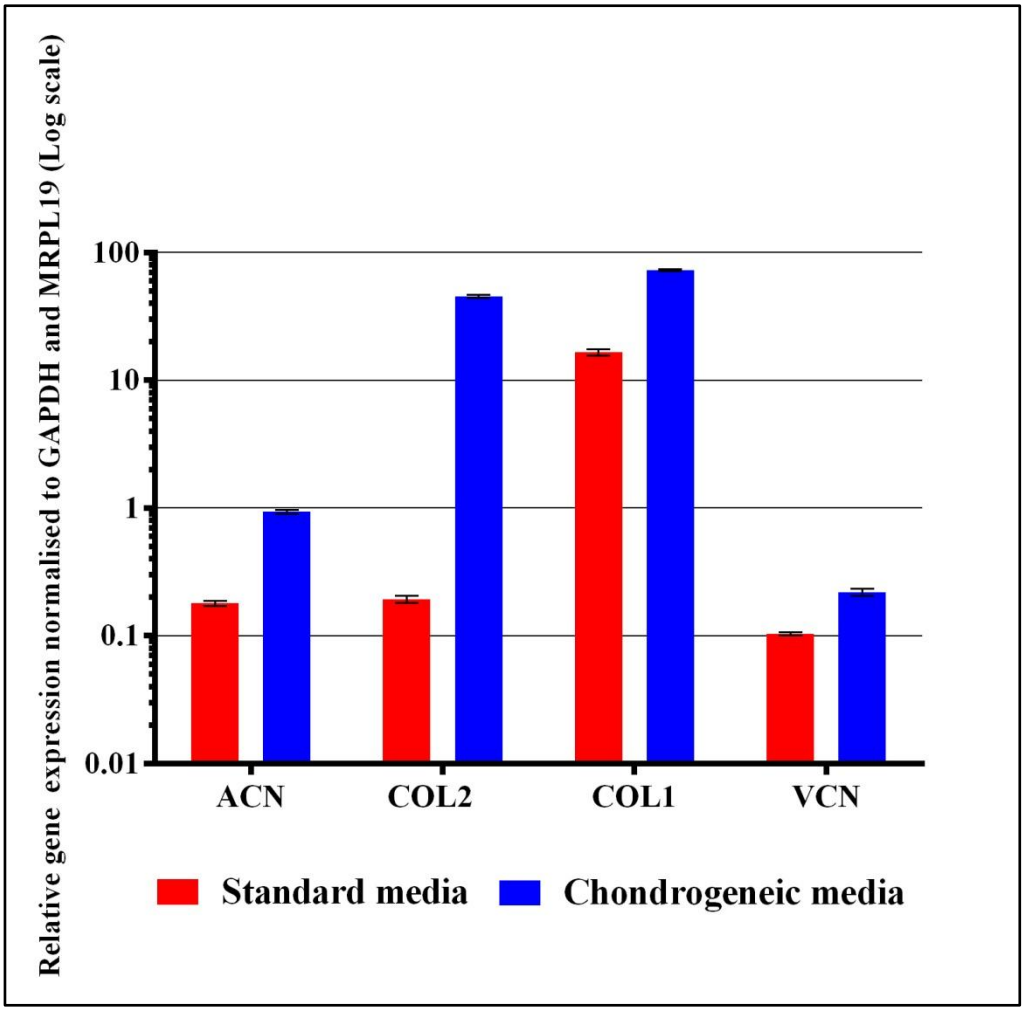

Figure 5.40. Chondrocyte Markers in Human NP Cells under Standard and Chondrogenic Media Conditions.

Human NP cells seeded in alginate and cultured under standard or chondrogenic media conditions for 21 days. qRT-PCR data for relative gene expression of chondrogenic marker (ACN, COL2, and VCN) normalised to housekeeping genes GAPDH and MRPL19. ACN= aggrecan, COL2= type II collagen, COL1= type I collagen, and VCN= versican.

5.5.3 AFM Imaging

5.5.3.1 Bovine NP Tissue

Bovine NP tissue was extracted by GuHCl, but purified as a D1 fraction with SEC. Aggrecan molecules from fraction 20, which was at the centre of the Vo peak (figure 5.41a), were selected for further AFM imaging. These molecules appeared as slender bottle brush structures (figure 5.41b) with a short GAG brush region. Aggrecan molecules with extended GAG chains were low in abundance. As previously observed with the D1D1 fraction (Chapter 3), there were a heterogeneous species of aggrecan molecules (figure 5.41a) with a low number (6%) of full-length monomers and a high abundance of non-intact aggrecan molecules (figure 5.41b).

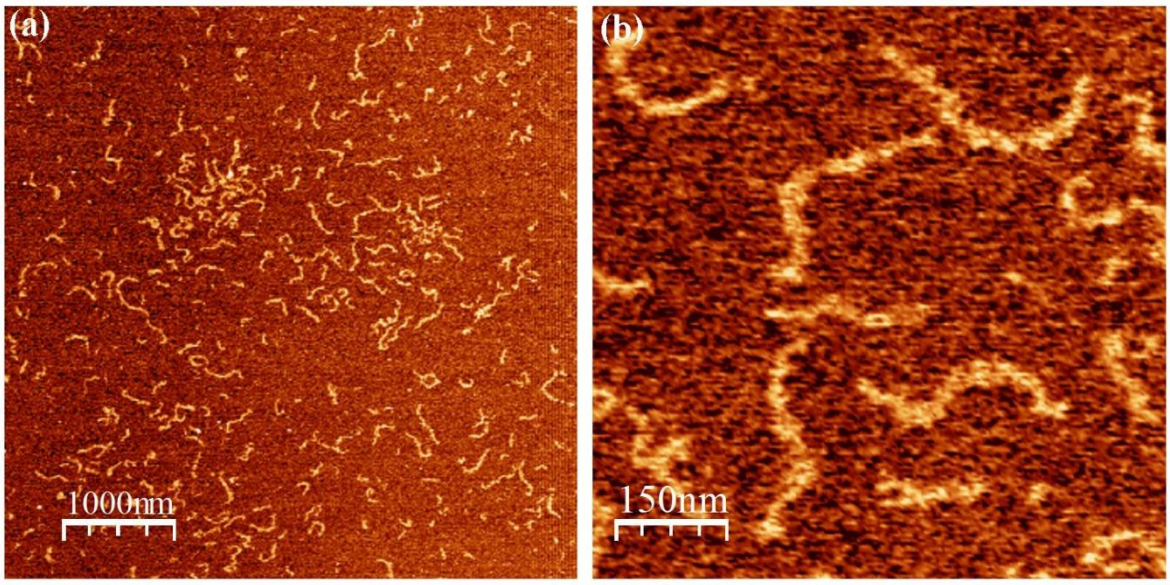

Figure 5.41. D1-SEC Isolated Aggrecan from Bovine NP Tissue.
(a) Aggrecan general species [height scale= 2.0nm]. (b) Non-intact aggrecan molecules with short GAG chains [|Height scale= 1.5 nm].

5.5.3.2 Human NP Cells

Human NP cells were expanded and cultured in alginate beads in SM or CM. Aggrecan isolated from human NP cells seeded in alginate was extracted by GuHCl as described previously but purified using a D1 CsCl density gradient centrifugation followed by SEC. The top peak Vo fraction (F19) was selected for AFM imaging for both SM and CM conditions. AFM imaging revealed aggrecan isolated from both culture conditions as the same bottle brush structure (core protein and GAG chains) as previously seen/reported in Chapter 3 and 4. However, there was a notable observation in that CS GAG chains were more extended in aggrecan isolated from alginate cultures in CM compared to aggrecan molecules isolated from SM (figure 5.42a and c). Aggrecan derived NP tissue (figure 5.42a and b) showed an opposite description where GAG chains were short in length however CP was long in length. It was also found that CM aggrecan species contained predominantly non-intact species (full intact brush region with no or one (partial or full) globular end on either N or C terminal end) with no observable full-length aggrecan monomers. The types of non-intact species observed with SM were mostly fragmented aggrecan molecules (figure 5.42a and b).

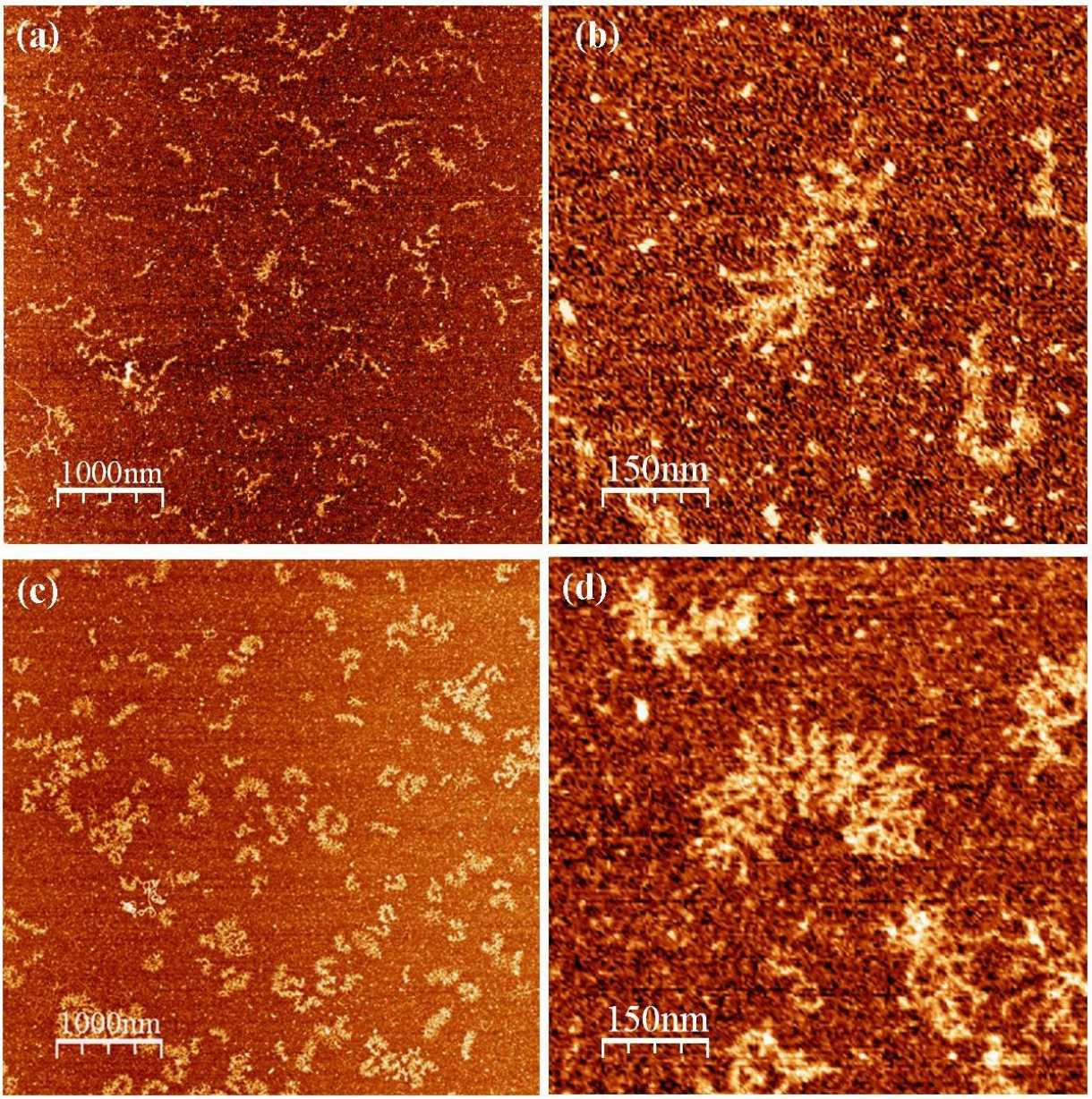

Figure 5.42. Aggrecan Isolated from Human NP Cells under Standard and Chondrogenic Media.

(a) Aggrecan general species of aggrecan cultured under SM conditions [Height scale = 2.0 nm]. (b) Fragmented aggrecan molecule isolated from alginate cultures under SM conditions [Height scale= 1.5 nm]. (c) Aggrecan general species of aggrecan cultured under CM conditions [Height scale = 2.0 nm]. (d) Fragmented aggrecan molecule with extended CS GAG chain isolated from alginate cultures under CM conditions [Height scale= 1.5 nm].

5.5.4 Aggrecan Dimensions

5.5.4.1 Bovine NP Tissue

Aggrecan dimensions, core protein contour length, GAG brush length, and GAG brush width were quantified as previously described in Chapter 2. The General species refers to all aggrecan observed (n= 300), non-intact species (n= 283) refers to all aggrecan molecules that are degraded or partially degraded, and full length (n= 17) are aggrecan monomers with their N and C terminal globular domains present.

CP length frequency distributions for all species (general, non-intact, and full length) were unimodal with no differences between general (367 ± 2 nm) and non-intact (366 ± 2 nm) species since the majority of aggrecan molecules existed as non-intact molecules (figure 5.43a and d). Only a small cohort (n= 17) of full-length aggrecan species (figure 5.43g) were found in bovine NP tissue. Full-length CP length was longer (449 ± 2 nm) compared to general and non-intact species with a limited range from 400 to 550 nm compared to general and non-intact species which had an extended range between 200-500 nm.

GAG brush length was found to be unimodal for all species. Both general (249 ± 4 nm) and non-intact (246 ± 4 nm) species were similar in brush length and range (100-400 nm) (figure 5.43b and e). Full-length monomers had a mean value of 300 ± 6nm with a variety of brush lengths that ranged between 200-450 nm (figure 5.43h).

GAG brush width was bimodal for all species. The predominant brush width size was 36 ± 0.5nm for both general and non-intact populations and a small species of aggrecan molecules with a wider GAG brush mean value at 56-57 ± 0.5nm (Figure 5.43c and f). Full-length aggrecan monomers showed a bimodal distribution of two sub-populations. However, there was no difference between general and non-intact populations since their GAG brush width range were similar to the full-length species (figure 5.43i).

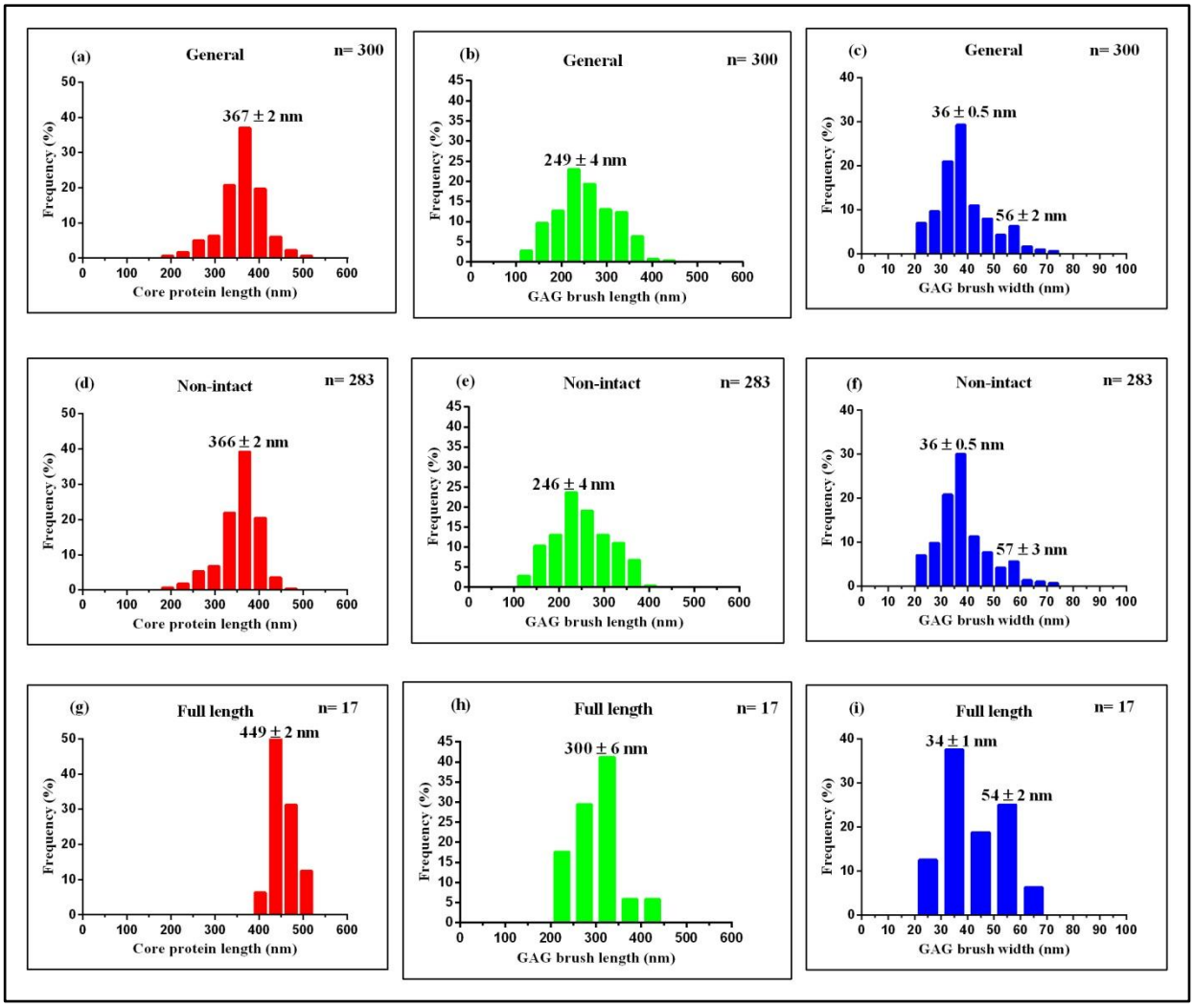

Figure 5.43. D1 Isolated Aggrecan Dimension from Bovine NP Tissue.
Aggrecan dimensions, core protein contour length (red), GAG brush length (green), and GAG brush width (blue) were quantified for general (a-c), non-intact (d-f), and full length (g-i) populations. All data was represented as mean ± SEM.

5.5.4.2 Human NP Cells Cultured in Standard and Chondrogenic media

Aggrecan was isolated from human NP cells seeded in alginate beads and cultured in SM or CM for 21 days. A similar number of alginate beads from SM (30 beads) and CM (28 beads) for AFM imaging were used. The aggrecan general species (n= 300) from SM and CM (n= 300) were predominantly non-intact with no full-length monomers identified. As a result the term SM or CM species will be used to describe both SM and CM aggrecan general species. Aggrecan dimension statistics (general species; figure 5.44a-c) from bovine NP tissue were included for comparison between SM and CM conditions.

The SM species for aggrecan CP length was unimodal similar to CM (figure5.44a and b). However, the mean CP length value for CM (376 ± 2 nm) was greater than the SM species (314 ± 2 nm). The length range for SM species ranged from 150 to 500 nm whereas the CM species had a different range starting from 200 to over 550 nm. The range differences

point towards the different CP length size of aggrecan molecules present in their respective populations. This indicates that SM species contained a smaller range of aggrecan molecules and fragments of CP length. However, CM species also showed a small presence of fragmented aggrecan molecules with CP length< 300 nm. Figure 5.44c SM and CM CP mean length were considered to be significantly different ($p<0.0001$). Aggrecan mean CP length of from NP tissue (367 ± 2 nm) was found to be longer compared to aggrecan species from SM, but shorter compared to aggrecan species from CM. Aggrecan mean CP length from NP tissue of general species was found to be significantly different between both SM (314 ± 2 nm; $p<0.0001$) and CM (376 ± 2 nm; $p=0.0018$) conditions.

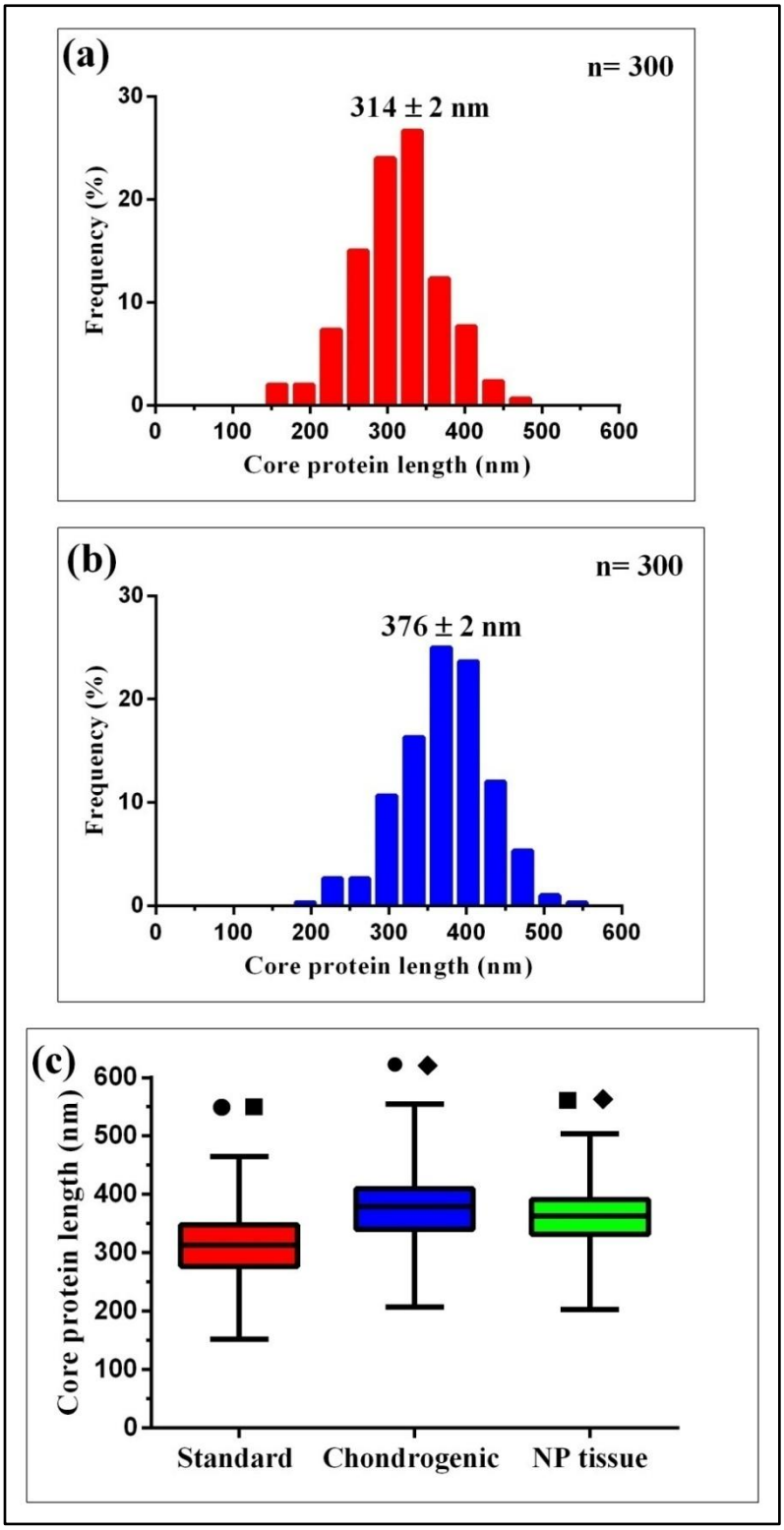

Figure 5.44. Aggrecan Core Protein Length Quantification.
(a) Aggrecan core protein length from human NP cells seeded in alginate and cultured in SM (n= 300). (b) Aggrecan core protein length from human NP cells seeded in alginate and cultured in CM (n= 300). (c) Box and whisker plots of parameter distributions of aggrecan CP length of SM, CM, and bovine NP tissue. ●= vs. tissue ($p< 0.0001$) by Mann-Whitney test; ■= vs. CM ($p< 0.0001$) by Mann-Whitney test; ♦= vs. SM ($p< 0.0001$) by Mann-Whitney test. All data was represented as mean ± SEM (a-b).

GAG brush length for both SM and CM populations were both found to have unimodal distributions (figure 5.45a and b). However, SM and CM species mean GAG brush length values were different in values (248 ± 3 nm and 290 ± 1 nm, respectively). The GAG brush length range between the SM and CM species were also different, where SM had a lower GAG brush length range from 100 to 400 nm compared to its counterpart, CM, which possessed a higher GAG brush length range (150-450 nm). GAG brush length of both SM and CM species were significantly different (248 ± 3 nm and 290 ± 1 nm; $p<0.0001$) (figure 5.45c). However, there was no significant difference between bovine NP tissue and SM (249 ± 4 nm and 248 ± 3 nm; $p=0.2864$) which have a similar mean GAG brush length values and brush length range (100-400 nm) (figure 5.45c).

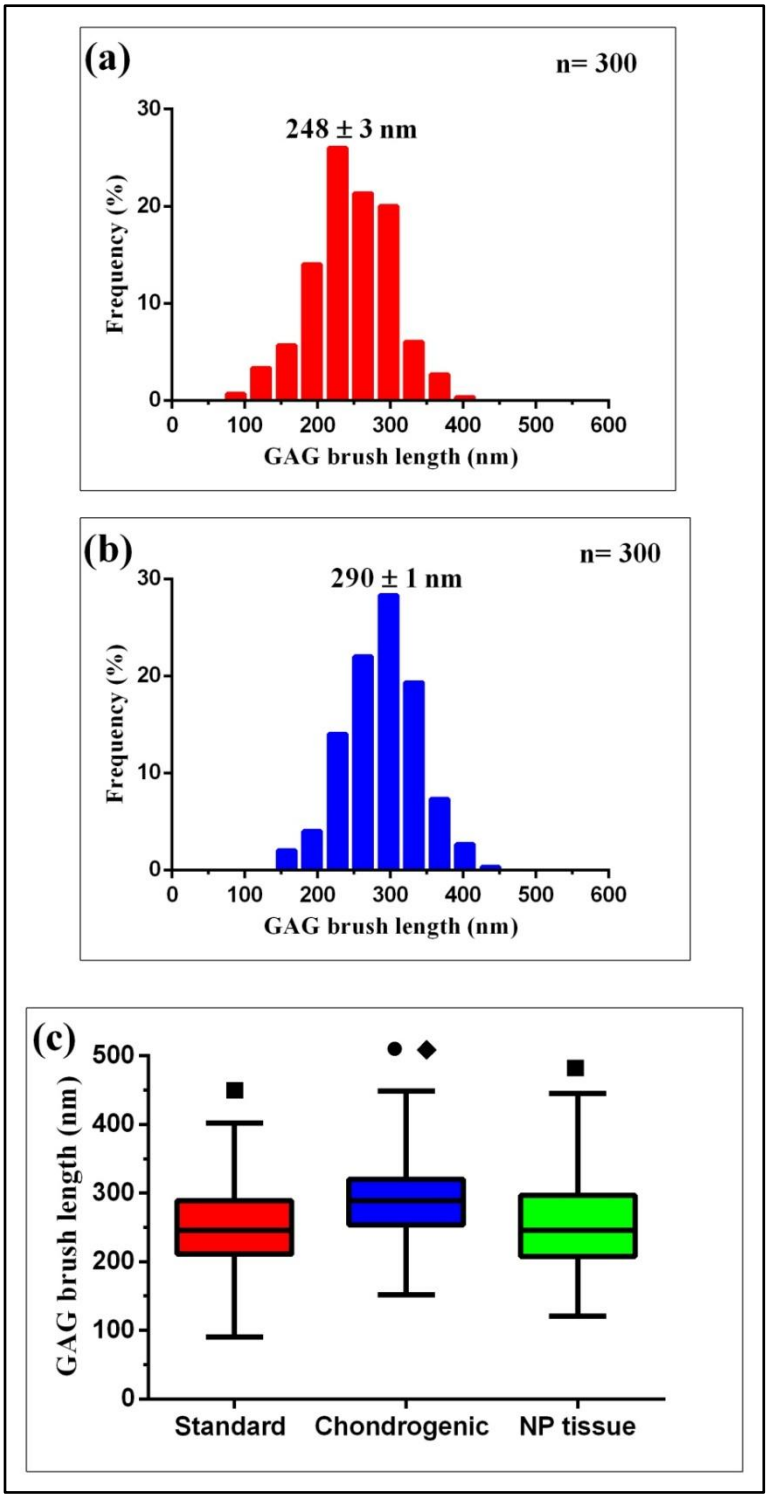

Figure 5.45. Aggrecan GAG Brush Length Quantification.
(a) Aggrecan GAG brush length from human NP cells seeded in alginate and cultured in SM (n= 300). (b) Aggrecan GAG brush length from human NP cells seeded in alginate and cultured in CM (n= 300). (c) Box and whisker plots of parameter distributions of aggrecan GAG brush length of SM, CM, and bovine NP tissue. ●= vs. tissue ($p< 0.0001$) by Mann-Whitney test; ■= vs. CM ($p< 0.0001$) by Mann-Whitney test; ♦= vs. SM ($p< 0.0001$) by a unpaired t-test since both distributions were parametric according to a Sharpio-Wilk normality test. All data was represented as mean ± SEM (a-b).

Figure 5.46c showed both GAG brush width of SM (49 ± 1 nm) and CM (57 ± 2 nm) with different mean GAG brush width values were significantly different ($p < 0.0001$). However, the data ranges for both groups were found to be similar from 20 to 120 nm. Figure 5.46a show the percentage of aggrecan molecules with a GAG brush widths less than 60 nm were found to be at 78.6% and the percentage of aggrecan molecules greater than 60 nm were 21.3%. The percentage of aggrecan molecules found in CM species with GAG brush width values less than 60 nm were 54.3% however the percentage of aggrecan molecules greater than 60 nm were found to be 45.6% which was 2 times more than the SM species (figure 5.46b).

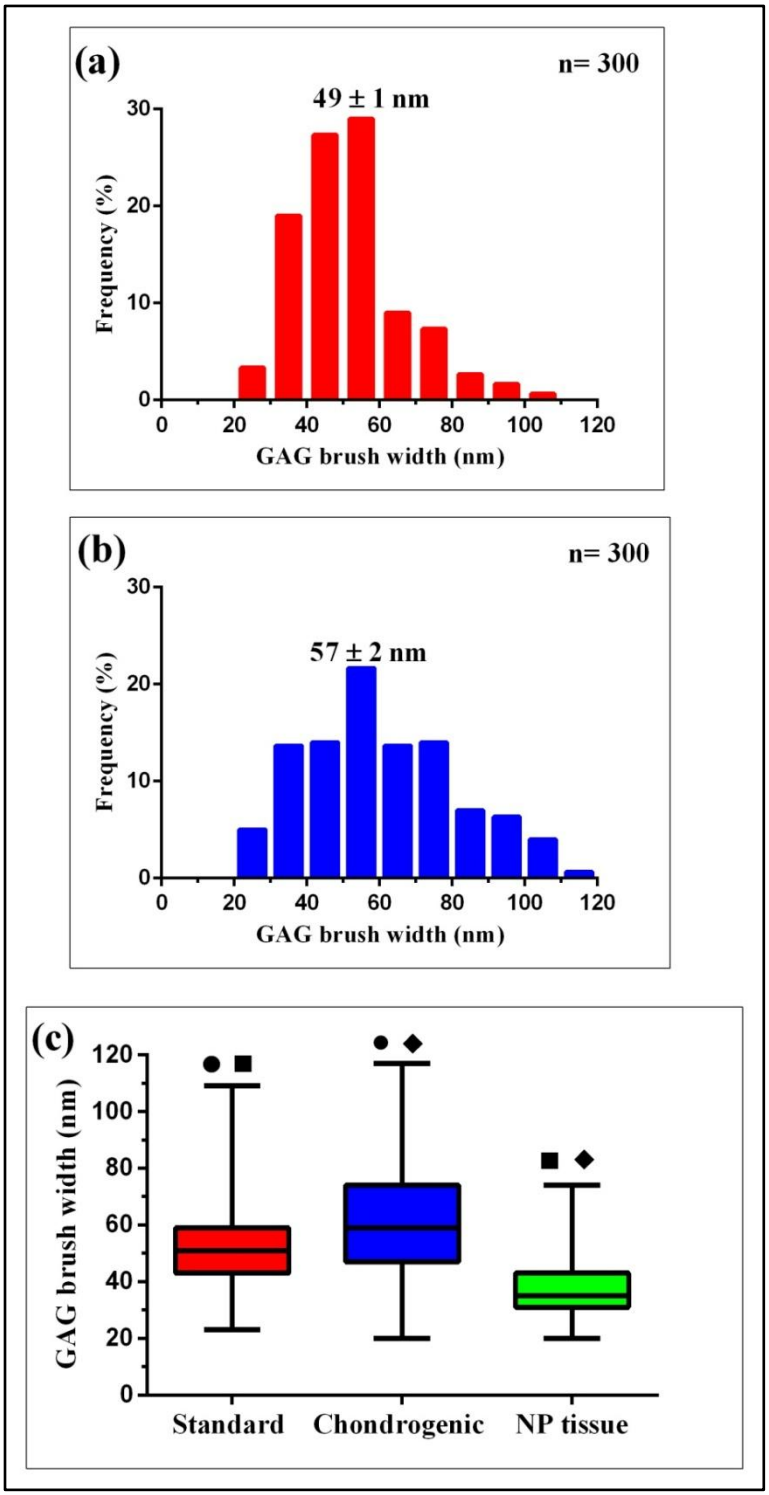

Figure 5.46. Aggrecan GAG Brush Width Quantification.
(a) Aggrecan GAG brush width from human NP cells seeded in alginate and cultured in SM (n= 300). (b) Aggrecan GAG brush width from human NP cells seeded in alginate and cultured in CM (n= 300). (c) Box and whisker plots of parameter distributions of aggrecan GAG brush width of SM, CM, and bovine NP tissue. ●= vs. tissue ($p< 0.0001$) by Mann-Whitney test; ■= vs. CM ($p< 0.0001$) by Mann-Whitney test; ♦= vs. SM ($p< 0.0001$) by Mann-Whitney test. All data was represented as mean ± SEM (a-b).

5.5.4.3 GAG Brush Width and Aggrecan Structural Changes

It has been proposed in previous studies that GAG chain extension may lead to aggrecan structural changes through extending CP length compared to those aggrecan molecules with a shorter GAG chain length (Morgelin et al., 1989, Ng et al., 2003, Lee et al., 2013). Aggrecan molecules cultured under CM conditions showed a significant increase in GAG brush width and CP length compared to SM and NP tissue. Figure 5.47a-c illustrates a set of graphs plotted with GAG brush width (nm) against CP length (nm) for SM, CM, and NP tissue (aggrecan general species). Figure 5.47d is a graph of full-length aggrecan from NP tissue. The correlation of coefficient (r) was calculated to find any correlation between aggrecan CP length and GAG brush width. Figures 5.47a and b showed SM and CM with positive r values indicating low levels correlation between CP length and GAG brush width. NP tissue indicated no correlation (-0.01) between CP length and GAG brush width found in the aggrecan general population. However, the full-length species on its own revealed a high r value (r= 0.5) compared to SM and CM suggesting a higher correlation with full-length aggrecan monomers (figure 5.47d).

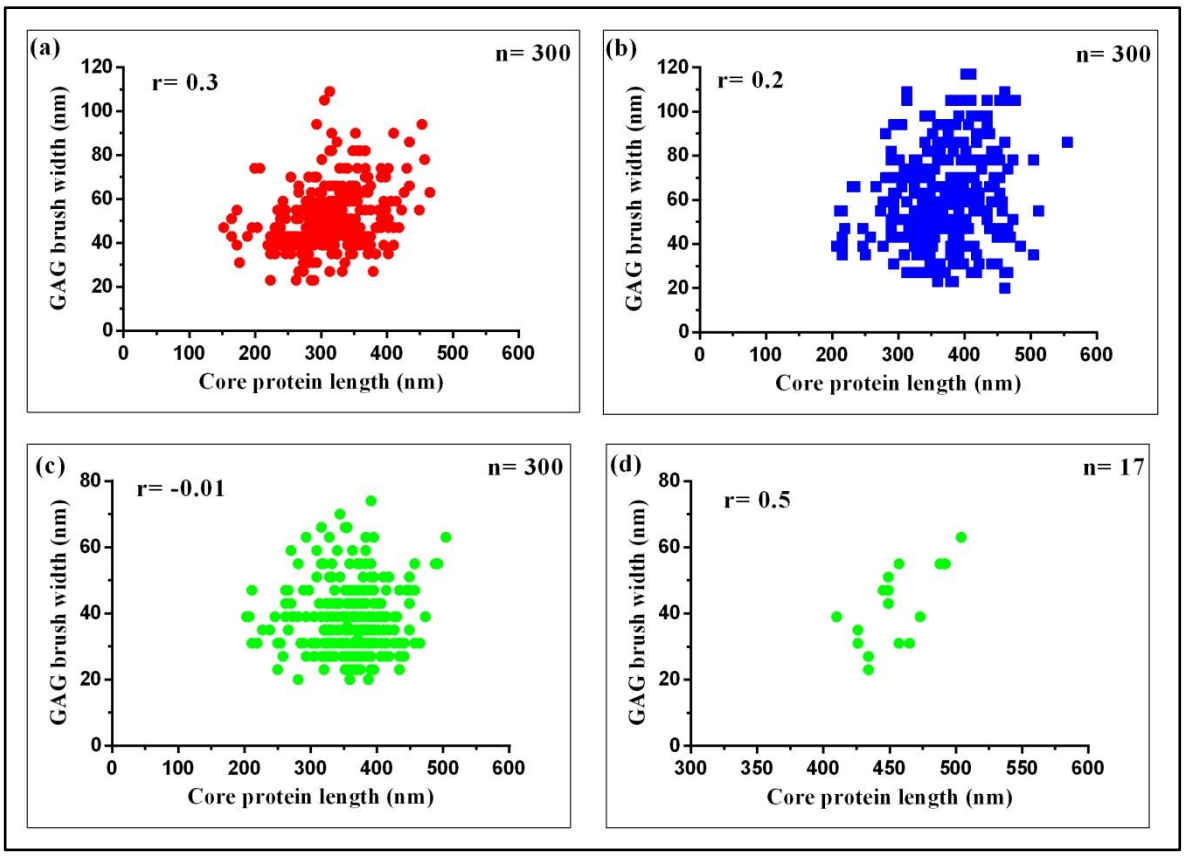

Figure 5.47. Correlation between Aggrecan GAG Brush Width and CP Length.
(a) SM aggrecan general population. (b) CM aggrecan general population. (c) Bovine NP tissue aggrecan general population. (d) Bovine NP tissue aggrecan full-length population. Correlation coefficient values (r) calculated from Spearman's ranking correlation.

5.6 Discussion

Human NP cells from the same donor were cultured in alginate under different media conditions (standard or chondrogenic media) to investigate the effect of growth factor on aggrecan ultrastructure. The scarcity of normal / healthy human NP tissue leads to the utilisation of bovine NP tissue instead as a reference model. Bovine NP tissue was prepared (aggrecan isolation techniques) in the same manner (except tissue was not dissolved in EDTA) as aggrecan isolated from human NP cells cultured in alginate.

Pre-existing techniques of extraction and purifying aggrecan as described in previous studies (Kopesky et al., 2010, Lee et al., 2010) and in Chapter 3 and 4 were applied to obtain aggrecan from cells seeded in constructs for subsequent AFM imaging. This entailed GuHCl extraction followed by a D1 CsCl density gradient centrifugation. The last stage of aggrecan purification was with SEC to remove any residual alginate fragments. According to the dot blotting analysis, the majority of eluted fractionated aggrecan was concentrated in the Vo position with both SM and CM samples eluting in the same fraction number (F19).

5.6.1 Aggrecan Gene Expression

Human NP cells are described as chondrocyte-like and express chondrocyte ECM gene markers (ACN, COL2, and VCN). Detection of these markers in NP cells cultured in alginate would indicate expression of these genes and point towards chondrogenesis i.e. extracellular matrix formation. The expression of chondrocyte markers were evident (especially under CM) that NP cells cultured in alginate retain chondrocytic gene expression. However, high expression of type I collagen was also observed and increased with chondrogenic media. Type I collagen is usually expressed in low levels in normal human NP cells and it is indicated as a sign of de-differentiation to a fibroblastic phenotype. However, this may not be the case since previous studies have reported that cells suspended in alginate have been shown to promote and prolong chondrocyte phenotype (Hauselmann et al., 1994, Mok et al., 1994, Lee et al., 2003). The high expression of COL1 could be due to the human NP cells undergoing a prolonged expansion and cell passage on a 2D surface prior to seeding in alginate where they do retain some fibroblastic phenotype even after redifferentiation in alginate beads (Darling and Athanasiou, 2005, Hegewald et al., 2011). Data presented in this study showed evidence chondrogenic marker expression, however the levels of expression is much reduced compared to the native NP tissue (Minogue et al., 2010).

5.6.2 Aggrecan Ultrastructure and Media Conditions

AFM imaging of isolated aggrecan showed a notable difference in the structure between media conditions. Statistical analysis revealed a significant increase in all aggrecan dimensions (CP length, GAG brush length, and GAG brush width) under CM conditions. Aggrecan species from CM condition showed an increase in GAG brush chain extension compared to aggrecan molecules cultured under SM conditions. These changes may be due to the chondrogenic media supplemented with a combination of factors which include TGF-β3 and dexamethasone. It has been reported that the combination of TGF-β3 and dexamethasone influence chondrogenesis (Mackay et al., 1998, Barry et al., 2001, Risbud et al., 2006). TGF-β has also been shown to be implicated in GAG chain elongation (Schonherr et al., 1993, Little et al., 2008). GAG chain elongation has been shown to be enhanced by growth factors (e.g. TGF-β1). As a result this has an effect on downstream signalling mechanisms that enhance transcription and translation of the CS-GAG synthesising a series of glycostransferases which in certain combinations increase GAG chain polymerisation (Little et al., 2008, Mikami and Kitagawa, 2013).

5.6.3 Comparison to NP tissue

The scarcity of human NP tissue leads to the use of bovine NP tissue as a reference model for comparison since bovine IVD tissue in general has been used in past studies which represent a non-degenerate healthy tissue (Walsh et al., 2004, Demers et al., 2004, Le Maitre et al., 2009, Minogue et al., 2010). Aggrecan isolated from bovine NP tissue was separated in the same manner as alginate beads. Since no full-length aggrecan monomers were identified only the general aggrecan species of bovine NP tissue was used for comparison. Table 5.2 is a summary of aggrecan dimensions from bovine NP tissue, SM, and CM media conditions reported in this study. The key question of this study was whether human NP cells cultured in SM or CM conditions influence the synthesis of aggrecan as compared to NP tissue. Table 5.2 suggest that media conditions do influence aggrecan structure by enhancing aggrecan dimensions however, aggrecan dimensions from aggrecan molecules derived from culture media conditions were not comparable to aggrecan dimensions found in bovine NP tissue.

Table 5.3. Summary of reported aggrecan dimensions from bovine NP tissue, human NP cells cultured from standard and chondrogenic media.

Aggrecan Dimension	Bovine NP tissue (n=300)	Standard media (n= 300)	Chondrogenic media (n= 300)
Core protein length	367 ± 2 nm	314 ± 2 nm	376 ± 2 nm
GAG brush length	249 ± 4 nm	248 ± 3 nm	290 ± 1 nm
GAG brush width	36 ± 0.5 nm 56 ± 2 nm	49 ± 2 nm	57± 2 nm

5.6.4 Aggrecan structural features and GAG brush width

Another outstanding key question was the correlation of GAG brush width and their influence on CP length. It has been postulated that increase in aggrecan GAG chain length has an effect on CP length (Morgelin et al., 1989, Ng et al., 2003, Kopesky et al., 2010, Lee et al., 2013). This is due to the fact that the elongated GAG chains produce a high anionic charge density when packed close together on the CP which leads to a higher GAG-GAG repulsive force which in turn can extend the CP length (Kopesky et al., 2010). Data analysis from figure 5.10 show evidence of low levels of correlation with SM and CM (r= 0.3 and 0.2 respectively). However, NP tissue showed no evidence of correlation between GAG brush width and CP length with aggrecan general species. The interesting finding was when full-length aggrecan monomers from NP tissue were analysed that a higher correlation (r= 0.5) was found. The data obtained from this study compared with data from other studies were base on experimental work from EM (Morgelin et al., 1989) and recently from AFM (Lee et al., 2013). The aggrecan population used by Lee et al., (2013) only based their findings on full-length aggrecan monomers. When full-length species in this study were analysed in this way there was a correlation, which agrees with other studies where full length has been measured. However, the data obtained from this study was limited to the general species since full-length aggrecan species were low in abundance with SM and CM. However, the observation of increase GAG brush width and CP length of aggrecan (general species) found in CM condition compared to aggrecan from SM and aggrecan derived tissue suggest this may cause aggrecan structural changes.

5.6.5 Comparison to other studies

There are a number of studies that have described the application of TGF to mature chondrocytes or NP cells seeded in constructs (Risbud et al., 2006, Byers et al., 2008, Reza and Nicoll, 2010). There was only one study that reported the use of CM with TGF-β1 by Kopesky et al., (2010) and imaged the aggrecan molecules by AFM. They reported that CS

GAG chain extension of equine BMSCs (from foetal and mature) and chondrocytes (from foetal and mature) cells. Although they do report aggrecan dimensions (CP length and CS GAG chain length) of adult mature chondrocytes with TGF-β1, however they do not disclose any AFM imaging or data of aggrecan structure from mature chondrocytes without TGF-β1. The data reported showed a mean CP length between 412-437 nm with a wide range of CP lengths 100-650 nm with three peaks around 100, 400, and 600 nm which represent a heterogeneous population. The aggrecan from chondrocytes cultured in CM (TGF-β1) were longer in length compared to the findings of this study and the CM aggrecan species distribution was unimodal with a range from 200-550 nm. However Kopesky et al., 2010 did not report any findings of GAG brush length and width which was unique to this study and could not be compared since no other studies have described these parameters from 3D cell cultures.

5.7 Conclusion

Human NP cells were seeded in alginate constructs under SM and CM conditions. CM contained TGF-β3 that was known to increase proteoglycan synthesis. Aggrecan isolated from alginate constructs that were cultured under SM or CM was imaged by AFM to investigate their respective aggrecan ultrastructures. Data analysis found a significant difference in aggrecan ultrastructure when human NP cells were cultured under CM conditions. The observable key change was the GAG chain extension which in turn has a profound effect on the overall structure by the negative charge density of extended GAG chains that may increase CP length. The comparison of aggrecan ultrastructure from alginate constructs to tissue has shown that cells seeded in constructs especially cultured with CM conditions show a significant increase in most aggrecan dimensions (CP length, GAG brush, and GAG brush width) which influences its consequential structure.

Chapter 6

General Conclusions and Future Work

6.1 General Conclusions

Aggrecan is an important extracellular matrix component in the IVD with regards to providing osmotic pressure to counteract compressive load (Comper and Laurent, 1978, Chahine et al., 2005). This is due to negatively charged chondroitin and keratan sulphate (CS and KS) GAG side chains which consist of carboxylate and sulphate groups which influences the mechanical properties of the proteoglycan (Maroudas et al., 1969, Hardingham and Fosang, 1992). In addition to this important mechanical role, aggrecan has other roles such as being a structural component forming aggregates to build a three-dimensional ECM network in tissue with other proteins and GAGs (e.g. collagens, link protein, and HA) (Kiani et al., 2002, Dudhia, 2005, Heinegard, 2009).

Previous studies have shown that structural changes to aggrecan have a profound effect on the mechanical properties of tissue and cell seeded constructs (Roughley, 2004, Han et al., 2011). Our current knowledge of aggrecan ultrastructure from the past 40 years has been gained predominantly from EM studies (Rosenberg et al., 1970, Roughley and White, 1980, Buckwalter and Rosenberg, 1982, Buckwalter et al., 1994) and more recently from AFM (Ng et al., 2003, Kopesky et al., 2010, Lee et al., 2010, Lee et al., 2013). Compared with EM approaches, AFM imaging is non-destructive and can yield high signal-to-noise ratio images of unstained molecules. Sample preparation is rapid and crucially, the structure and mechanical properties of biological samples can be characterised in native conditions. As a consequence AFM was employed in these studies to characterise the ultrastructure of aggrecan isolated from both tissues and tissue engineered constructs.

6.12 Characterising Aggrecan Ultrastructure from Bovine NP Tissue

The aims of the first experimental chapter (3) were: i) to optimise an extraction and purification protocol based on past studies, ii) to determine the optimal substrate surface conditions in order to immobilise aggrecan for subsequent AFM imaging, and iii) to develop image analysis protocols in a public domain software environment (ImageJ) to analyse aggrecan ultrastructure (CP length, GAG brush length, and GAG brush width).

In the first part of Chapter 3, the application of Guanidine-HCl solubilisation and CsCl density gradient centrifugation (D1D1) made it possible to successfully isolate aggrecan from bovine NP tissue which was confirmed by biochemical assays (DMMB and BCA) and dot blotting. Secondly, APTES-coated mica was found to be a suitable substrate for

aggrecan immobilisation having a low surface roughness (~ 0.1 nm; deposition time point of 30 minutes) and being hydrophilic in nature. This enabled the immobilisation of aggrecan on APTES-mica and AFM imaging in air. AFM height imaging revealed that aggrecan molecules in tissue predominantly exist as non-intact forms which consist of either a partial CS brush region with one globular end, a cleaved and degraded aggrecan fragment with no globular terminal ends, or aggrecan monomers with only one or no globular domain end. Only a small population of full-length species (5%) with both N and C terminal globular domains were observed.

Thirdly, the development of image analysis protocols to measure CP length and GAG brush length as previously reported in other studies (Ng et al., 2003) was undertaken . However, a key change to analysis was included which was the quantification of total brush width (GAG brush width) rather than measurement of individual GAG chains. Having established these protocols (i.e. aggrecan isolation, immobilisation and imaging/image analysis), an aggrecan population of 300 molecules was measured which confirmed that in terms of CP and GAG brush length two distinct populations of aggrecan molecules existed. This probably reflects the normal tissue homeostasis processing (enzymatic degradation) of aggrecan molecules in healthy NP tissue. The novel approach of quantifying GAG brush width (rather than measuring selected individual GAG chains) from AFM height imaging allowed a larger cohort of samples to be measured. Full-length aggrecan monomers showed variation in GAG brush width which could be possibly due to a combination of inter-linked biological factors such as nutrient supply and expression of specific glycosyltransferases in CS chain polymerisation.

The comparison of aggrecan CP length noted in this study was limited to one previous study where equine AC aggrecan (220 ± 142 nm) (Lee et al., 2010) was reported to be similar to that noted here for bovine NP tissue (215 ± 2 nm). GAG brush length has only been analysed in one previous study (Ng et al., 2003) where data of 268 ± 73 nm (from full-length aggrecan monomers) from bovine AC was reported. This is similar to the findings of this study where GAG brush width was 277 ± 2 nm (general population only).

The findings in Chapter 3 support the conclusion of previous studies in terms of AFM height imaging in air in observing similar aggrecan moieties (CP, globular regions, and GAG brush chains) from normal tissue. There was a degree of similarity of CP length and GAG brush length despite the species/tissue type. The two key novelties of this study were

the isolation of aggrecan and quantification of their dimensions from bovine NP tissue which has not been previously reported and the measurement of GAG brush width allowed the entire aggrecan GAG brush domain to be measured where others studies were limited in measuring selected individual GAG chains.

6.13 Development of Aggrecan Isolation from Alginate for AFM Imaging

Alginate is an exemplar hydrogel that has been used for studying chondrocyte and IVD cell function and behaviour in a three-dimensional environment. Two aims were addressed in Chapter 4; i) assessment of the variability of manually produced alginate bead sizes to ensure there was no significant variation between individual alginate beads which may affect aggrecan synthesis by cells and ii) optimisation of aggrecan isolation from alginate beads with the addition of size exclusion chromatography to separate aggrecan molecules from residual alginate fragments for subsequent AFM imaging. Alginate beads were produced manually and size variation assessed as differences in alginate bead size could influence number of cells seeded in each bead, affect cellular proliferation and extracellular matrix production due to the nutrient and oxygen gradient within the alginate bead microenvironment. Statistical analysis found that alginate bead size was unimodally distributed and bead size was relatively consistent (i.e. ~3.8 ± 0.05 mm^2).

In order to remove contaminating alginate molecules from the aggrecan preparation, the aggrecan isolation protocol was modified which involved the addition of SEC to CsCl density gradient centrifugation. Bovine NP cells were cultured in alginate beads and aggrecan molecules were isolated. Evidence of aggrecan isolation was confirmed by antibody detection (dot blotting) and visualisation of the aggrecan bottle-brush structure (central CP and densely packed GAG chains) by AFM height imaging. To date, no studies have reported the isolation and visualisation of aggrecan molecules from alginate constructs and thus the data here is novel. However, comparison to other studies was limited since qualitative data (AFM height imaging) was taken and no quantitative data of aggrecan dimensions were performed as in this study. Nonetheless, AFM imaging was found to support those findings reported by Lee and colleagues and Kopesky et al in that aggrecan isolated from cells seeded in hydrogel constructs showed a similar bottle-brush structure with the typical aggrecan moieties (central CP and densely packed GAG chains) (Lee et al., 2010, Kopesky et al., 2010).

6.14 Media Conditions Influence Aggrecan Ultrastructure

Developmental work of aggrecan isolation and purification for both tissue and alginate constructs (Chapter 3 and 4) led to the last part of this thesis. It was hypothesised that IVD disc cells (adult mature human NP cells) seeded into a hydrogel would synthesise aggrecan with an ultrastructure similar to that found in NP tissue and that media conditions would influence structure.

TGF-β3, a growth factor known to increase proteoglycan synthesis was incorporated in CM media conditions which also included other components (see table 7 in Chapter 7) that are known to promote chondrogenesis. AFM imaging and data analysis showed a significant change in aggrecan ultrastructure isolated from CM cell cultures compared to that isolated from cells cultured under standard conditions. Under CM conditions, a significant increase in all three aggrecan dimensions (CP length, GAG brush length, and GAG brush width) was observed. Two previous studies have reported similar findings where aggrecan isolated from equine chondrocytes or BM MSCs seeded in a 3D-peptide hydrogel constructs and cultured in chondrogenic media supplemented with TGF-β1 had an increase in CP length and GAG chain length (Lee et al., 2010, Kopesky et al., 2010) as observed in this study

Interestingly neither culture condition induced human NP cells to synthesise aggrecan which was structurally comparable to that isolated from bovine NP tissue as summarised in table 5.3. This variability highlights a biological significance in differences in aggrecan moiety size between tissue and seeded constructs especially with GAG brush width. An increase in GAG brush width represents an increase in CS-GAG chain elongation by TGF-β3 (Little et al., 2008). This increase of GAG content would be beneficial to NP tissue by attracting more water molecules thereby increasing osmotic pressure to counteract compressive load.

6.15 Concluding Remarks

Common aggrecan isolation techniques in combination with advanced technologies such as AFM have added to our understanding of aggrecan ultrastructure from IVD tissue and cell seeded constructs. As a result this work has been considered to be novel according to the three unique findings which have not been previously reported. i) the characterisation of aggrecan ultrastructure isolated from bovine NP tissue and adult human NP cells seeded in alginate constructs by AFM height imaging. ii) A new approach in quantifying the size of

GAG chain domains (GAG brush width) has allowed the entire aggrecan molecule/monomer to be quantified from AFM height imaging. iii) The demonstration of chondrogenic media conditions influence aggrecan ultrastructure by significantly enhancing aggrecan size compared to native NP tissue.

The characterisation of aggrecan ultrastructure from bovine NP tissue and adult human NP cell seeded in alginate constructs has contributed to IVD biology in the understanding on how the aggrecan ultrastructure exists inside bovine NP tissue and alginate constructs. The development work from this study will allow the contribution to future work towards cell-based therapy in IVD tissue engineering.

6.2 Future Work

6.21 Characterising Species and Tissue Differences in Aggrecan Structure

In this study aggrecan isolated from human NP cells was compared with aggrecan derived from bovine NP tissue. Currently there is insufficient data analysing aggrecan ultrastructure from human NP tissue. Although animal tissue such as bovine is used as an alternative model to human IVD, bovine caudal IVDs are exposed to different mechanical loads as bovines are a quadrupedal animal species as oppose to humans which are bipedal (Oshima et al., 1993, Horner et al., 2002, Demers et al., 2004). The differences in mechanical load may affect ECM components such as aggrecan molecules. Therefore it would important to acquire human NP tissue for isolation and purification for AFM imaging in order to quantify aggrecan dimensions as described in Chapter 2. Data obtained from adult human NP tissue would aid in the comparison of aggrecan molecules from bovine NP tissue and human NP cell seeded in alginate constructs.

Another area of for future investigation is the possible difference in aggrecan structure between two tissue types such as AC and NP tissue. The differences of ECM composition, mechanical properties, and cell phenotypes between AC and NP tissue are known (Buckwalter et al., 1989, Sive et al., 2002, Mwale et al., 2004, Minogue et al., 2010, Rodrigues-Pinto et al., 2013) but it is not known whether the ultrastructure differs. This indicates a gap in this area of research regarding the comparison of aggrecan ultrastructure between human IVD tissue and articular cartilage. Lee et al., 2013 characterised aggrecan

molecules from one human adult using the same isolation procedure and imaging techniques described in Chapter 3.

6.22 Cellular Distribution and ECM Accumulation in Alginate Constructs

No histological work was performed in this study. This would be beneficial to illustrate ECM formation by cells seeded in alginate constructs. Gradual ECM formation from 7, 14, and 21 day cell cultures (under SM and CM culture conditions) could be monitored by histological methods such as haematoxylin and eosin (H&E) staining to look at cell distribution within the individual alginate beads. Proteoglycan accumulation could be investigated by Safranin O staining, and immunohistochemistry for other ECM such as type II and type I collagen in order to monitor their distribution throughout individual alginate constructs (Ma et al., 2003, Richardson et al., 2008). Chapter 3 showed that aggrecan existed predominately as a mixed sized population of non-intact molecules that was possibly due to degradation from enzymatic activity. The application of in situ zymography would be useful in localising enzymatic activity within individual alginate beads (George and Johnson, 2010). This could possibly reveal how human NP cells and adult human MSCs behave with proteoglycan enzymatic degradation in alginate constructs.

6.23 Identification of Aggrecan Core Protein Heterogeneity

This study has shown that the majority of aggrecan molecules exist predominantly as a non-intact population (species) in healthy NP tissue. However, in IVD disc degeneration aggrecan molecules are broken down due to aggrecan degrading enzymes such as MMPs and ADAMTS. The current method (dot blotting) of aggrecan detection was only limited in detecting the presence of aggrecan molecules with G1-IGD-G2 domain and could not detect the presence of full-length aggrecan monomers. The application of Western blotting (Struglics and Larsson, 2010, Roughley and Mort, 2012) could be used to detect the presence of full-length and degraded aggrecan molecules by quantifying protein molecular weight of CP. This would be valuable in investigating CP length of aggrecan fragments from tissue (normal and disease) and constructs seeded with MSCs or NP cells. However, Western blotting is limited to quantifying relative molecular weight. Other proteomic techniques could be explored such as peptide mapping by matrix assisted laser desorption ionisation time of flight (MALDI-TOF) mass spectrometry. This would allow

identification aggrecan core protein as biomarkers for normal and disease states (Cillero-Pastor et al., 2013).

6.24 IVD Tissue Engineering: The Application of Human MSCs

6.24.1 The Seeding of Human Adult MSCs in Alginate Constructs

From a tissue engineering standpoint, figure 1.11 in Chapter 1 illustrates the long term goal for a cell-based therapy for IVD regeneration by the application of adult human BM or AD-MSCs (Ma et al., 2003, Colombini et al., 2008, Richardson et al., 2010, Vadala et al., 2013). This would entail the seeding of human BM or AD-MSCs into alginate under standard and chondrogenic media conditions. Again this would involve characterising aggrecan ultrastructure from both human BM or AD-MSCs seeded constructs under standard and chondrogenic media conditions. In an addition to characterising aggrecan, this would answer two outstanding questions. i) Would stems cells from different sources produce a different aggrecan structure? ii) Would CM culturing conditions have the same effect as with human NP cells described in Chapter 5?

6.24.2 Stimulation of Chondrogenesis with Other Growth Factors

Chapter 5 described the use of chondrogenic media with TGF-β3 which showed a significant increase in CP length, GAG brush length, and GAG brush width. There are other alternative growth factors such as growth and differentiation factor 5 and 6 (GDF-5 and GDF-6) which can also direct chondrogenesis. Current unpublished work in the research group seeded patient matched human AD and BM-MSCs into type I collagen hydrogels (Devro) (Clarke et al., 2013). Gene expression data showed chondrogenic markers expression was significantly greater with GDF-5 and 6 with BM and AD-MSCs compared with TGF-β3. A similar strategy could be employed where the BM-MSCs and AD-MSCs could be cultured in alginate constructs under chondrogenic media conditions with either TGF-β3, GDF-5, or GDF-6 at specific time points such as 7, 14, and 21 days and the aggrecan isolated to ascertain whether these growth factors influence GAG dimensions.

6.25 Investigating Changes in Aggrecan Structure and Micromechanics

Extracellular matrix composition of tissue especially in the IVD is important since it influences the biomechanics of the tissue in resisting tensile and compressive loads (Nerurkar et al., 2010). To date, there has been a limited number of studies investigating changes in aggrecan structure and micromechanics of tissue or cell seeded constructs (Lee

et al., 2010, Kopesky et al., 2010). However, there have been no specific studies on aggrecan structure changes relating to mechanic properties involving IVD tissue and IVD cell seeded constructs. There are two techniques that could be employed to investigate the micromechanical differences between NP tissue and ECM synthesised in alginate constructs by specific cell types such as nanoindentation and scanning acoustic microscopy (SAM) (Radmacher, 1997, Lewis et al., 2008, Miller and Morgan, 2010, Zhao et al., 2012, Sherratt, 2013). Nanoindentation is a technique in measuring mechanical properties of a material at microscopic resolution by physically indenting the material with a hard probe with known mechanical properties to a softer material of unknown stiffness and/or resilience. Conventional nanoindenters have a lateral and depth resolution of greater than 10μm and nanometre to micrometer scale respectively and ideal for NP tissue and ECM components, but are limited to resolve fine biomechanical detail. AFM-based nanoindentation apply a small scale probes that allow both lateral and depth resolution at the nanoscale (<10nm) of cellular components and small ECM assemblies (i.e. aggregates) (Radmacher, 1997, Han et al., 2011). SAM is a non-invasive method which uses high frequency waves (GHz range) to rapidly map local sample wave speed which is related to stiffness. Clarke et. al.,(2013) included a second part of their study by applying SAM on collagen hydrogel constructs seeded with BM and AD-MSCs to measure the micromechanics. They found GDF-6 treated AD-MSCs have a less stiff matrix composition suggesting the growth factor was inducing a matrix that was more akin to the gelatinous native tissue. SAM is an attractive option to employ for investigating micromechanics of matrix composition in alginate constructs. If potential findings described in Section 6.21 (investigating aggrecan structures differences between species/tissue types) were true then, would structural differences relate to mechanical properties. These findings could be further investigated with nanoindentation or SAM to see if changes in aggrecan ultrastructure effect mechanical properties in different tissue types and alginate constructs seeded with various cell types (i.e. Human NP cells and human MSCs). These findings would be critical for future IVD tissue engineering development.

Overall, the long term goal is the use of tissue engineering approaches such as cell-based therapy for IVD repair/regeneration with autologous MSCs from either the patient's BM or AD tissue. Before this approach can be considered, key ECM components such as aggrecan were investigated in order to study its ultrastructure from bovine NP tissue and human NP cells seeded in alginate constructs. With the use of classic proteoglycan

isolation techniques and nanotechnology (AFM), a reproducible aggrecan isolation and purification methods were established, aggrecan isolated from NP tissue was visualised and its structure characterised, and the demonstration of different media conditions influence aggrecan ultrastructure and thus comparing these findings to bovine NP tissue to find a contrast between tissue and alginate constructs are the goals met in this study. This work has contributed to the ongoing understanding in IVD biology and preliminary work for IVD tissue engineering.

Chapter 7

Appendices

7. 0 Appendices

7.1 Dimethylmethylene Blue (DMMB) Solution Preparation

The first step was to add the following together:
3.04g glycine
2.37g NaCl
9.6ml 1M HCl
800 ml of deionised water

Mix until all reagents have completely dissolved then add 16mg DMMB and made up to 1L in water.

7.2 Supplement Data for RMS roughness Analysis for APTES

Box size (pixels)	Box dimension (nm)	RMS roughness (nm)						
		Mica	1min	5 min	15 min	20 min	30min	60 min
5	10	0.04183	0.08494	0.06928	0.05629	0.05773	0.05554	0.05773
10	20	0.04356	0.11363	0.07971	0.06411	0.06498	0.06201	0.06657
15	29	0.04418	0.13347	0.08502	0.06800	0.06762	0.06428	0.07038
20	39	0.04478	0.14953	0.08814	0.06985	0.06882	0.06555	0.07197
25	49	0.04537	0.16167	0.09051	0.07165	0.06951	0.06653	0.07366
30	59	0.04606	0.16961	0.09263	0.07304	0.07092	0.06688	0.07498
35	68	0.04689	0.18016	0.09473	0.07373	0.07078	0.06778	0.07580
40	78	0.04784	0.18712	0.09467	0.07437	0.07132	0.06816	0.07670
45	88	0.04864	0.19181	0.09597	0.07604	0.07169	0.06849	0.07708
50	98	0.04963	0.19557	0.09809	0.07675	0.07200	0.06869	0.07707
55	107	0.05071	0.20785	0.09926	0.07748	0.07248	0.06917	0.07780
60	117	0.05195	0.21037	0.09864	0.07764	0.07234	0.06994	0.07860
65	127	0.05340	0.22146	0.10069	0.07756	0.07405	0.07098	0.07951
70	137	0.05424	0.21726	0.10111	0.07948	0.07350	0.07069	0.07901
75	146	0.05601	0.22509	0.10184	0.07854	0.07370	0.07213	0.07975
80	156	0.05692	0.23026	0.10198	0.08075	0.07454	0.07169	0.07975
85	166	0.05807	0.22624	0.10317	0.08212	0.07564	0.07164	0.07943
90	176	0.05989	0.22930	0.10380	0.08089	0.07475	0.07376	0.08071
95	186	0.06097	0.23759	0.10457	0.08290	0.07483	0.07393	0.08046
100	195	0.06230	0.24179	0.10510	0.08427	0.07586	0.07346	0.07986

Table 7.4. APTES-mica RMS analysis Raw Data.

The above table is the complied data from RMS analysis (Sherratt et al., 2004) routine where all scan size images at 512 pixel size. The box dimensions are box sizes multiplied by the pixel size (1.95312). The overall data is plotted in figure 2.10a. Values indicted in yellow are RMS roughness mean values for box dimensions of 195 nm presented in figure 2.10b.

7.3 IC tapping and PeakForce Tapping Mode Settings

The following settings are for the older Multimode models with IC tapping mode:

- Scan rate = 1.0 Hz
- Scan sizes = 2 µm x 2 µm.
- Gain: 0.3/0.5
- Drive amplitude: Less than 100 mV recommended
- Drive frequency and setpoint: variable according to autotuning
- Data scale = 1- 2 nm
- Height and amplitude: On
- Pixel line: 512
- AFM probe: OTESPA (Bruker AFM Probes).

The following settings are for the Multimode 8 model with Peak Force tapping mode:

- ScanAsyst: On
- Scan rate = 0.488 Hz
- Scan sizes = 8 µm x 8 µm.
- Gain: Variable according to ScanAsyst
- Setpoint: Variable according to ScanAsyst
- Data scale = 2 nm
- Height: on
- Pixel line: 2048
- AFM probe: ScanAsyst in air (Bruker AFM Probes).

The following settings are for the Multimode 8 model with Peak Force tapping mode under high humidity:

- ScanAsyst: Off
- Scan rate = 0.244 Hz
- Scan sizes = 8 µm x 8 µm.
- Gain: 16-20 (Variable according to user discretion)
- Setpoint: Variable according to user discretion
- Data scale = 2 nm
- Height: on
- Pixel line: 2048

AFM probe: ScanAsyst in air (Bruker AFM Probes).

Table 7.5. Atomic force microscopy parameters for IC tapping and Peak force tapping mode

7.4 Defining the Aggrecan Molecular Perimeter

A second RAW file was generated to define the mean surface substrate height without subtracting the background, but arrange a set z-range value via the AFM Image Manipulation. The conversion factor was noted and image was opened in ImageJ and a 51 x 51 pixel box was drawn at three different points of the image. A histogram analysis was done for each box where the pixel SD was noted and converted to height in nanometres and calculated as an average to define molecular perimeter to determine GAG brush width.

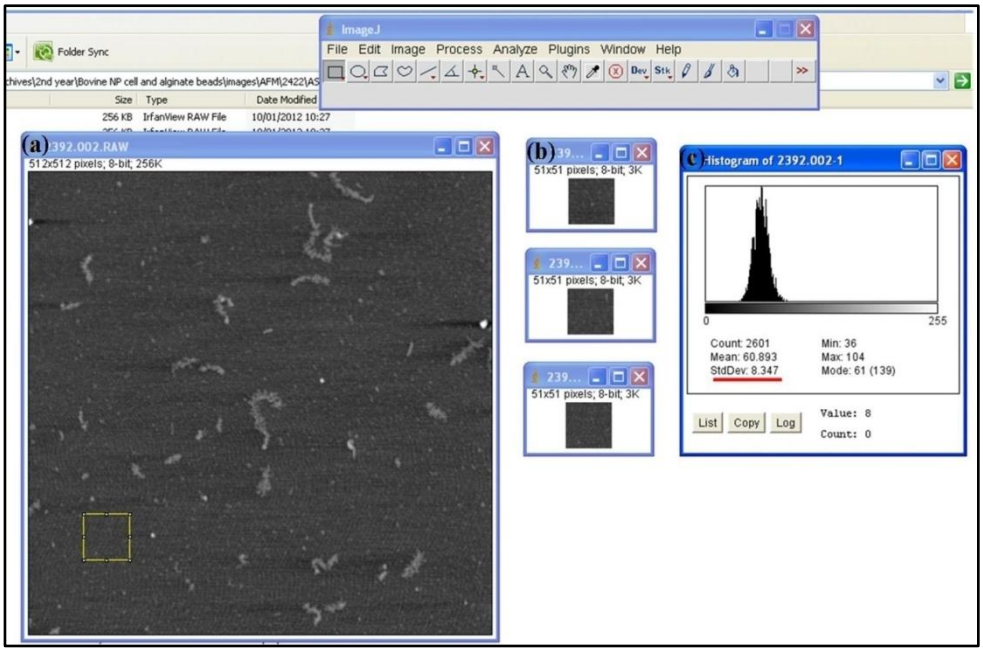

Figure 7.48. Determining Aggrecan Molecular Perimeter.

(a) Second RAW file without background subtraction. (b) Triplicates of 51 x 51 pixel boxes taken from different sections of the image. (c) Histogram values from one 51 x 51 pixel box. The standard deviation (SD) was noted from all three pixel boxes (not shown) to obtain a mean SD value which is converted to height (nm).

7.5 Alginate Beads Size Determination

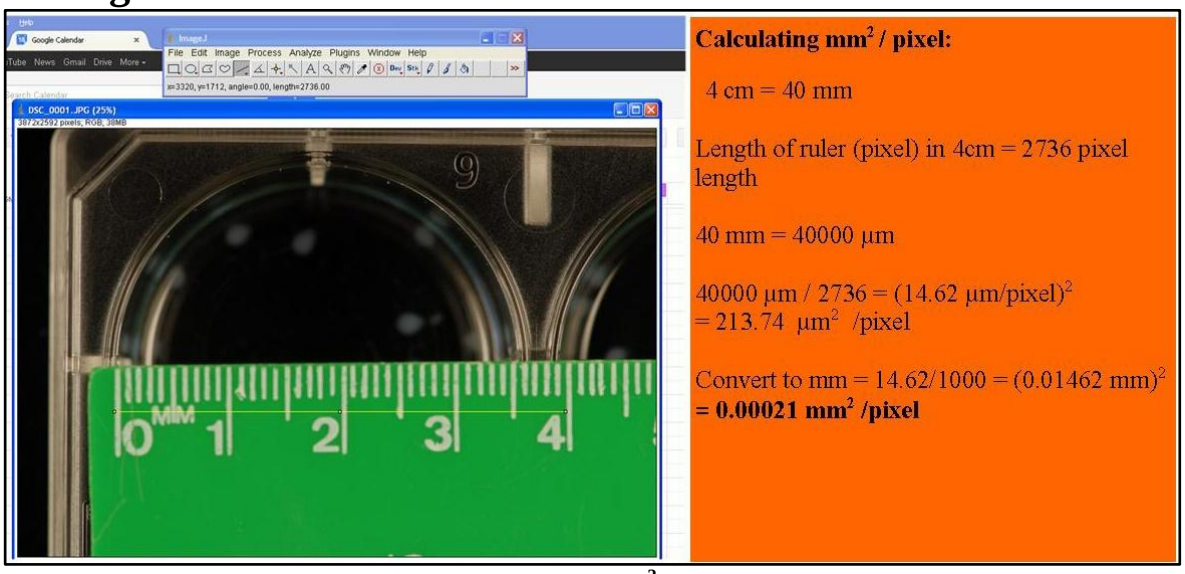

Figure 7.49. Calculating mm^2/pixel with ImageJ

Figure 7.50 Determining Alginate Bead Size with ImageJ

7.6 Standard and Chondrogenic Media Reagents

Table 7.6 Standard and Chondrogenic Media Formulation

Standard media		**Chondrogenic media**	
Reagent	**Final concentration**	**Reagent**	**Final concentration**
DMEM, AQmedia (with 4500 mg/L glucose, L-alanyl-glutamine, and sodium bicarbonate, without sodium pyruvate)		DMEM, AQmedia with 4500 mg/L glucose, L-alanyl-glutamine, and sodium bicarbonate, without sodium pyruvate)	
Antibiotics	100units/ml pen, 100µg/ml strep, 0.25µg/ml amphotericin	Antibiotics	100units/ml pen, 100µg/ml strep, 0.25µg/ml amphotericin
FCS	5%	FCS	1%
L-ascorbate acid	25 µg/ml	Ascorbic acid 2-phosphate	100µM
Sodium pyruvate	1 mM	Sodium pyruvate	1 mM
		BSA	1.25mg/ml
		Dexamethasone	$5x10^{-8}$ M
		ITS-X	Insulin 10µg/ml Transferrin 5.5µg/ml Selenium 6.7ng/ml
		L-proline	40µg/ml
		TGF-β3	10ng/ml

7.7 RT sample preparation procedure

Table 7.7. Reaction Mixture of RT

Volume (µl)	**Reagent**
2µl	10X RT Buffer
0.8µl	25X dNTP mix (100mM)
2µl	10X RT Random Primers
1µl	MultiScribe Reverse Transcriptase
1µl	RNAse Inhibitor
3.2µl	molecular biology grade H_2O

Incubate the reaction tubes under the following conditions on thermal cycler:

25°C for 10 minutes

37°C for 120 minutes

85°C for 5 seconds

4°C (standby).

7.8 Supplementary Data for CsCl Density Gradient fraction

The following is data for Chapter 3 results for bovine NP tissue D1D1 fraction for aggrecan purification.

Fraction no	Sample type	Fraction	density (g/ml)
1	NP D1		1.36
2	NP D1		1.40
3	NP D1		1.34
4	NP D1		1.43
5	NP D1		1.50
6	NP D1	D1D1	1.56
7	NP D1	D1D1	1.62
8	NP D1	D1D1	1.74
9	NP D1	D1D1	1.67
10	NP D1	D1D1	1.77
11	NP D1	D1D1	1.86

Table 7.8 D1D1 Fraction from Bovine NP tissue

The following is data for Chapter 4 results for bovine NP cells in alginate for 21 days. D1 fraction for aggrecan purification.

Fraction no	Sample type	Fraction	density (g/ml)
1	NP -cell alginate		1.39
2	NP -cell alginate		1.32
3	NP -cell alginate		1.37
4	NP -cell alginate		1.34
5	NP -cell alginate		1.49
6	NP -cell alginate		1.49
7	NP -cell alginate	D1	1.59
8	NP -cell alginate	D1	1.57
9	NP -cell alginate	D1	1.62
10	NP -cell alginate	D1	1.69
11	NP -cell alginate	D1	1.74

Table 7.9. Bovine NP Cells D1 fractions

The following is data for Chapter 5 results for bovine NP tissue in alginate for 21 days under standard media conditions for aggrecan purification (D1 fraction).

Fraction no	Sample type	Fraction	density (g/ml)
1	PG extract		1.41
2	PG extract		1.38
3	PG extract		1.48
4	PG extract		1.45
5	PG extract		1.50
6	PG extract		1.60
7	PG extract	D1	1.61
8	PG extract	D1	1.69
9	PG extract	D1	1.76
10	PG extract	D1	1.85
11	PG extract	D1	less than 1 ml

Table 7.10. Bovine NP Tissue D1 fractions

The following is data for Chapter 5 results for human NP cells culture in alginate for 21 days under standard media conditions for aggrecan purification (D1 fraction).

PM16 _standard		
Fraction no	**Fraction**	**Density (g/ml)**
1	PG extract	1.43
2	PG extract	1.39
3	PG extract	1.5
4	PG extract	1.46
5	PG extract	1.51
6	D1	1.59
7	D1	1.59
8	D1	1.81
9	D1	1.76
10	D1	1.73
11	D1	less than 1 ml

Table 7.11 Human NP Cells D1 Fraction for Standard Media

The following is data for Chapter 5 results for human NP cells culture in alginate for 21 days under chondrogenic media conditions for aggrecan purification (D1 fraction).

PM16 _chondrogenic		
Fraction no	**Fraction**	**Density (g/ml)**
1	PG extract	1.38
2	PG extract	1.39
3	PG extract	1.43
4	PG extract	1.49
5	PG extract	1.47
6	D1	1.63
7	D1	1.63
8	D1	1.8
9	D1	1.76
10	D1	1.78
11	D1	less than 1 ml

Table 7.12. Human NP Cells D1 Fraction for Chondrogenic Media

8.0 References

ABBOTT, R. D., PURMESSUR, D., MONSEY, R. D. & IATRIDIS, J. C. 2012. Regenerative potential of TGF beta 3 + Dex and notochordal cell conditioned media on degenerated human intervertebral disc cells. *Journal of Orthopaedic Research,* 30**,** 482-488.

ADAMS, M. (ed.) 2002. *The Biomechanics of Back Pain*: Churchill Livingstone.

ADAMS, M. A. 2004. Biomechanics of back pain. *Acupuncture in Medicine,* 22**,** 178-188.

ADAMS, M. A., DOLAN, P. & MCNALLY, D. S. 2009. The internal mechanical functioning of intervertebral discs and articular cartilage, and its relevance to matrix biology. *Matrix Biology,* 28**,** 384-389.

ADAMS, M. A. P. & ROUGHLEY, P. J. P. 2006. What is Intervertebral Disc Degeneration, and What Causes It? [Review]. *Spine,* 31**,** 2151-2161.

ALADIN, D. M., CHEUNG, K. M., NGAN, A. H., CHAN, D., LEUNG, V. Y., LIM, C. T., LUK, K. D. & LU, W. W. 2010. Nanostructure of collagen fibrils in human nucleus pulposus and its correlation with macroscale tissue mechanics. *J Orthop Res,* 28**,** 497-502.

ALINI, M., ROUGHLEY, P. J., ANTONIOU, J., STOLL, T. & AEBI, M. 2002. A biological approach to treating disc degeneration: not for today, but maybe for tomorrow. *Eur Spine J,* 11 Suppl 2**,** S215-20.

ALSTEENS, D., DUPRES, V., YUNUS, S., LATGÉ, J.-P., HEINISCH, J. J. & DUFRÊNE, Y. F. 2012. High-Resolution Imaging of Chemical and Biological Sites on Living Cells Using Peak Force Tapping Atomic Force Microscopy. *Langmuir,* 28**,** 16738-16744.

ARIGA, K., YONENOBU, K., NAKASE, T., KANEKO, M., OKUDA, S., UCHIYAMA, Y. & YOSHIKAWA, H. 2001. Localization of cathepsins D, K, and L in degenerated human intervertebral discs. *Spine (Phila Pa 1976),* 26**,** 2666-72.

AUGST, A. D., KONG, H. J. & MOONEY, D. J. 2006. Alginate hydrogels as biomaterials. *Macromol Biosci,* 6**,** 623-33.

BARRY, F., BOYNTON, R. E., LIU, B. & MURPHY, J. M. 2001. Chondrogenic differentiation of mesenchymal stem cells from bone marrow: differentiation-dependent gene expression of matrix components. *Exp Cell Res,* 268**,** 189-200.

BARRY, F. P., NEAME, P. J., SASSE, J. & PEARSON, D. 1994. Length variation in the keratan sulfate domain of mammalian aggrecan. *Matrix Biol,* 14**,** 323-8.

BARTELS, E. M., FAIRBANK, J. C. T., WINLOVE, C. P. & URBAN, J. P. G. 1998. Oxygen and Lactate Concentrations Measured in Vivo in the Intervertebral Discs of Patients With Scoliosis and Back Pain. *Spine,* 23**,** 1-7.

BATTIE, M. C., VIDEMAN, T., LEVALAHTI, E., GILL, K. & KAPRIO, J. 2008. Genetic and environmental effects on disc degeneration by phenotype and spinal level: a multivariate twin study. *Spine (Phila Pa 1976),* 33**,** 2801-8.

BENNEKER, L. M., HEINI, P. F., ANDERSON, S. E., ALINI, M. & ITO, K. 2005. Correlation of radiographic and MRI parameters to morphological and biochemical assessment of intervertebral disc degeneration. *Eur Spine J,* 14**,** 27-35.

BENYA, P. D. & SHAFFER, J. D. 1982. Dedifferentiated chondrocytes reexpress the differentiated collagen phenotype when cultured in agarose gels. *Cell,* 30**,** 215-24.

BERTAGNOLI, R., YUE, J. J., SHAH, R. V., NANIEVA, R., PFEIFFER, F., FENK-MAYER, A., KERSHAW, T. & HUSTED, D. S. 2005. The treatment of disabling single-level lumbar discogenic low back pain with total disc arthroplasty utilizing the Prodisc prosthesis: a prospective study with 2-year minimum follow-up. *Spine (Phila Pa 1976),* 30**,** 2230-6.

BINNIG, G., & ROHRER, H. 1982. Scanning Tunnelling Microscope. *Helvetica Physica Acta,* 55**,** 726-735.

BINNIG, G., QUATE, C. F. & GERBER, C. 1986. Atomic Force Microscope. *Physical Review Letters,* 56**,** 930.

BLUMENTHAL, S., MCAFEE, P. C., GUYER, R. D., HOCHSCHULER, S. H., GEISLER, F. H., HOLT, R. T., GARCIA, R., JR., REGAN, J. J. & OHNMEISS, D. D. 2005. A prospective, randomized, multicenter Food and Drug Administration investigational device exemptions study of lumbar total disc replacement with the CHARITE artificial disc versus lumbar fusion: part I: evaluation of clinical outcomes. *Spine (Phila Pa 1976),* 30**,** 1565-75; discussion E387-91.

BOGDUK, N. 2004. Management of chronic low back pain. *Med J Aust,* 180**,** 79-83.

BRISSETT, N. C. & PERKINS, S. J. 1998. Conserved basic residues in the C-type lectin and short complement repeat domains of the G3 region of proteoglycans. *Biochem J,* 329 (Pt 2)**,** 415-24.

BRODELIUS, P., DEUS, B., MOSBACH, K. & ZENK, M. H. 1979. Immobilized plant cells for the production and transformation of natural products. *FEBS Lett,* 103**,** 93-7.

BRODIN, H. 1955a. Longitudinal bone growth, the nutrition of the epiphyseal cartilages and the local blood supply; an experimental study in the rabbit. *Acta Orthop Scand Suppl,* 20**,** 1-92.

BRODIN, H. 1955b. Paths of nutrition in articular cartilage and intervertebral discs. *Acta Orthop Scand,* 24**,** 177-83.

BUCKWALTER, J. A. 1983. Proteoglycan structure in calcifying cartilage. *Clin Orthop Relat Res***,** 207-32.

BUCKWALTER, J. A. 1995. Aging and degeneration of the human intervertebral disc. *Spine (Phila Pa 1976),* 20**,** 1307-14.

BUCKWALTER, J. A., PEDRINIMILLE, A., PEDRINI, V. & TUDISCO, C. 1985. PROTEOGLYCANS OF HUMAN INFANT INTERVERTEBRAL-DISK - ELECTRON-MICROSCOPIC AND BIOCHEMICAL-STUDIES. *Journal of Bone and Joint Surgery-American Volume,* 67A**,** 284-294.

BUCKWALTER, J. A. & ROSENBERG, L. C. 1982. Electron microscopic studies of cartilage proteoglycans. Direct evidence for the variable length of the chondroitin sulfate-rich region of proteoglycan subunit core protein. *J Biol Chem,* 257**,** 9830-9.

BUCKWALTER, J. A. & ROSENBERG, L. C. 1988. Electron microscopic studies of cartilage proteoglycans. *Electron Microsc Rev,* 1**,** 87-112.

BUCKWALTER, J. A., ROSENBERG, L. C. & TANG, L. H. 1984. The effect of link protein on proteoglycan aggregate structure. An electron microscopic study of the molecular architecture and dimensions of proteoglycan aggregates reassembled from the proteoglycan monomers and link proteins of bovine fetal epiphyseal cartilage. *J Biol Chem,* 259**,** 5361-3.

BUCKWALTER, J. A., ROUGHLEY, P. J. & ROSENBERG, L. C. 1994. Age-related changes in cartilage proteoglycans: quantitative electron microscopic studies. *Microsc Res Tech,* 28**,** 398-408.

BUCKWALTER, J. A., SMITH, K. C., KAZARIEN, L. E., ROSENBERG, L. C. & UNGAR, R. 1989. ARTICULAR-CARTILAGE AND INTERVERTEBRAL-DISK PROTEOGLYCANS DIFFER IN STRUCTURE - AN ELECTRON-MICROSCOPIC STUDY. *Journal of Orthopaedic Research,* 7**,** 146-151.

BUENO, E. M., BILGEN, B. & BARABINO, G. A. 2005. Wavy-walled bioreactor supports increased cell proliferation and matrix deposition in engineered cartilage constructs. *Tissue Eng,* 11**,** 1699-709.

BYERS, B. A., MAUCK, R. L., CHIANG, I. E. & TUAN, R. S. 2008. Transient exposure to transforming growth factor beta 3 under serum-free conditions enhances the

biomechanical and biochemical maturation of tissue-engineered cartilage. *Tissue Eng Part A,* 14**,** 1821-34.

CAMPBELL, R. E., MOSIMANN, S. C., VAN DE RIJN, I., TANNER, M. E. & STRYNADKA, N. C. 2000. The first structure of UDP-glucose dehydrogenase reveals the catalytic residues necessary for the two-fold oxidation. *Biochemistry,* 39**,** 7012-23.

CHAHINE, N. O., CHEN, F. H., HUNG, C. T. & ATESHIAN, G. A. 2005. Direct measurement of osmotic pressure of glycosaminoglycan solutions by membrane osmometry at room temperature. *Biophys J,* 89**,** 1543-50.

CHAN, D., SONG, Y., SHAM, P. & CHEUNG, K. M. 2006. Genetics of disc degeneration. *Eur Spine J,* 15 Suppl 3**,** S317-25.

CHANDRAN, P. L. & HORKAY, F. 2012. Aggrecan, an unusual polyelectrolyte: review of solution behavior and physiological implications. *Acta Biomater,* 8**,** 3-12.

CHEETHAM, P. S. J., BLUNT, K. W. & BOCKE, C. 1979. Physical Studies on Cell Immobilization Using Calcium Alginate Gels. *Biotechnology and Bioengineering,* 21**,** 2155-2168.

CHEUNG, K. M., KARPPINEN, J., CHAN, D., HO, D. W., SONG, Y. Q., SHAM, P., CHEAH, K. S., LEONG, J. C. & LUK, K. D. 2009. Prevalence and pattern of lumbar magnetic resonance imaging changes in a population study of one thousand forty-three individuals. *Spine (Phila Pa 1976),* 34**,** 934-40.

CHIBA, K., ANDERSSON, G. B., MASUDA, K. & THONAR, E. J. 1997. Metabolism of the extracellular matrix formed by intervertebral disc cells cultured in alginate. *Spine (Phila Pa 1976),* 22**,** 2885-93.

CHOU, A. I. & NICOLL, S. B. 2009. Characterization of photocrosslinked alginate hydrogels for nucleus pulposus cell encapsulation. *Journal of Biomedical Materials Research Part A,* 91A**,** 187-194.

CILLERO-PASTOR, B., EIJKEL, G. B., KISS, A., BLANCO, F. J. & HEEREN, R. M. A. 2013. Matrix-assisted laser desorption ionization–imaging mass spectrometry: A new methodology to study human osteoarthritic cartilage. *Arthritis & Rheumatism,* 65**,** 710-720.

CLARKE, L. E., MCCONNELL, J., SHERRATT, M. J., DERBY, B., RICHARDSON, S. M. & HOYLAND, J. A. 2013. GDF6 Drives Discogenic Differentiation of Adipose Derived Mesenchymal Stem Cells (In press).

CLOUET, J., VINATIER, C., MERCERON, C., POT-VAUCEL, M., HAMEL, O., WEISS, P., GRIMANDI, G. & GUICHEUX, J. 2009. The intervertebral disc: From pathophysiology to tissue engineering. *Joint Bone Spine,* 76**,** 614-618.

COLOMBINI, A., LOMBARDI, G., CORSI, M. M. & BANFI, G. 2008. Pathophysiology of the human intervertebral disc. *Int J Biochem Cell Biol,* 40**,** 837-42.

COMPER, W. D. & LAURENT, T. C. 1978. Physiological function of connective tissue polysaccharides. *Physiological Reviews,* 58**,** 255-315.

CREVENSTEN, G., WALSH, A. J., ANANTHAKRISHNAN, D., PAGE, P., WAHBA, G. M., LOTZ, J. C. & BERVEN, S. 2004. Intervertebral disc cell therapy for regeneration: mesenchymal stem cell implantation in rat intervertebral discs. *Ann Biomed Eng,* 32**,** 430-4.

DADLANI, H., BALLINGER, M. L., OSMAN, N., GETACHEW, R. & LITTLE, P. J. 2008. Smad and p38 MAP kinase-mediated signaling of proteoglycan synthesis in vascular smooth muscle. *J Biol Chem,* 283**,** 7844-52.

DAGENAIS, S., CARO, J. & HALDEMAN, S. 2008. A systematic review of low back pain cost of illness studies in the United States and internationally. *The Spine Journal,* 8**,** 8-20.

DANG, J. M., SUN, D. D., SHIN-YA, Y., SIEBER, A. N., KOSTUIK, J. P. & LEONG, K. W. 2006. Temperature-responsive hydroxybutyl chitosan for the culture of mesenchymal stem cells and intervertebral disk cells. *Biomaterials,* 27**,** 406-18.

DARLING, E. M. & ATHANASIOU, K. A. 2005. Rapid phenotypic changes in passaged articular chondrocyte subpopulations. *J Orthop Res,* 23**,** 425-32.

DEAN, D., HAN, L., GRODZINSKY, A. J. & ORTIZ, C. 2006. Compressive nanomechanics of opposing aggrecan macromolecules. *J Biomech,* 39**,** 2555-65.

DEAN, D., HAN, L., ORTIZ, C. & GRODZINSKY, A. J. 2005. Nanoscale Conformation and Compressibility of Cartilage Aggrecan Using Microcontact Printing and Atomic Force Microscopy. *Macromolecules,* 38**,** 4047-4049.

DEGROOT, J., VERZIJL, N., WENTING-VAN WIJK, M. J., JACOBS, K. M., VAN EL, B., VAN ROERMUND, P. M., BANK, R. A., BIJLSMA, J. W., TEKOPPELE, J. M. & LAFEBER, F. P. 2004. Accumulation of advanced glycation end products as a molecular mechanism for aging as a risk factor in osteoarthritis. *Arthritis Rheum,* 50**,** 1207-15.

DEMERS, C. N., ANTONIOU, J. & MWALE, F. 2004. Value and limitations of using the bovine tail as a model for the human lumbar spine. *Spine (Phila Pa 1976),* 29**,** 2793-9.

DEYO, R. A. & WEINSTEIN, J. N. 2001. Low back pain. *N Engl J Med,* 344**,** 363-70.

DIAMANT, B., KARLSSON, J. & NACHEMSON, A. 1968. Correlation between lactate levels and pH in discs of patients with lumbar rhizopathies. *Experientia,* 24**,** 1195-6.

DISCHER, D. E., MOONEY, D. J. & ZANDSTRA, P. W. 2009. Growth factors, matrices, and forces combine and control stem cells. *Science,* 324**,** 1673-7.

DIWAN, A. D., PARVATANENI, H. K., KHAN, S. N., SANDHU, H. S., GIRARDI, F. P. & CAMMISA, F. P., JR. 2000. Current concepts in intervertebral disc restoration. *Orthop Clin North Am,* 31**,** 453-64.

DOEGE, K. J., COULTER, S. N., MEEK, L. M., MASLEN, K. & WOOD, J. G. 1997. A human-specific polymorphism in the coding region of the aggrecan gene. Variable number of tandem repeats produce a range of core protein sizes in the general population. *J Biol Chem,* 272**,** 13974-9.

DOEGE, K. J., SASAKI, M., KIMURA, T. & YAMADA, Y. 1991. Complete coding sequence and deduced primary structure of the human cartilage large aggregating proteoglycan, aggrecan. Human-specific repeats, and additional alternatively spliced forms. *Journal of Biological Chemistry,* 266**,** 894-902.

DONOHUE, P. J., JAHNKE, M. R., BLAHA, J. D. & CATERSON, B. 1988. Characterization of link protein(s) from human intervertebral-disc tissues. *Biochem J,* 251**,** 739-47.

DRAGET, K. I., SKJAK-BRAEK, G. & SMIDSROD, O. 1997. Alginate based new materials. *Int J Biol Macromol,* 21**,** 47-55.

DUDHIA, J. 2005. Aggrecan, aging and assembly in articular cartilage. *Cell Mol Life Sci,* 62**,** 2241-56.

ENGLER, A. J., SEN, S., SWEENEY, H. L. & DISCHER, D. E. 2006. Matrix elasticity directs stem cell lineage specification. *Cell,* 126**,** 677-89.

ERRICO, T. J. 2005. Lumbar disc arthroplasty. *Clinical Orthopaedics and Related Research***,** 106-117.

EYRE, D. R. & MUIR, H. 1977. Quantitative analysis of types I and II collagens in human intervertebral discs at various ages. *Biochim Biophys Acta,* 492**,** 29-42.

FASSETT, D. R., KURD, M. F. & VACCARO, A. R. 2009. Biologic solutions for degenerative disk disease. *J Spinal Disord Tech,* 22**,** 297-308.

FOSTER, B. 2012. New Atomic Force Microscopy (AFM) Approaches Life Sciences Gently, Quantitatively, and Correlatively. *American Laboratory.*

FOTIADIS, D., SCHEURING, S., MULLER, S. A., ENGEL, A. & MULLER, D. J. 2002. Imaging and manipulation of biological structures with the AFM. *Micron,* 33**,** 385-97.

FREEMAN, B. J. & DAVENPORT, J. 2006. Total disc replacement in the lumbar spine: a systematic review of the literature. *Eur Spine J,* 15 Suppl 3**,** S439-47.

FREEMONT, A. J., PEACOCK, T. E., GOUPILLE, P., HOYLAND, J. A., OBRIEN, J. & JAYSON, M. I. V. 1997. Nerve ingrowth into diseased intervertebral disc in chronic back pain. *Lancet,* 350**,** 178-181.

FUKUTA, S., MIYAMOTO, K., SUZUKI, K., MAEHARA, H., INOUE, T., HARA, A., KIKUIKE, K., TAGUCHI, A. & SHIMIZU, K. 2011. Abundance of calpain and aggrecan-cleavage products of calpain in degenerated human intervertebral discs. *Osteoarthritis Cartilage,* 19**,** 1254-62.

FUNDERBURGH, J. L. 2000. Keratan sulfate: structure, biosynthesis, and function. *Glycobiology,* 10**,** 951-8.

GAETANI, P., TORRE, M. L., KLINGER, M., FAUSTINI, M., CROVATO, F., BUCCO, M., MARAZZI, M., CHLAPANIDAS, T., LEVI, D., TANCIONI, F., VIGO, D. & RODRIGUEZ Y BAENA, R. 2008. Adipose-derived stem cell therapy for intervertebral disc regeneration: an in vitro reconstructed tissue in alginate capsules. *Tissue Eng Part A,* 14**,** 1415-23.

GEORGE, S. & JOHNSON, J. 2010. In Situ Zymography. *In:* CLARK, I. M. (ed.) *Matrix Metalloproteinase Protocols.* Humana Press.

GILBERT, H., T. J., HOYLAND, J., A. & MILLWARD-SADLER, S., J 2010. The response of human annulus fibrosus cells to cyclic tensile strain: Effects of frequency and degeneration. *Arthritis & Rheumatism,* 9999**,** NA.

GRAHAM, H. K., HODSON, N. W., HOYLAND, J. A., MILLWARD-SADLER, S. J., GARROD, D., SCOTHERN, A., GRIFFITHS, C. E. M., WATSON, R. E. B., COX, T. R., ERLER, J. T., TRAFFORD, A. W. & SHERRATT, M. J. 2010. Tissue section AFM: In situ ultrastructural imaging of native biomolecules. *Matrix Biology,* 29**,** 254-260.

GRANDOLFO, M., D'ANDREA, P., PAOLETTI, S., MARTINA, M., SILVESTRINI, G., BONUCCI, E. & VITTUR, F. 1993. Culture and differentiation of chondrocytes entrapped in alginate gels. *Calcif Tissue Int,* 52**,** 42-8.

GRANT, G. T., MORRIS, E. R., REES, D. A., SMITH, P. J. C. & THOM, D. 1973. Biological interactions between polysaccharides and divalent cations: The egg-box model. *FEBS Letters,* 32**,** 195-198.

GRUBER, H. E. P., INGRAM, J. A. B. S., NORTON, H. J. P. & HANLEY, E. N. J. M. D. 2007. Senescence in Cells of the Aging and Degenerating Intervertebral Disc: Immunolocalization of Senescence-Associated [beta]-Galactosidase in Human and Sand Rat Discs. *Spine,* 32**,** 321-327.

GRUNHAGEN, T., WILDE, G., SOUKANE, D. M., SHIRAZI-ADL, S. A. & URBAN, J. P. G. 2006. Nutrient Supply and Intervertebral Disc Metabolism. *J Bone Joint Surg Am,* 88**,** 30-35.

GUO, J. F., JOURDIAN, G. W. & MACCALLUM, D. K. 1989. Culture and growth characteristics of chondrocytes encapsulated in alginate beads. *Connect Tissue Res,* 19**,** 277-97.

HALLE, J. P., LANDRY, D., FOURNIER, A., BEAUDRY, M. & LEBLOND, F. A. 1993. Method for the quantification of alginate in microcapsules. *Cell Transplant,* 2**,** 429-36.

HAN, L., GRODZINSKY, A. J. & ORTIZ, C. 2011. Nanomechanics of the Cartilage Extracellular Matrix. *Annu Rev Mater Res,* 41**,** 133-168.

HANDA, T., ISHIHARA, H., OHSHIMA, H., OSADA, R., TSUJI, H. & OBATA, K. 1997. Effects of hydrostatic pressure on matrix synthesis and matrix

metalloproteinase production in the human lumbar intervertebral disc. *Spine (Phila Pa 1976),* 22**,** 1085-91.

HARDER, A., WALHORN, V., DIERKS, T., FERNÀNDEZ-BUSQUETS, X. & ANSELMETTI, D. 2010. Single-Molecule Force Spectroscopy of Cartilage Aggrecan Self-Adhesion. *Biophysical Journal,* 99**,** 3498-3504.

HARDINGHAM, T. E. & FOSANG, A. J. 1992. Proteoglycans: many forms and many functions. *FASEB J,* 6**,** 861-70.

HASCALL, V., CALABRO, A., MIDURA, R. J., YANAGISHITA, M., WILLIAM, J. L. & GERALD, W. H. 1994. Isolation and characterization of proteoglycans. *Methods in Enzymology.* Academic Press.

HASSLER, O. 1969. The Human Intervertebral Disc: A Micro-Angiographical Study on Its Vascular Supply at Various Ages. *Acta Orthopaedica,* 40**,** 765-772.

HAUG, A., & LARSEN, B. 1962. Qunantitative Determination of the Uronic Acid Composition of Alginates. *Acta Chemica Scandinavica,* 16**,** 1908-1918.

HAUSELMANN, H. J., AYDELOTTE, M. B., SCHUMACHER, B. L., KUETTNER, K. E., GITELIS, S. H. & THONAR, E. 1992. SYNTHESIS AND TURNOVER OF PROTEOGLYCANS BY HUMAN AND BOVINE ADULT ARTICULAR CHONDROCYTES CULTURED IN ALGINATE BEADS. *Matrix,* 12**,** 116-129.

HAUSELMANN, H. J., FERNANDES, R. J., MOK, S. S., SCHMID, T. M., BLOCK, J. A., AYDELOTTE, M. B., KUETTNER, K. E. & THONAR, E. J. 1994. Phenotypic stability of bovine articular chondrocytes after long-term culture in alginate beads. *J Cell Sci,* 107 (Pt 1)**,** 17-27.

HAUSELMANN, H. J., MASUDA, K., HUNZIKER, E. B., NEIDHART, M., MOK, S. S., MICHEL, B. A. & THONAR, E. J. 1996. Adult human chondrocytes cultured in alginate form a matrix similar to native human articular cartilage. *Am J Physiol,* 271**,** C742-52.

HEGEWALD, A. A., ENZ, A., ENDRES, M., SITTINGER, M., WOICIECHOWSKY, C., THOMÉ, C. & KAPS, C. 2011. Engineering of polymer-based grafts with cells derived from human nucleus pulposus tissue of the lumbar spine. *Journal of Tissue Engineering and Regenerative Medicine,* 5**,** 275-282.

HEINEGARD, D. 2009. Proteoglycans and more--from molecules to biology. *Int J Exp Pathol,* 90**,** 575-86.

HEINEGARD, D. & HASCALL, V. C. 1974. Aggregation of cartilage proteoglycans. 3. Characteristics of the proteins isolated from trypsin digests of aggregates. *J Biol Chem,* 249**,** 4250-6.

HODSON, N. W., KIELTY, C. M. & SHERRATT, M. J. 2009. ECM macromolecules: height-mapping and nano-mechanics using atomic force microscopy. *Methods Mol Biol,* 522**,** 123-41.

HORNER, H. A., ROBERTS, S., BIELBY, R. C., MENAGE, J., EVANS, H. & URBAN, J. P. 2002. Cells from different regions of the intervertebral disc: effect of culture system on matrix expression and cell phenotype. *Spine (Phila Pa 1976),* 27**,** 1018-28.

HORTON, W. G. 1958. Further observations on the elastic mechanism of the intervertebral disc. *J Bone Joint Surg Br,* 40-B**,** 552-7.

HSIEH, A. H. & TWOMEY, J. D. 2010. Cellular mechanobiology of the intervertebral disc: New directions and approaches. *Journal of Biomechanics,* 43**,** 137-145.

HUANG, K. & WU, L. D. 2008. Aggrecanase and aggrecan degradation in osteoarthritis: a review. *J Int Med Res,* 36**,** 1149-60.

HUMZAH, M. D. & SOAMES, R. W. 1988. Human intervertebral disc: structure and function. *Anat Rec,* 220**,** 337-56.

HUTTON, W. C., ELMER, W. A., BODEN, S. D., HYON, S., TORIBATAKE, Y., TOMITA, K. & HAIR, G. A. 1999a. The effect of hydrostatic pressure on intervertebral disc metabolism. *Spine (Phila Pa 1976),* 24**,** 1507-15.

HUTTON, W. C., ELMER, W. A., BODEN, S. D., HYON, S., TORIBATAKE, Y., TOMITA, K. & HAIR, G. A. 1999b. The effect of hydrostatic pressure on intervertebral disc metabolism. *Spine,* 24**,** 1507-1515.

INOUE, H. 1973. Three-dimensional observation of collagen framework of intervertebral discs in rats, dogs and humans. *Arch Histol Jpn,* 36**,** 39-56.

IOZZO, R. V. & SCHAEFER, L. 2010. Proteoglycans in health and disease: novel regulatory signaling mechanisms evoked by the small leucine-rich proteoglycans. *FEBS J,* 277**,** 3864-75.

ISHIHARA, H. & URBAN, J. P. 1999. Effects of low oxygen concentrations and metabolic inhibitors on proteoglycan and protein synthesis rates in the intervertebral disc. *J Orthop Res,* 17**,** 829-35.

IZUMIKAWA, T., KOIKE, T., SHIOZAWA, S., SUGAHARA, K., TAMURA, J. & KITAGAWA, H. 2008. Identification of chondroitin sulfate glucuronyltransferase as chondroitin synthase-3 involved in chondroitin polymerization: chondroitin polymerization is achieved by multiple enzyme complexes consisting of chondroitin synthase family members. *J Biol Chem,* 283**,** 11396-406.

IZUMIKAWA, T., UYAMA, T., OKUURA, Y., SUGAHARA, K. & KITAGAWA, H. 2007. Involvement of chondroitin sulfate synthase-3 (chondroitin synthase-2) in chondroitin polymerization through its interaction with chondroitin synthase-1 or chondroitin-polymerizing factor. *Biochem J,* 403**,** 545-52.

IZZO, R., GUARNIERI, G., GUGLIELMI, G. & MUTO, M. 2013. Biomechanics of the spine. Part I: Spinal stability. *European Journal of Radiology,* 82**,** 118-126.

JAHNKE, M. R. & MCDEVITT, C. A. 1988. Proteoglycans of the human intervertebral disc. Electrophoretic heterogeneity of the aggregating proteoglycans of the nucleus pulposus. *Biochem J,* 251**,** 347-56.

JENSEN, M. C., BRANT-ZAWADZKI, M. N., OBUCHOWSKI, N., MODIC, M. T., MALKASIAN, D. & ROSS, J. S. 1994. Magnetic resonance imaging of the lumbar spine in people without back pain. *N Engl J Med,* 331**,** 69-73.

JOHNSON, W. E., SIVAN, S., WRIGHT, K. T., EISENSTEIN, S. M., MAROUDAS, A. & ROBERTS, S. 2006. Human intervertebral disc cells promote nerve growth over substrata of human intervertebral disc aggrecan. *Spine (Phila Pa 1976),* 31**,** 1187-93.

JOHNSTONE, B. & BAYLISS, M. T. 1995. The large proteoglycans of the human intervertebral disc. Changes in their biosynthesis and structure with age, topography, and pathology. *Spine (Phila Pa 1976),* 20**,** 674-84.

KALAMAJSKI, S. & OLDBERG, A. 2010. The role of small leucine-rich proteoglycans in collagen fibrillogenesis. *Matrix Biol,* 29**,** 248-53.

KIANI, C., CHEN, L., WU, Y. J., YEE, A. J. & YANG, B. B. 2002. Structure and function of aggrecan. *Cell Res,* 12**,** 19-32.

KIELTY, C. M., STEPHAN, S., SHERRATT, M. J., WILLIAMSON, M. & SHUTTLEWORTH, C. A. 2007. Applying elastic fibre biology in vascular tissue engineering. *Philosophical Transactions of the Royal Society B: Biological Sciences,* 362**,** 1293-1312.

KIERSTAN, M. & BUCKE, C. 1977. The immobilization of microbial cells, subcellular organelles, and enzymes in calcium alginate gels. *Biotechnology and Bioengineering,* 19**,** 387-397.

KIM, D. H., KIM, S.-H., HEO, S.-J., SHIN, J. W., LEE, S. W., PARK, S. A. & SHIN, J.-W. 2009a. Enhanced differentiation of mesenchymal stem cells into NP-like cells

via 3D co-culturing with mechanical stimulation. *Journal of Bioscience and Bioengineering,* 108**,** 63-67.

KIM, K.-W., CHUNG, H.-N., HA, K.-Y., LEE, J.-S. & KIM, Y.-Y. 2009b. Senescence mechanisms of nucleus pulposus chondrocytes in human intervertebral discs. *The Spine Journal,* 9**,** 658-666.

KITAGAWA, H., IZUMIKAWA, T., UYAMA, T. & SUGAHARA, K. 2003. Molecular cloning of a chondroitin polymerizing factor that cooperates with chondroitin synthase for chondroitin polymerization. *J Biol Chem,* 278**,** 23666-71.

KITAGAWA, H., UYAMA, T. & SUGAHARA, K. 2001. Molecular cloning and expression of a human chondroitin synthase. *J Biol Chem,* 276**,** 38721-6.

KLOCK, G., PFEFFERMANN, A., RYSER, C., GROHN, P., KUTTLER, B., HAHN, H. J. & ZIMMERMANN, U. 1997. Biocompatibility of mannuronic acid-rich alginates. *Biomaterials,* 18**,** 707-13.

KOCSIS, E., TRUS, B. L., STEER, C. J., BISHER, M. E. & STEVEN, A. C. 1991. Image averaging of flexible fibrous macromolecules: the clathrin triskelion has an elastic proximal segment. *J Struct Biol,* 107**,** 6-14.

KOLETTAS, E., BULUWELA, L., BAYLISS, M. T. & MUIR, H. I. 1995. Expression of cartilage-specific molecules is retained on long-term culture of human articular chondrocytes. *J Cell Sci,* 108 (Pt 5)**,** 1991-9.

KOPESKY, P. W., LEE, H. Y., VANDERPLOEG, E. J., KISIDAY, J. D., FRISBIE, D. D., PLAAS, A. H., ORTIZ, C. & GRODZINSKY, A. J. 2010. Adult equine bone marrow stromal cells produce a cartilage-like ECM mechanically superior to animal-matched adult chondrocytes. *Matrix Biol*.

KORECKI, C. L., KUO, C. K., TUAN, R. S. & IATRIDIS, J. C. 2009. Intervertebral disc cell response to dynamic compression is age and frequency dependent. *J Orthop Res,* 27**,** 800-6.

LAMARI, F. N. & KARAMANOS, N. K. 2006. Structure of chondroitin sulfate. *Adv Pharmacol,* 53**,** 33-48.

LANSDOWN, A. B. & PAYNE, M. J. 1994. An evaluation of the local reaction and biodegradation of calcium sodium alginate (Kaltostat) following subcutaneous implantation in the rat. *J R Coll Surg Edinb,* 39**,** 284-8.

LE MAITRE, C. L., BAIRD, P., FREEMONT, A. J. & HOYLAND, J. A. 2009. An in vitro study investigating the survival and phenotype of mesenchymal stem cells following injection into nucleus pulposus tissue. *Arthritis Res Ther,* 11**,** R20.

LE MAITRE, C. L., FRAIN, J., FOTHERINGHAM, A. P., FREEMONT, A. J. & HOYLAND, J. A. 2008. Human cells derived from degenerate intervertebral discs respond differently to those derived from non-degenerate intervertebral discs following application of dynamic hydrostatic pressure. *Biorheology,* 45**,** 563-575.

LE MAITRE, C. L., FREEMONT, A. J. & HOYLAND, J. A. 2004. Localization of degradative enzymes and their inhibitors in the degenerate human intervertebral disc. *J Pathol,* 204**,** 47-54.

LE MAITRE, C. L., FREEMONT, A. J. & HOYLAND, J. A. 2007a. Accelerated cellular senescence in degenerate intervertebral discs: a possible role in the pathogenesis of intervertebral disc degeneration. *Arthritis Res Ther,* 9**,** R45.

LE MAITRE, C. L., POCKERT, A., BUTTLE, D. J., FREEMONT, A. J. & HOYLAND, J. A. 2007b. Matrix synthesis and degradation in human intervertebral disc degeneration. *Biochem Soc Trans,* 35**,** 652-5.

LEBOVITS, A., HAINLINE, B., STONE, L. S., SEMINOWICZ, D. A., BRUNZ, J. T., ROSENQUIST, R. W. & COWAN, P. 2009. Struck From Behind: Maintaining Quality of Life With Chronic Low Back Pain. *The Journal of Pain,* 10**,** 927-931.

LEE, D. A., REISLER, T. & BADER, D. L. 2003. Expansion of chondrocytes for tissue engineering in alginate beads enhances chondrocytic phenotype compared to conventional monolayer techniques. *Acta Orthop Scand,* 74**,** 6-15.

LEE, H. Y., HAN, L., ROUGHLEY, P. J., GRODZINSKY, A. J. & ORTIZ, C. 2013. Age-related nanostructural and nanomechanical changes of individual human cartilage aggrecan monomers and their glycosaminoglycan side chains. *J Struct Biol,* 181**,** 264-73.

LEE, H. Y., KOPESKY, P. W., PLAAS, A., SANDY, J., KISIDAY, J., FRISBIE, D., GRODZINSKY, A. J. & ORTIZ, C. 2010. Adult bone marrow stromal cell-based tissue-engineered aggrecan exhibits ultrastructure and nanomechanical properties superior to native cartilage. *Osteoarthritis Cartilage,* 18**,** 1477-86.

LEE, K. Y. & MOONEY, D. J. 2001. Hydrogels for tissue engineering. *Chem Rev,* 101**,** 1869-79.

LEWIS, N. T., HUSSAIN, M. A. & MAO, J. J. 2008. Investigation of nano-mechanical properties of annulus fibrosus using atomic force microscopy. *Micron,* 39**,** 1008-19.

LI, Z., KUPCSIK, L., YAO, S. J., ALINI, M. & STODDART, M. J. 2009. Mechanical Load Modulates Chondrogenesis of Human Mesenchymal Stem Cells through the TGF-beta Pathway. *J Cell Mol Med*.

LIM, F. & SUN, A. M. 1980. Microencapsulated islets as bioartificial endocrine pancreas. *Science,* 210**,** 908-10.

LITTLE, P. J., BALLINGER, M. L., BURCH, M. L. & OSMAN, N. 2008. Biosynthesis of natural and hyperelongated chondroitin sulfate glycosaminoglycans: new insights into an elusive process. *Open Biochem J,* 2**,** 135-42.

LIVAK, K. J. & SCHMITTGEN, T. D. 2001. Analysis of Relative Gene Expression Data Using Real-Time Quantitative PCR and the 2−ΔΔCT Method. *Methods,* 25**,** 402-408.

LOHMANDER, L. S., NEAME, P. J. & SANDY, J. D. 1993. The structure of aggrecan fragments in human synovial fluid. Evidence that aggrecanase mediates cartilage degradation in inflammatory joint disease, joint injury, and osteoarthritis. *Arthritis Rheum,* 36**,** 1214-22.

LOTZ, J. C., STAPLES, A., WALSH, A. & HSIEH, A. H. 2004. Mechanobiology in intervertebral disc degeneration and regeneration. *Conf Proc IEEE Eng Med Biol Soc,* 7**,** 5459.

LUNDON, K. & BOLTON, K. 2001. Structure and function of the lumbar intervertebral disk in health, aging, and pathologic conditions. *J Orthop Sports Phys Ther,* 31**,** 291-303; discussion 304-6.

LUO, W., GUO, C., ZHENG, J., CHEN, T. L., WANG, P. Y., VERTEL, B. M. & TANZER, M. L. 2000. Aggrecan from start to finish. *J Bone Miner Metab,* 18**,** 51-6.

LUOMA, K., RIIHIMAKI, H., LUUKKONEN, R., RAININKO, R., VIIKARI-JUNTURA, E. & LAMMINEN, A. 2000. Low back pain in relation to lumbar disc degeneration. *Spine (Phila Pa 1976),* 25**,** 487-92.

LYONS, G. & SWEET, M. B. E. 1986. AGE-RELATED-CHANGES IN PROTEOGLYCAN OF BOVINE INTERVERTEBRAL-DISK. *South African Journal of Science,* 82**,** 151-155.

LYUBCHENKO, Y., SHLYAKHTENKO, L., HARRINGTON, R., ODEN, P. & LINDSAY, S. 1993. Atomic force microscopy of long DNA: imaging in air and under water. *Proc Natl Acad Sci U S A,* 90**,** 2137-40.

MA, H. L., HUNG, S. C., LIN, S. Y., CHEN, Y. L. & LO, W. H. 2003. Chondrogenesis of human mesenchymal stem cells encapsulated in alginate beads. *J Biomed Mater Res A,* 64**,** 273-81.

MACKAY, A. M., BECK, S. C., MURPHY, J. M., BARRY, F. P., CHICHESTER, C. O. & PITTENGER, M. F. 1998. Chondrogenic differentiation of cultured human mesenchymal stem cells from marrow. *Tissue Eng,* 4**,** 415-28.

MACLEAN, J. J., LEE, C. R., ALINI, M. & IATRIDIS, J. C. 2004. Anabolic and catabolic mRNA levels of the intervertebral disc vary with the magnitude and frequency of in vivo dynamic compression. *J Orthop Res,* 22**,** 1193-200.

MALDONADO, B. A. & OEGEMA, T. R., JR. 1992. Initial characterization of the metabolism of intervertebral disc cells encapsulated in microspheres. *J Orthop Res,* 10**,** 677-90.

MALLADI, P., XU, Y., CHIOU, M., GIACCIA, A. J. & LONGAKER, M. T. 2006. Effect of reduced oxygen tension on chondrogenesis and osteogenesis in adipose-derived mesenchymal cells. *Am J Physiol Cell Physiol,* 290**,** C1139-46.

MANIADAKIS, N. & GRAY, A. 2000. The economic burden of back pain in the UK. *Pain,* 84**,** 95-103.

MAROUDAS, A., MUIR, H. & WINGHAM, J. 1969. The correlation of fixed negative charge with glycosaminoglycan content of human articular cartilage. *Biochim Biophys Acta,* 177**,** 492-500.

MAROUDAS, A., STOCKWELL, R. A., NACHEMSON, A. & URBAN, J. 1975. Factors involved in the nutrition of the human lumbar intervertebral disc: cellularity and diffusion of glucose in vitro. *J Anat,* 120**,** 113-30.

MARTINSEN, A., SKJAK-BRAEK, G. & SMIDSROD, O. 1989. Alginate as immobilization material: I. Correlation between chemical and physical properties of alginate gel beads. *Biotechnol Bioeng,* 33**,** 79-89.

MASUDA, K. 2008. Biological repair of the degenerated intervertebral disc by the injection of growth factors. *Eur Spine J,* 17 Suppl 4**,** 441-51.

MASUDA, K. & LOTZ, J. C. 2010. New Challenges for Intervertebral Disc Treatment Using Regenerative Medicine. *Tissue Engineering Part B-Reviews,* 16**,** 147-158.

MAYER, J. E., IATRIDIS, J. C., CHAN, D., QURESHI, S. A., GOTTESMAN, O. & HECHT, A. C. 2013. Genetic polymorphisms associated with intervertebral disc degeneration. *Spine J,* 13**,** 299-317.

MCCANLESS, J. D., COLE, J. A., SLACK, S. M., BUMGARDNER, J. D., ZAMORA, P. O. & HAGGARD, W. O. 2011. Modeling Nucleus Pulposus Regeneration In Vitro: Mesenchymal Stem Cells, Alginate Beads, Hypoxia, Bone Morphogenetic Protein-2, and Synthetic Peptide B2A. *Spine,* 36**,** 2275-2285 10.1097/BRS.0b013e31820cd1b1.

MELROSE, J. & ROUGHLEY, P. 2014. Proteoglycans of the Intervertebral Disc. *In:* SHAPIRO, I. M. & RISBUD, M. V. (eds.) *The Intervertebral Disc.* Springer Vienna.

MELROSE, J., SMITH, S. & GHOSH, P. 2000. Differential expression of proteoglycan epitopes by ovine intervertebral disc cells. *J Anat,* 197 (Pt 2)**,** 189-98.

MIKAMI, T. & KITAGAWA, H. 2013. Biosynthesis and function of chondroitin sulfate. *Biochimica et Biophysica Acta (BBA) - General Subjects,* 1830**,** 4719-4733.

MILLER, G. J. & MORGAN, E. F. 2010. Use of microindentation to characterize the mechanical properties of articular cartilage: comparison of biphasic material properties across length scales. *Osteoarthritis Cartilage,* 18**,** 1051-7.

MINOGUE, B. M., RICHARDSON, S. M., ZEEF, L. A., FREEMONT, A. J. & HOYLAND, J. A. 2010. Transcriptional profiling of bovine intervertebral disc cells: implications for identification of normal and degenerate human intervertebral disc cell phenotypes. *Arthritis Res Ther,* 12**,** R22.

MOBASHERI, A. 1998. Correlation between [Na+], [glycosaminoglycan] and Na+/K+ pump density in the extracellular matrix of bovine articular cartilage. *Physiol Res,* 47**,** 47-52.

MOK, S. S., MASUDA, K., HAUSELMANN, H. J., AYDELOTTE, M. B. & THONAR, E. J. 1994. Aggrecan synthesized by mature bovine chondrocytes suspended in alginate. Identification of two distinct metabolic matrix pools. *J Biol Chem,* 269**,** 33021-7.

MORGELIN, M., PAULSSON, M., MALMSTROM, A. & HEINEGARD, D. 1989. Shared and distinct structural features of interstitial proteoglycans from different bovine tissues revealed by electron microscopy. *J Biol Chem,* 264**,** 12080-90.

MORRIS, E. R., REES, D. A., THOM, D. & BOYD, J. 1978. Chiroptical and stoichiometric evidence of a specific, primary dimerisation process in alginate gelation. *Carbohydrate Research,* 66**,** 145-154.

MWALE, F., ROUGHLEY, P. & ANTONIOU, J. 2004. Distinction between the extracellular matrix of the nucleus pulposus and hyaline cartilage: a requisite for tissue engineering of intervertebral disc. *Eur Cell Mater,* 8**,** 58-63; discussion 63-4.

NAGASE, H. & KASHIWAGI, M. 2003. Aggrecanases and cartilage matrix degradation. *Arthritis Res Ther,* 5**,** 94-103.

NEAME, P. J. & BARRY, F. P. 1993. THE LINK PROTEINS. *Experientia,* 49**,** 393-402.

NERURKAR, N. L., ELLIOTT, D. M. & MAUCK, R. L. 2010. Mechanical design criteria for intervertebral disc tissue engineering. *Journal of Biomechanics,* 43**,** 1017-1030.

NG, L., GRODZINSKY, A. J., PATWARI, P., SANDY, J., PLAAS, A. & ORTIZ, C. 2003. Individual cartilage aggrecan macromolecules and their constituent glycosaminoglycans visualized via atomic force microscopy. *Journal of Structural Biology,* 143**,** 242-257.

NILSSON, K. & MOSBACH, K. 1980. Preparation of Immobilized animal cells. *FEBS Letters,* 118**,** 145-150.

NOMURA, T., MOCHIDA, J., OKUMA, M., NISHIMURA, K. & SAKABE, K. 2001. Nucleus pulposus allograft retards intervertebral disc degeneration. *Clin Orthop Relat Res***,** 94-101.

O'HALLORAN, D. M. & PANDIT, A. S. 2007. Tissue-engineering approach to regenerating the intervertebral disc. *Tissue Engineering,* 13**,** 1927-1954.

OEGEMA, T. R., JOHNSON, S. L., AGUIAR, D. J. & OGILVIE, J. W. 2000. Fibronectin and its fragments increase with degeneration in the human intervertebral disc. *Spine,* 25**,** 2742-2747.

OHLSON, S., LARSSON, P.-O. & MOSBACH, K. 1979. Steroid transformation by living cells immobilized in calcium alginate. *European journal of applied microbiology and biotechnology,* 7**,** 103-110.

OSHIMA, H., ISHIHARA, H., URBAN, J. P. & TSUJI, H. 1993. The use of coccygeal discs to study intervertebral disc metabolism. *J Orthop Res,* 11**,** 332-8.

PATTAPPA, G., LI, Z., PEROGLIO, M., WISMER, N., ALINI, M. & GRAD, S. 2012. Diversity of intervertebral disc cells: phenotype and function. *J Anat,* 221**,** 480-96.

PEARCE, R. H., GRIMMER, B. J. & ADAMS, M. E. 1987. Degeneration and the chemical composition of the human lumbar intervertebral disc. *J Orthop Res,* 5**,** 198-205.

PERKINS, S. J., NEALIS, A. S., DUNHAM, D. G., HARDINGHAM, T. E. & MUIR, I. H. 1991. Molecular modeling of the multidomain structures of the proteoglycan binding region and the link protein of cartilage by neutron and synchrotron X-ray scattering. *Biochemistry,* 30**,** 10708-16.

POCKERT, A. J., RICHARDSON, S. M., LE MAITRE, C. L., LYON, M., DEAKIN, J. A., BUTTLE, D. J., FREEMONT, A. J. & HOYLAND, J. A. 2009. Modified expression of the ADAMTS enzymes and tissue inhibitor of metalloproteinases 3 during human intervertebral disc degeneration. *Arthritis Rheum,* 60**,** 482-91.

PUETZER, J. L., PETITTE, J. N. & LOBOA, E. G. 2010. Comparative review of growth factors for induction of three-dimensional in vitro chondrogenesis in human

mesenchymal stem cells isolated from bone marrow and adipose tissue. *Tissue Eng Part B Rev,* 16**,** 435-44.

RADMACHER, M. 1997. Measuring the elastic properties of biological samples with the AFM. *IEEE Eng Med Biol Mag,* 16**,** 47-57.

REZA, A. T. & NICOLL, S. B. 2010. Characterization of novel photocrosslinked carboxymethylcellulose hydrogels for encapsulation of nucleus pulposus cells. *Acta Biomater,* 6**,** 179-86.

RICHARDSON, S. M., CURRAN, J. M., CHEN, R., VAUGHAN-THOMAS, A., HUNT, J. A., FREEMONT, A. J. & HOYLAND, J. A. 2006a. The differentiation of bone marrow mesenchymal stem cells into chondrocyte-like cells on poly-L-lactic acid (PLLA) scaffolds. *Biomaterials,* 27**,** 4069-78.

RICHARDSON, S. M., HOYLAND, J. A., MOBASHERI, R., CSAKI, C., SHAKIBAEI, M. & MOBASHERI, A. 2010. Mesenchymal stem cells in regenerative medicine: opportunities and challenges for articular cartilage and intervertebral disc tissue engineering. *J Cell Physiol,* 222**,** 23-32.

RICHARDSON, S. M., HUGHES, N., HUNT, J. A., FREEMONT, A. J. & HOYLAND, J. A. 2008. Human mesenchymal stem cell differentiation to NP-like cells in chitosan-glycerophosphate hydrogels. *Biomaterials,* 29**,** 85-93.

RICHARDSON, S. M., MOBASHERI, A., FREEMONT, A. J. & HOYLAND, J. A. 2007. Intervertebral disc biology, degeneration and novel tissue engineering and regenerative medicine therapies. *Histol Histopathol,* 22**,** 1033-41.

RICHARDSON, S. M., PURMESSUR, D., BAIRD, P., PROBYN, B., FREEMONT, A. J. & HOYLAND, J. A. 2012. Degenerate human nucleus pulposus cells promote neurite outgrowth in neural cells. *PLoS One,* 7**,** e47735.

RICHARDSON, S. M., WALKER, R. V., PARKER, S., RHODES, N. P., HUNT, J. A., FREEMONT, A. J. & HOYLAND, J. A. 2006b. Intervertebral disc cell-mediated mesenchymal stem cell differentiation. *Stem Cells,* 24**,** 707-16.

RISBUD, M. V., ALBERT, T. J., GUTTAPALLI, A., VRESILOVIC, E. J., HILLIBRAND, A. S., VACCARO, A. R. & SHAPIRO, I. M. 2004. Differentiation of mesenchymal stem cells towards a nucleus pulposus-like phenotype in vitro: implications for cell-based transplantation therapy. *Spine (Phila Pa 1976),* 29**,** 2627-32.

RISBUD, M. V., DI MARTINO, A., GUTTAPALLI, A., SEGHATOLESLAMI, R., DENARO, V., VACCARO, A. R., ALBERT, T. J. & SHAPIRO, I. M. 2006. Toward an optimum system for intervertebral disc organ culture: TGF-beta 3 enhances nucleus pulposus and anulus fibrosus survival and function through modulation of TGF-beta-R expression and ERK signaling. *Spine (Phila Pa 1976),* 31**,** 884-90.

RISBUD, M. V., SCHAER, T. P. & SHAPIRO, I. M. 2010a. Toward an understanding of the role of notochordal cells in the adult intervertebral disc: From discord to accord. *Dev Dyn*.

RISBUD, M. V., SCHIPANI, E. & SHAPIRO, I. M. 2010b. Hypoxic Regulation of Nucleus Pulposus Cell Survival From Niche to Notch. *American Journal of Pathology,* 176**,** 1577-1583.

ROBERTS, S., CATERSON, B., MENAGE, J., EVANS, E. H., JAFFRAY, D. C. & EISENSTEIN, S. M. 2000. Matrix metalloproteinases and aggrecanase: their role in disorders of the human intervertebral disc. *Spine (Phila Pa 1976),* 25**,** 3005-13.

RODRIGUES-PINTO, R., RICHARDSON, S. M. & HOYLAND, J. A. 2013. Identification of novel nucleus pulposus markers: Interspecies variations and implications for cell-based therapiesfor intervertebral disc degeneration. *Bone Joint Res,* 2**,** 169-78.

RODRIGUEZ, E., ROLAND, S. K., PLAAS, A. & ROUGHLEY, P. J. 2006. The glycosaminoglycan attachment regions of human aggrecan. *J Biol Chem,* 281**,** 18444-50.

ROSENBERG, L., HELLMANN, W. & KLEINSCHMIDT, A. K. 1970. Macromolecular models of proteinpolysaccharides from bovine nasal cartilage based on electron microscopic studies. *J Biol Chem,* 245**,** 4123-30.

ROSENBERG, L. & SCHUBERT, M. 1967. The proteinpolysaccharides of bovine nucleus pulposus. *J Biol Chem,* 242**,** 4691-701.

ROUGHLEY, P., MARTENS, D., RANTAKOKKO, J., ALINI, M., MWALE, F. & ANTONIOU, J. 2006. The involvement of aggrecan polymorphism in degeneration of human intervertebral disc and articular cartilage. *Eur Cell Mater,* 11**,** 1-7; discussion 7.

ROUGHLEY, P. J. 2004. Biology of intervertebral disc aging and degeneration: involvement of the extracellular matrix. *Spine (Phila Pa 1976),* 29**,** 2691-9.

ROUGHLEY, P. J. & MORT, J. S. 2012. Analysis of aggrecan catabolism by immunoblotting and immunohistochemistry. *Methods Mol Biol,* 836**,** 219-37.

ROUGHLEY, P. J. & WHITE, R. J. 1980. Age-related changes in the structure of the proteoglycan subunits from human articular cartilage. *J Biol Chem,* 255**,** 217-24.

RUAN, D., HE, Q., DING, Y., HOU, L., LI, J. & LUK, K. D. 2007. Intervertebral disc transplantation in the treatment of degenerative spine disease: a preliminary study. *Lancet,* 369**,** 993-9.

RUBIN, D. I. 2007. Epidemiology and risk factors for spine pain. *Neurol Clin,* 25**,** 353-71.

SAKAI, D., MOCHIDA, J., IWASHINA, T., HIYAMA, A., OMI, H., IMAI, M., NAKAI, T., ANDO, K. & HOTTA, T. 2006. Regenerative effects of transplanting mesenchymal stem cells embedded in atelocollagen to the degenerated intervertebral disc. *Biomaterials,* 27**,** 335-45.

SAKAI, D., MOCHIDA, J., IWASHINA, T., WATANABE, T., NAKAI, T., ANDO, K. & HOTTA, T. 2005. Differentiation of mesenchymal stem cells transplanted to a rabbit degenerative disc model: potential and limitations for stem cell therapy in disc regeneration. *Spine (Phila Pa 1976),* 30**,** 2379-87.

SAMBROOK, P. N., MACGREGOR, A. J. & SPECTOR, T. D. 1999. Genetic influences on cervical and lumbar disc degeneration: a magnetic resonance imaging study in twins. *Arthritis Rheum,* 42**,** 366-72.

SANDY, J. D., FLANNERY, C. R., BOYNTON, R. E. & NEAME, P. J. 1990. Isolation and characterization of disulfide-bonded peptides from the three globular domains of aggregating cartilage proteoglycan. *J Biol Chem,* 265**,** 21108-13.

SASSO, R. C., FOULK, D. M. & HAHN, M. 2008. Prospective, randomized trial of metal-on-metal artificial lumbar disc replacement. *Spine,* 33**,** 123-131.

SCHIZAS, C., KULIK, G. & KOSMOPOULOS, V. 2010. Disc degeneration: current surgical options. *Eur Cell Mater,* 20**,** 306-15.

SCHNEIDER, C. A., RASBAND, W. S. & ELICEIRI, K. W. 2012. NIH Image to ImageJ: 25 years of image analysis. *Nat Methods,* 9**,** 671-5.

SCHONHERR, E., JARVELAINEN, H. T., KINSELLA, M. G., SANDELL, L. J. & WIGHT, T. N. 1993. Platelet-derived growth factor and transforming growth factor-beta 1 differentially affect the synthesis of biglycan and decorin by monkey arterial smooth muscle cells. *Arterioscler Thromb,* 13**,** 1026-36.

SCOTT, J. E. & HAIGH, M. 1988. Keratan sulphate and the ultrastructure of cornea and cartilage: a 'stand-in' for chondroitin sulphate in conditions of oxygen lack? *J Anat,* 158**,** 95-108.

SETTON, L. A. & CHEN, J. 2006. Mechanobiology of the Intervertebral Disc and Relevance to Disc Degeneration. *J Bone Joint Surg Am,* 88**,** 52-57.

SHAPIRO, L. & COHEN, S. 1997. Novel alginate sponges for cell culture and transplantation. *Biomaterials,* 18**,** 583-90.

SHEN, B., WEI, A., TAO, H., DIWAN, A. D. & MA, D. D. 2009. BMP-2 enhances TGF-beta3-mediated chondrogenic differentiation of human bone marrow multipotent mesenchymal stromal cells in alginate bead culture. *Tissue Eng Part A,* 15**,** 1311-20.

SHERRATT, M. J. 2013. Structural proteins and arterial ageing. *Artery Research,* 7**,** 15-21.

SHERRATT, M. J., BALDOCK, C., MORGAN, A. & KIELTY, C. M. 2007. The morphology of adsorbed extracellular matrix assemblies is critically dependent on solution calcium concentration. *Matrix Biology,* 26**,** 156-166.

SHERRATT, M. J., BAX, D. V., CHAUDHRY, S. S., HODSON, N., LU, J. R., SARAVANAPAVAN, P. & KIELTY, C. M. 2005. Substrate chemistry influences the morphology and biological function of adsorbed extracellular matrix assemblies. *Biomaterials,* 26**,** 7192-206.

SHERRATT, M. J., HOLMES, D. F., SHUTTLEWORTH, C. A. & KIELTY, C. M. 2004. Substrate-dependent morphology of supramolecular assemblies: fibrillin and type-VI collagen microfibrils. *Biophys J,* 86**,** 3211-22.

SIKORSKI, P., MO, F., SKJAK-BRAEK, G. & STOKKE, B. R. T. 2007. Evidence for Egg-Box-Compatible Interactions in Calcium-Alginate Gels from Fiber X-ray Diffraction. *Biomacromolecules,* 8**,** 2098-2103.

SILBERT, J. E. & SUGUMARAN, G. 2002. Biosynthesis of chondroitin/dermatan sulfate. *IUBMB Life,* 54**,** 177-86.

SINGH, M., PIERPOINT, M., MIKOS, A. G. & KASPER, F. K. 2011. Chondrogenic differentiation of neonatal human dermal fibroblasts encapsulated in alginate beads with hydrostatic compression under hypoxic conditions in the presence of bone morphogenetic protein-2. *J Biomed Mater Res A,* 98**,** 412-24.

SITTERBERG, J., OZCETIN, A., EHRHARDT, C. & BAKOWSKY, U. 2010. Utilising atomic force microscopy for the characterisation of nanoscale drug delivery systems. *Eur J Pharm Biopharm,* 74**,** 2-13.

SIVAN, S. S., TSITRON, E., WACHTEL, E., ROUGHLEY, P. J., SAKKEE, N., VAN DER HAM, F., DEGROOT, J., ROBERTS, S. & MAROUDAS, A. 2006. Aggrecan turnover in human intervertebral disc as determined by the racemization of aspartic acid. *J Biol Chem,* 281**,** 13009-14.

SIVE, J. I., BAIRD, P., JEZIORSK, M., WATKINS, A., HOYLAND, J. A. & FREEMONT, A. J. 2002. Expression of chondrocyte markers by cells of normal and degenerate intervertebral discs. *Mol Pathol,* 55**,** 91-7.

SMETANA, K., JR. 1993. Cell biology of hydrogels. *Biomaterials,* 14**,** 1046-50.

SMITH, L. J. & FAZZALARI, N. L. 2009. The elastic fibre network of the human lumbar anulus fibrosus: architecture, mechanical function and potential role in the progression of intervertebral disc degeneration. *European Spine Journal,* 18**,** 439-448.

SOLOVIEVA, S., NOPONEN, N., MANNIKKO, M., LEINO-ARJAS, P., LUOMA, K., RAININKO, R., ALA-KOKKO, L. & RIIHIMAKI, H. 2007. Association between the aggrecan gene variable number of tandem repeats polymorphism and intervertebral disc degeneration. *Spine (Phila Pa 1976),* 32**,** 1700-5.

SPICER, A. P., KABACK, L. A., SMITH, T. J. & SELDIN, M. F. 1998. Molecular cloning and characterization of the human and mouse UDP-glucose dehydrogenase genes. *J Biol Chem,* 273**,** 25117-24.

STECK, E., BERTRAM, H., ABEL, R., CHEN, B. H., WINTER, A. & RICHTER, W. 2005. Induction of intervertebral disc-like cells from adult mesenchymal stem cells. *Stem Cells,* 23**,** 403-411.

STEVENS, R. L., DONDI, P. G. & MUIR, H. 1979. Proteoglycans of the intervertebral disc. Absence of degradation during the isolation of proteoglycans from the intervertebral disc. *Biochem J,* 179**,** 573-8.

STOLZ, M., GOTTARDI, R., RAITERI, R., MIOT, S., MARTIN, I., IMER, R., STAUFER, U., RADUCANU, A., DUGGELIN, M., BASCHONG, W., DANIELS, A. U., FRIEDERICH, N. F., ASZODI, A. & AEBI, U. 2009. Early detection of aging cartilage and osteoarthritis in mice and patient samples using atomic force microscopy. *Nat Nano,* 4**,** 186-192.

STRUGLICS, A. & LARSSON, S. 2010. A comparison of different purification methods of aggrecan fragments from human articular cartilage and synovial fluid. *Matrix Biology,* 29**,** 74-83.

STRUGLICS, A., LARSSON, S., PRATTA, M. A., KUMAR, S., LARK, M. W. & LOHMANDER, L. S. 2006. Human osteoarthritis synovial fluid and joint cartilage contain both aggrecanase- and matrix metalloproteinase-generated aggrecan fragments. *Osteoarthritis and Cartilage,* 14**,** 101-113.

SUN, J. C. & TAN, H. P. 2013. Alginate-Based Biomaterials for Regenerative Medicine Applications. *Materials,* 6**,** 1285-1309.

SUN, J. Y., ZHAO, X., ILLEPERUMA, W. R., CHAUDHURI, O., OH, K. H., MOONEY, D. J., VLASSAK, J. J. & SUO, Z. 2012. Highly stretchable and tough hydrogels. *Nature,* 489**,** 133-6.

SZTROLOVICS, R., ALINI, M., ROUGHLEY, P. J. & MORT, J. S. 1997. Aggrecan degradation in human intervertebral disc and articular cartilage. *Biochemical Journal,* 326**,** 235-241.

TANAKA, K. 1978. Physicochemical Properties of Chondroitin Sulfate: I. Ion Binding and Secondary Structure. *Journal of Biochemistry,* 83**,** 647-653.

TANIGAWA, M. & OKADA, T. 1998. Atomic force microscopy of supercoiled DNA structure on mica. *Analytica Chimica Acta,* 365**,** 19-25.

TEGEDER, I. 2009. Current evidence for a modulation of low back pain by human genetic variants. *Journal of Cellular and Molecular Medicine,* 13**,** 1605-1619.

THOMAS, K. J., MACPHERSON, H., THORPE, L., BRAZIER, J., FITTER, M., CAMPBELL, M. J., ROMAN, M., WALTERS, S. J. & NICHOLL, J. 2006. Randomised controlled trial of a short course of traditional acupuncture compared with usual care for persistent non-specific low back pain. *BMJ,* 333**,** 623.

THOMPSON, J. P., OEGEMA, T. R., JR. & BRADFORD, D. S. 1991. Stimulation of mature canine intervertebral disc by growth factors. *Spine (Phila Pa 1976),* 16**,** 253-60.

TORTONESE, M. 1997. Cantilevers and tips for atomic force microscopy. *Engineering in Medicine and Biology Magazine, IEEE,* 16**,** 28-33.

TORTORELLA, M. D., BURN, T. C., PRATTA, M. A., ABBASZADE, I., HOLLIS, J. M., LIU, R., ROSENFELD, S. A., COPELAND, R. A., DECICCO, C. P., WYNN, R., ROCKWELL, A., YANG, F., DUKE, J. L., SOLOMON, K., GEORGE, H., BRUCKNER, R., NAGASE, H., ITOH, Y., ELLIS, D. M., ROSS, H., WISWALL, B. H., MURPHY, K., HILLMAN, M. C., JR., HOLLIS, G. F., NEWTON, R. C., MAGOLDA, R. L., TRZASKOS, J. M. & ARNER, E. C. 1999. Purification and cloning of aggrecanase-1: a member of the ADAMTS family of proteins. *Science,* 284**,** 1664-6.

TORTORELLA, M. D., PRATTA, M., LIU, R.-Q., AUSTIN, J., ROSS, O. H., ABBASZADE, I., BURN, T. & ARNER, E. 2000. Sites of Aggrecan Cleavage by Recombinant Human Aggrecanase-1 (ADAMTS-4). *Journal of Biological Chemistry,* 275**,** 18566-18573.

TROUT, J. J., BUCKWALTER, J. A., MOORE, K. C. & LANDAS, S. K. 1982. Ultrastructure of the human intervertebral disc. I. Changes in notochordal cells with age. *Tissue Cell,* 14**,** 359-69.

URBAN, J. P. G. 2002. The role of the physicochemical environment in determining disc cell behaviour. *Biochem. Soc. Trans.,* 30**,** 858-864.

URBAN, J. P. G. & MAROUDAS, A. 1979. The measurement of fixed charged density in the intervertebral disc. *Biochimica et Biophysica Acta (BBA) - General Subjects,* 586**,** 166-178.

URBAN, J. P. G., ROBERTS, S. & RALPHS, J. R. 2000. The Nucleus of the Intervertebral Disc from Development to Degeneration. *Amer. Zool.,* 40**,** 53-61.

URBAN, J. P. G., SMITH, S. & FAIRBANK, J. C. T. 2004. Nutrition of the intervertebral disc. *Spine,* 29**,** 2700-2709.

VADALA, G., RUSSO, F., DI MARTINO, A. & DENARO, V. 2013. Intervertebral disc regeneration: from the degenerative cascade to molecular therapy and tissue engineering. *J Tissue Eng Regen Med*.

VAN SUSANTE, J. L., BUMA, P., VAN OSCH, G. J., VERSLEYEN, D., VAN DER KRAAN, P. M., VAN DER BERG, W. B. & HOMMINGA, G. N. 1995. Culture of chondrocytes in alginate and collagen carrier gels. *Acta Orthop Scand,* 66**,** 549-56.

VERZIJL, N., DEGROOT, J., THORPE, S. R., BANK, R. A., SHAW, J. N., LYONS, T. J., BIJLSMA, J. W., LAFEBER, F. P., BAYNES, J. W. & TEKOPPELE, J. M. 2000. Effect of collagen turnover on the accumulation of advanced glycation end products. *J Biol Chem,* 275**,** 39027-31.

VICTOR, X. V., NGUYEN, T. K., ETHIRAJAN, M., TRAN, V. M., NGUYEN, K. V. & KUBERAN, B. 2009. Investigating the elusive mechanism of glycosaminoglycan biosynthesis. *J Biol Chem,* 284**,** 25842-53.

VINATIER, C., MRUGALA, D., JORGENSEN, C., GUICHEUX, J. & NOEL, D. 2009. Cartilage engineering: a crucial combination of cells, biomaterials and biofactors. *Trends Biotechnol,* 27**,** 307-14.

VO, N. V., HARTMAN, R. A., YURUBE, T., JACOBS, L. J., SOWA, G. A. & KANG, J. D. 2013. Expression and regulation of metalloproteinases and their inhibitors in intervertebral disc aging and degeneration. *The Spine Journal,* 13**,** 331-341.

WALSH, A. J., BRADFORD, D. S. & LOTZ, J. C. 2004. In vivo growth factor treatment of degenerated intervertebral discs. *Spine (Phila Pa 1976),* 29**,** 156-63.

WANG, J. Y., BAER, A. E., KRAUS, V. B. & SETTON, L. A. 2001. Intervertebral disc cells exhibit differences in gene expression in alginate and monolayer culture. *Spine (Phila Pa 1976),* 26**,** 1747-51; discussion 1752.

WATANABE, H., CHEUNG, S. C., ITANO, N., KIMATA, K. & YAMADA, Y. 1997. Identification of hyaluronan-binding domains of aggrecan. *J Biol Chem,* 272**,** 28057-65.

WENGER, K. H., WOODS, J. A., HOLECEK, A., ECKSTEIN, E. C., ROBERTSON, J. T. & HASTY, K. A. 2005. Matrix remodeling expression in anulus cells subjected to increased compressive load. *Spine (Phila Pa 1976),* 30**,** 1122-6.

WILBUR JL, K. A., BIEBUYCK HA, KIM E, WHITESIDES GM. 1996. Microcontact printing of self-assembled monolayers: applications in microfabrication. *Nanotechnology,* 7**,** 452.

WILKE, H. J., NEEF, P., CAIMI, M., HOOGLAND, T. & CLAES, L. E. 1999. New in vivo measurements of pressures in the intervertebral disc in daily life. *Spine (Phila Pa 1976),* 24**,** 755-62.

WUERTZ, K., GODBURN, K., MACLEAN, J. J., BARBIR, A., DONNELLY, J. S., ROUGHLEY, P. J., ALINI, M. & IATRIDIS, J. C. 2009. In vivo remodeling of intervertebral discs in response to short- and long-term dynamic compression. *J Orthop Res,* 27**,** 1235-42.

YAMAMOTO, Y., MOCHIDA, J., SAKAI, D., NAKAI, T., NISHIMURA, K., KAWADA, H. & HOTTA, T. 2004. Upregulation of the viability of nucleus pulposus cells by bone marrow-derived stromal cells: significance of direct cell-to-cell contact in coculture system. *Spine (Phila Pa 1976),* 29**,** 1508-14.

YANG, S. H., LIN, C. C., HU, M. H., SHIH, T. T., SUN, Y. H. & LIN, F. H. 2010. Influence of age-related degeneration on regenerative potential of human nucleus pulposus cells. *J Orthop Res,* 28**,** 379-83.

YEH, M. L. & LUO, Z. P. 2004. The structure of proteoglycan aggregate determined by atomic force microscopy. *Scanning,* 26**,** 273-276.

YU, J. 2002. Elastic tissues of the intervertebral disc. *Biochem Soc Trans,* 30**,** 848-52.

ZHANG, Y., CAO, L., KIANI, C., YANG, B. L., HU, W. & YANG, B. B. 1999. Promotion of chondrocyte proliferation by versican mediated by G1 domain and EGF-like motifs. *J Cell Biochem,* 73**,** 445-57.

ZHAO, C. Q., JIANG, L. S. & DAI, L. Y. 2006. Programmed cell death in intervertebral disc degeneration. *Apoptosis,* 11**,** 2079-88.

ZHAO, C. Q., WANG, L. M., JIANG, L. S. & DAI, L. Y. 2007. The cell biology of intervertebral disc aging and degeneration. *Ageing Res Rev,* 6**,** 247-61.

ZHAO, X., AKHTAR, R., NIJENHUIS, N., WILKINSON, S. J., MURPHY, L., BALLESTREM, C., SHERRATT, M. J., WATSON, R. E. B. & DERBY, B. 2012. Multi-layer phase analysis: quantifying the elastic properties of soft tissues and live cells with ultra-high-frequency scanning acoustic microscopy. *Ultrasonics, Ferroelectrics and Frequency Control, IEEE Transactions on,* 59**,** 610-620.

ZHENG, J., LUO, W. & TANZER, M. L. 1998. Aggrecan synthesis and secretion. A paradigm for molecular and cellular coordination of multiglobular protein folding and intracellular trafficking. *J Biol Chem,* 273**,** 12999-3006.